INSIGHTS INTO THE ROLE OF THE MEMBRANE ON PHOSPHOLIPASE C BETA AND G ALPHA Q-MEDIATED ACTIVATION

by

Brianna N. Hudson

A Dissertation

Submitted to the Faculty of Purdue University

In Partial Fulfillment of the Requirements for the degree of

Doctor of Philosophy

Department of Chemistry

West Lafayette, Indiana

August 2019

THE PURDUE UNIVERSITY GRADUATE SCHOOL
STATEMENT OF COMMITTEE APPROVAL

Dr. Angeline Lyon, Chair

Departments of Chemistry and Biological Sciences

Dr. Chittaranjan Das

Department of Chemistry

Dr. Nicholas Noinaj

Department of Biological Sciences

Dr. David Thompson

Department of Chemistry

Approved by:

Dr. Christine Hrycyna

Head of the Graduate Program

To my family, especially my mom and grandma Annette, for their continued support and encouragement.

ACKNOWLEDGMENTS

I would first like to thank my advisor, Dr. Angeline Lyon, who has been an excellent mentor over the years. One of the best decisions I have ever made was joining your lab! I am so grateful for your patience, support, encouragement, and guidance. Also, thank you for always being so positive and upbeat even when my experiments are not working. I would also like to thank my committee members, Dr. Chittaranjan Das, Dr. Nicholas Noinaj, and Dr. David Thompson for all of their guidance throughout my graduate career.

Thank you to the Lyon Lab members: Elisabeth Garland-Kuntz, Yvon Rugema, Monita Sieng, Candi Esquina, Michelle Van Camp, Kaushik Muralidharan, and Arielle Selvia. Thank you all for putting up with me and my craziness every day and for making the lab a fun environment. I would especially like to thank Elisabeth Garland-Kuntz for training me in numerous techniques and helping me get started in the lab, serving as my "lab mom," and being a great supportive friend! Additionally, I would like to recognize Monita Sieng for being my Starbucks and Stacked Pickle buddy, for always being willing to listen to me complain, and for being one of my closest friends at Purdue.

Finally, I would like to acknowledge my friends and family for always believing in me and reminding me to take breaks for fun. I would especially like to recognize my parents, step-dad, grandma, and two sisters for their endless prayers, support, and for always making me laugh. I definitely could not have made it through graduate school without all of you.

TABLE OF CONTENTS

LIST OF TABLES

LIST OF FIGURES

LIST OF ABBREVIATIONS

7TM	Seven Transmembrane-Spanning
AFM	Atomic Force Microscopy
ANTH	AP180 N-terminal homology
BAR	Bin-Amphiphysin-Rvsv167
CTD	C-terminal Domain
DAG	Diacylglycerol
DRM	Detergent Resistance Membrane
DSF	Differential Scanning Fluorimetry
ENTH	Epsin 1 N-terminal Homology
EM	Electron Microscopy
ER	Endoplasmic Reticulum
FRET	Förster Resonance Energy Transfer
GAP	Guanosine Triphosphatase Activating Protein
GDP	Guanosine Diphosphate
GEF	Guanine Nucleotide Exchange Factor
GPCR	G Protein-Coupled Receptor
GRK	G Protein-Coupled Receptor Kinase
GTP	Guanosine Triphosphate
HOPG	Highly Ordered Pyrolytic Graphite
IP_1	Inositol Monophosphate
IP_3	Inositol 1,4,5-triphosphate
L_d	Liquid-Disordered Phase
L_o	Liquid Ordered Phase
NLS	Nuclear Localization Signal
PC	Phosphatidylcholine
PE	Phosphatidylethanolamine
PS	Phosphatidylserine
PH	Pleckstrin Homology

PI	Phosphoinositides; Inositol Phospholipids
PI3K	Phosphoinositide-3-kinases
PI4K	Phosphoinositide-4-kinases
PIK	Phosphoinositide Lipid Kinases
PIP5K	Phosphatidylinositol-4-phosphate 5-kinases
PKC	Protein Kinase C
PLC	Phospholipase C
PPI	Polyphosphoinositides
PtdIns	Phosphatidylinositol
PtdIns-3-P	Phosphatidylinositol-3-phosphate
PtdIns-4-P	Phosphatidylinositol-4-phosphate
PtdIns-5-P	Phosphatidylinositol-5-phosphate
PtdIns-3,4-P_2	Phosphatidylinositol-3,4-bisphosphate
PtdIns-3,5-P_2	Phosphatidylinositol-3,5-bisphosphate
PtdIns-4,5-P_2; PIP_2	Phosphatidylinositol-4,5-bisphosphate
PtdIns-3,4,5-P_3	Phosphatidylinositol-3,4,5-triphosphate
PTEN	Phosphatase and Tensin Homolog
PX	Phox Homology Domains
RGS	Regulation of G Protein Signaling
SHIP	SH2-Containing Inositol Phosphatase
TIM	Triose Phosphate Isomerase

ABSTRACT

Author: Hudson, Brianna, N. PhD
Institution: Purdue University
Degree Received: August 2019
Title: Insights into the Role of the Membrane on Phospholipase C Beta and G Alpha Q-Mediated Activation
Committee Chair: Angeline Lyon

Phospholipase Cβ (PLCβ) cleaves phosphatidylinositol-4,5-bisphosphate (PIP_2) into the second messengers inositol-1,4,5-triphosphate (IP_3) and diacylglycerol (DAG). IP_3 increases intracellular Ca^{2+}, while DAG remains in the membrane, and together with increased Ca^{2+}, activates protein kinase C (PKC). PLCβ has low basal activity but is activated following stimulation of G_i- and G_q-coupled receptors through direct interactions with $G\alpha_q$ and $G\beta\gamma$. PLCβ is essential for normal cardiomyocyte and vascular smooth muscle function and regulates cell proliferation, survival, migration, and differentiation. However, increased PLCβ activity and expression results in arrhythmias, hypertrophy, and heart failure. PLCβ must interact with the cell membrane for its activity. While heterotrimeric G proteins stimulate PLCβ, they are insufficient for full activation, suggesting the membrane itself contributes to increased lipid hydrolysis, potentially via interfacial activation. However, how the composition of the membrane and its resulting properties, such as surface charge, contribute to adsorption and interfacial activation is not well-established. Furthermore, whether or how interfacial activation also impacts other regulatory elements in PLCβ and $G\alpha_q$-dependent activation is unknown. Using an innovative combination of atomic force microscopy on compressed lipid monolayers and biochemical assays, we are beginning to understand how the membrane itself, PLCβ autoinhibitory elements and $G\alpha_q$ regulate PLCβ activation. These studies provide the first structure-based approach to understanding how the cell membrane regulates the activity of this essential effector enzyme.

CHAPTER 1. INTRODUCTION

1.1 Cell Signaling

The ability of living cells to interact with and respond to changes in their extracellular environment is essential for fundamental cellular functions including proliferation, differentiation, transformation, and programmed cell death. The transmission of signals from the extracellular environment of a cell to its interior is achieved by the expression of diverse cell surface receptors that specifically respond to individual stimuli such as soluble molecules, a ligand bound to the surface of another cell, or the extracellular matrix itself. The extracellular signals are transduced across the plasma membrane upon detection and/or binding of stimuli to a specific cell surface receptor, resulting in the activation of intracellular pathways, and ultimately, leading to a physiological response. Dysregulation of the components within the cell that make up this complex network may result in human diseases, including cancer, cardiovascular disease, and autoimmune diseases. Thus, it is necessary to understand the function and mechanisms of the individual components that make up these complex cellular networks.

1.1.1 G Protein-Coupled Receptors

The largest family of cell-surface receptors involved in signal transduction are G protein-coupled receptors (GPCRs), which are also referred to as seven transmembrane-spanning (7TM) and heptahelical receptors. These receptors are encoded by the largest gene family in most animal genomes. For example, ~1% of the human genome encodes over 1,000 proteins with a predicted heptahelical structure[1]. Furthermore, countless previous studies have shown that these receptors play a substantial role in physiological functions, and their loss of function is directly involved in a large number of hereditary diseases[2–4]. As a result, ~34% of current Food and Drug Administration-approved drugs on the market target GPCRs and account for over 180 billion US dollars annually in global sales[5,6].

There are five families of GPCRs based on sequence and structural similarity: rhodopsin (family A), secretin (family B), glutamate (family C), adhesion, and Frizzled/Taste2[7,8]. Class A, B, and C receptors transmit extracellular signals through direct interactions with heterotrimeric G proteins, which consists of a Gα, Gβ, and Gγ subunit (Figure 1.1). The Gβ and Gγ subunits are tightly associated and form an obligate heterodimer. In the inactive state, the Gα subunit is bound

to guanosine diphosphate (GDP) and the Gβγ dimer[9,10]. Upon activation by extracellular stimuli, GPCRs undergo conformational changes which result in the activation of the bound Gα protein, wherein GDP is exchanged for guanosine triphosphate (GTP)[9,10]. This leads to the disassociation of the Gα subunit from Gβγ. Both the Gα subunit and Gβγ dimer can transmit receptor-generated signals to an array of downstream effector molecules. The specific downstream effector molecule targeted is dependent upon the particular type of GPCR, Gα subunit, and/or Gβγ dimer that is activated. Gα proteins are divided into four subfamilies based on functional and sequence homology: G_s, G_i, G_q, and $G_{12/13}$[11,12]. The G_s family ($G\alpha_s$ and $G\alpha_{olf}$), activates adenylyl cyclase, increasing cAMP concentration in the cell[1,2,11,13]. In contrast, the G_i family ($G\alpha_{i/o}$, $G\alpha_t$, $G\alpha_{gust}$, and $G\alpha_z$) inhibits adenylyl cyclase, opens K^+ channels, closes Ca^{2+} channels, and activates phosphodiesterases[1,7,11,13]. Members of the G_q family, including $G\alpha_q$, $G\alpha_{11}$, $G\alpha_{14}$, $G\alpha_{15/16}$ (mouse/human orthologs, respectively) stimulate phospholipase C β (PLCβ), which modulates calcium signals and activates protein kinase C (PKC) [1,7,11,14]. Finally, the $G_{12/13}$ family consisting of $G\alpha_{12}$ and $G\alpha_{13}$ activates Rho guanine nucleotide exchange factors (RhoGEFs), which regulate the Rho family of GTPases[1,7,11,15]. Currently, five different Gβ subunit and eleven different Gγ subunit genes have been identified in mammalian genomes[16,17]. These different subunit subtypes can pair together to form unique Gβγ dimer combinations. While the various roles of the different Gα families are well understood, the functional roles of the different Gβ and Gγ subunits and combinations of subunits is not well understood. However, previous studies have found that the Gβγ dimer can activate several different effectors, including PLCs, PKA, adenylyl cyclase, ion channels, and kinases[16,17].

GPCR signaling is desensitized through multiple mechanisms. Desensitization can occur through the degradation of the receptor agonist or by removal of the agonist from the vicinity of the receptor[18]. Furthermore, receptor signaling can also be controlled by the number of receptors present on a cell surface[19]. The activation of these receptors often results in the removal of receptors from the cell surface by internalization. Once internalized, receptors can be recycled back to the cell surface or targeted for degradation in lysosomes[19]. Recent studies have demonstrated that some GPCRs can continue signaling after internalization from endosomes and Golgi membranes[20]. Phosphorylation of GPCRs by at least two different classes of serine/threonine kinases through second messenger-dependent kinases (e.g., PKC) or independent kinases (e.g., GPCR kinases [GRKs][21]. Previous studies have shown that receptor phosphorylation recruits

arrestins to activated receptors, which prevent G protein binding and/or promote receptor internalization to endosomes[18,19,21]. In addition, the intrinsic GTPase activity by the Gα subunit hydrolyzes GTP to GDP, resulting in the re-association of the Gα and Gβγ subunits into the inactive heterotrimeric G protein[19]. GTPase activating proteins, such as the regulator of G protein signaling (RGS) family, accelerate this deactivation[18,19] (Figure 1.2).

1.2 Phosphoinositides

One of the ways in which GPCRs modulate cellular responses is through phosphoinositide (PI; also called inositol phospholipids) cascades, which are initiated by Gα and Gβγ subunits of heterotrimeric G proteins. PIs make up a small fraction of glycerol-based phospholipids and are concentrated at the inner leaflet of the plasma membrane. The cleavage of these lipids leads to the formation of lipid mediators that can serve as extracellular signaling molecules or intracellular second messengers[22,23]. This, in turn, controls a number of signaling events including membrane trafficking, actin remodeling, and ion channel function[24–26].

The parent PI, phosphatidylinositol (PtdIns) is synthesized in the endoplasmic reticulum (ER) and is composed of a diacylglycerol (DAG) backbone attached to an exposed inositol ring via phosphatidylinositol synthase, which attaches a di-ester phosphate bond at the D-1 position of the inositol ring[22,23]. PtsIns is then delivered to other membranes by vesicular transport or cytosolic PtsIns transport proteins[27,28]. The DAG moiety helps localize PIs to the cell membrane, while the headgroups on the inositol ring bind effector proteins such as PLC enzymes[29].

1.2.1 Polyphosphoinositides

There are eight naturally occurring PIs, seven of which are phosphorylated derivatives of PtdIns and are referred to as polyphosphoinositides (PPIs) (Figure 1.3). Of the seven PPIs, there are three monophosphoinositides: PtnIns-3-phosphate (PtnIns-3-P), PtnIns-4-phosphate (PtnIns-4-P), and PtnIns-5-phosphate (PtnIns-5-P). There are three bisphosphates: PtnIns-3,4-bisphosphate (PtnIns-3,4-P_2), PtnIns-3,5-bisphosphate (PtnIns-3,5-P_2), and PtnIns-4,5-bisphosphate (PtnIns-4,5-P_2; referred to as PIP_2 in subsequent sections). Finally, there is one triphosphoinositide: PtnIns-3,4,5-triphosphate (PtnIns-3,4,5-P_3). PtnIns-4-P represent ~95% of all monophosphoinositides found in mammalian cells, with PtnIns-3-P and PtnIns-5-P representing the additional 5% equally[30–32]. Out of the three bisphosphophosphate PPIs, PtnIns-4,5-P_2 (PIP_2) is the

most abundant and represents ~1% of total phospholipids in the cell membrane[30–32]. Mammalian cells contain varying levels of PtnIns-3,4,5-P_3; however, levels are typically thought to be similar in range to PtnIns-3,4-P_2 and PtnIns-3,5-P_2[30–32].

PPIs are phosphorylated in varying combinations at the –OH groups of the inositol ring by phosphoinositide lipid kinases (PIKs) (Figure 1.3)[29,33]. PIKs can be subdivided into three broad categories: phosphoinositide 3-kinases (PI3Ks), phosphatidylinositol (PtdIns) 4-kinases (PI4Ks), and PtdIns-4-phosphate 5-kinases (PIP5Ks)[34]. All of the lipid kinases transfer the γ-phosphate from ATP to various positions on the inositol headgroup of PtsIns[34]. Generally, most phosphorylation by PI3K and PI4K occurs in endomembranes, such as endosomes and the Golgi. In contrast, phosphorylation by PIP5K is thought to primarily occur in the plasma membrane[34]. Phosphate groups can also be removed from specific positions on the inositol ring by two major classes of inositol lipid phosphatases: phosphatase and tensin homolog deleted on chromosome ten (PTEN) and SH2-containing inositol phosphatase (SHIP)[35,36]. PTENs remove phosphates in the 3-position on the inositol ring, while SHIPs remove phosphates in the 5-position on the inositol ring[35].

1.2.2 Phosphoinositide Recognition Domains

The rapid phosphorylation and/or dephosphorylation of PtnIns allows for the creation of membrane targeting signals at distinct locations (Figure 1.3). Spatial and temporal recruitment of specific proteins to the membrane is essential for the regulation of intracellular signaling and trafficking events. There are a large number of proteins that contain specific phosphoinositide recognition domains, which are involved in an array of cell signaling events[31]. Over eleven different cytosolic PtnIns domains have been identified, including pleckstrin homology (PH), epsin 1 N-terminal homology (ENTH), AP180 N-terminal homology (ANTH), Bin-Amphiphysin-Rvsv167 (BAR) and Phox homology (PX) domains[29,31]. These PtnIns domains have a broad spectrum and affinity for PtnIns. For example, some PH domains which bind PtdIns-3,4,5-P_3, PtdIns-4,5-P_2 (PIP_2) and/or PtdIns-3,4-P_2, interact with the lipid headgroups through non-specific electrostatic interactions[29,31,37]. As a result, many PH domains bind phosphoinositides with poor specificity and low affinity. However, some PH domains, such as those that bind PtdIns-3,4,5-P_3, display high affinity for phosphoinsositides by forming specific contacts with lipid headgroups[31]. In contrast, ENTH and BAR domains, which bind PtdIns-4,5-P_2 (PIP_2), require an additional step

of insertion into the membrane to promote bilayer curvature[29,31,38]. The insertions of these domains into the membrane is thought to help stabilize these proteins at the membrane[38].

1.2.3 Phosphoinositides and Lipid Rafts

Another way in which PIs regulate diverse cellular functions is by temporally and spatially concentrating particular PIs into discrete domains, called lipid rafts, on the cell membrane based on their acyl chains[39,40]. Saturated acyl chains are thought to partition into the liquid-ordered phase (L_o), which is characterized by tight chain packing, reduced fluidity, and extended lipid chains. In contrast, unsaturated acyl chains partition into the fluid, liquid disordered phase (L_d)[39–41]. Lipid rafts are ~10-200 nm in size and are enriched in phospholipids, sphingolipids, and cholesterol[39,41]. Rafts are stabilized through intramolecular hydrogen bonds between the headgroups of neighboring sphingomyelin molecules, as well as through protein-lipid interactions[39]. Rafts are also characterized biochemically as being resistant to solubilization in detergents and dependent on cholesterol. Cholesterol serves as the dynamic glue that holds lipid rafts together by serving as a spacer between the hydrocarbons of the sphingolipids. In addition, cholesterol has also been shown to form intermolecular hydrogen bonds with sphingolipids[39]. Early studies employing membrane fractionation experiments found that a significant amount of PIP_2 is associated with the detergent-resistant membrane (DRM) resistant fraction, which is thought to represent discrete membrane domains[42–44]. However, the functional significance of PIP_2 compartmentalization is not well understood and remains controversial[41]. One possible mechanism for partitioning PIP_2 into lipid rafts could potentially be to compartmentalize the effects of PIP_2 depletion by PLC-dependent cellular processes. Alternatively, depletion of PIP_2 in lipid raft regions may activate the synthesis of PIP_2 in non-raft regions. Furthermore, the increased concentration of PIP_2 in these microdomains could also increase the synthesis of PtdIns-3,4,5-P_3, which controls an additional array of signaling reactions. In support of this, previous studies have shown that PI3K is targeted to lipid-raft regions in cells[45].

1.3 Phospholipase C Enzymes

There are several PI-specific proteins that recognize and bind to specific lipid headgroups. One of the most extensively studied PI-specific proteins is PLC enzymes, which hydrolyze PIP_2 into two second messengers: DAG and inositol-1,4,5-triphosphate (IP_3) (Figure 1.4). DAG

remains in the membrane and stimulates the activity of different enzymes by binding to C1 domains and serves as the substrate for phosphatidic acid synthesis. IP_3, which is the rate-limiting substrate for the synthesis of PPIs, is soluble and can bind to IP_3 receptors in the ER to release Ca^{2+} into the cell. This increase in Ca^{2+} triggers the association of PKC isozymes with the membrane, where they interact with DAG to stimulate kinase activity[46–48]. Some PKC isoforms are activated by the binding of both Ca^{2+} and DAG via their C1 and C2 domains, respectively[49,50]. In these isoforms, the binding of DAG is thought to increase its affinity for phosphatidylserine (PS) and Ca^{2+}, resulting in a conformational change that increases the catalytic activity of the enzyme[48]. In addition to generating DAG and IP_3, PLC enzymes also activate or inactivate downstream signaling pathways that rely on PIP_2 for membrane association and/or activity.

1.3.1 Phospholipase C Conserved Core Domains

There are 13 isozymes of PLC enzymes in mammals that are categorized into six subfamilies: PLCβ, PLCγ, PLCδ, PLCε, PLCζ, and PLCη[51,52] (Figure 1.5). All of the PLC subfamilies, with the exception of PLCζ, share a conserved catalytic core. The catalytic core is believed to be the minimal fragment necessary for lipase activity and is composed of a PH domain, four tandem EF hands, a triose phosphate isomerase-like (TIM) barrel domain that is split into an X and Y half by an X-Y linker, and a C2 domain[51–53]. Individual PLC subfamilies arise from the presence of conserved insertions within the catalytic core and/or regulatory domains at the N- and/or C- termini of the protein.

1.3.1.1 PH Domain

PH domains typically play a role in membrane association by binding negatively charged lipids, such as the PPIs[31]. The PLCδ and PLCγ PH domains can bind with high affinity to PIP_2 and PtdIns-3,4,5-P_3, respectively, and help translocate the protein to the membrane[54–56]. In contrast, the PLCβ PH domain only weakly contributes to non-specific membrane binding[57,58]. Instead, the PLCβ PH domain is thought to be involved in protein-protein interactions with Gβγ and/or Rac1[51,59]. The PH domains in the other PLC subfamilies have not been characterized with respect to their lipid binding properties.

1.3.1.2 EF Hands

The EF hands traditionally function as Ca^{2+} binding motifs in other well-known proteins such as calmodulin and topinin[60]. For the most part, the role of the EF hands in PLC enzymes is not well understood. The EF hands in PLCζ enzymes have been proposed to bind Ca^{2+}; however, this hypothesis has not been tested directly[51,52]. Similarly, previous studies have shown that deletion of all or part of this region in PLCδ1 results in a decrease in enzyme activity[52]. However, this is controversial, as Ca^{2+} is not bound to the EF hands in the crystal structure of PLCδ1[51]. The EF hands in PLCβ do not bind Ca^{2+}; instead, they serve as a scaffold and contain a loop responsible for stimulating the GTP hydrolysis of $G\alpha_q$ upon binding[61].

1.3.1.3 TIM Barrel Domain

All PLC enzymes catalyze the same PIP_2 hydrolysis reaction, and as a result, the TIM barrel is the most highly conserved domain between PLC subfamilies. The domain shares a 60-70% sequence identity between subfamilies and an even greater similarity between isoforms[51]. The general mechanism for PLC catalysis was determined with the help of a crystal structure of the catalytic core of PLCδ-1 in complex with IP_3[54,62,63](Figure 1.6). Deprotonation of the 2-hydroxyl group of the inositol ring is facilitated by a decrease of its pKa by the catalytic Ca^{2+}. A conserved glutamine residue (Glu341 in PLCδ-1 and Glu341 in PLCβ3) acts a base, resulting in the formation of a 1,2-monophosphate intermediate and DAG. This intermediate is stabilized via the 1-phosphate by a conserved histidine (His311 in PLCδ1 and His332 in PLCβ3) and Ca^{2+}. Next, a second histidine (His356 in PLCδ1 and His379 in PLCβ3) removes a proton from water and promotes a nucleophilic attack on the cyclic intermediate to form DAG and IP_3. All of the residues involved in Ca^{2+} coordination as well as PIP_2 recognition, specificity, and hydrolysis, are conserved across the PLC family[51]. The crystal structure of PLCδ1 also revealed a conserved hydrophobic ridge surrounding the active site that is proposed to facilitate catalysis by insertion into the membrane[62]. Previous studies showed that mutation of residues within the PLCδ1 or PLCβ3 hydrophobic ridge decreases basal activity and/or protein expression[63,64]. Early compressed lipid monolayer studies found that increasing the surface pressure of lipid monolayers significantly reduces the ability of PLCβ1 and PLCβ2 to hydrolyze PIP_2[65]. These studies are consistent with a mechanism in which the hydrophobic ridge penetrates the lipid bilayer to increase catalytic activity by maximizing the access of the active site to its substrate.

It is important to note that PLC enzymes have been shown to hydrolyze several PI substrates *in vitro* with the following rank order of specificity PIP_2 > PtdIns-4-P > PtdIns, however, data supporting direct hydrolysis of PtdIns-4-P and PtdIns by PLCs *in vivo* is lacking and not well understood[51,52,66]. Previous studies have shown that PLCε is responsible for PtsIns-4-P hydrolysis at the Golgi-nuclear envelope[67,68]. However, it is not yet known whether other PLC isoforms hydrolyze PtdIns-4-P and/or PtdIns in response to GPCR stimulation in cells.

1.3.1.4 X-Y Linker

PLC catalysis also involves the X-Y linker, which has been proposed to occlude the active site under basal conditions. Deletions of all or part of the negatively charged X-Y linker increases PIP_2 hydrolysis in PLCβ, PLCδ, and PLCε, demonstrating an autoinhibitory role for the X-Y linker[51,52,69–71]. Similarly, PLCζ is constitutively active due to the presence of a positively charged X-Y linker and has lower activity when the linker is removed[72]. The mechanism involved in the displacement of the negatively charged X-Y linker from the active site is not well understood and could potentially vary between the PLC isoforms. However, a general mechanism has been proposed involving interfacial activation. In this mechanism, electrostatic repulsion between the negatively charged membrane and the negatively charged X-Y linker result in conformational changes that expose the active site for substrate binding[61]. It is also possible that proteins that regulate PLC isozymes may also cause the release of the X-Y linker from the active site.

1.3.1.5 C2 Domain

The C2 domain is found in a variety of membrane-associated proteins such as PKC[50]. Traditionally, C2 domains bind Ca^{2+}, which increases the association of the domain with phospholipids. The C2 domain of PLCδ1 functions in this role and binds Ca^{2+} to promote translocation of the protein to the plasma membrane[62]. The PLCβ and PLCζ C2 domains lack critical Ca^{2+} binding residues, suggesting a non-conventional role for the C2 domain[51,61,73]. For example, the PLCβ C2 domain contributes to intra- and intermolecular regulatory binding sites[61].

1.3.2 Phospholipase C Subfamilies

1.3.2.1 Phospholipase Cγ

Two mammalian PLCγ isoforms have been identified, PLCγ1 and PLCγ2. PLCγ1 is expressed ubiquitously, while PLCγ2 is only expressed in the hematopoietic system[74]. PLCγ1 is essential for development, as PLCγ1-deficient mice showed embryonic lethality due to loss of both erythroid progenitors required for vasculogenesis[75,76]. In comparison, PLCγ2 is involved in signaling responses of B cells to immunoglobins[77]. This subfamily contains an insertion between the X and Y halves of the TIM barrel that consists of a split PH domain, two SH2 domains, and an SH3 domain. The PLCγ SH2 domains bind phosphorylated residues on tyrosine kinase receptors with high affinity[78]. This allows for the recruitment of the enzyme to the plasma membrane and phosphorylation of PLCγ, followed by increased catalytic activity through the release of autoinhibition[51,52]. Other mechanisms of PLCγ regulation have also been identified including phosphorylation by non-receptor tyrosine kinases, activation of immunoglobin receptors, and stimulation of GPCRs[55]. PLCγ2 has also been shown to be activated independently of receptor tyrosine kinases and PtnIns-3,4,5-P_3 generation through a mechanism involving Rac GTPases[79].

1.3.2.2 Phospholipase Cδ

There are three isoforms of PLCδ: 1, 3, and 4, all of which are expressed in almost every mammalian cell and share ~50% homology[80]. These isoforms have the highest expression in the brain, heart, and lungs. The PLCδ isoforms are the simplest PLC enzymes and only contain the core domains. They are all typically in equilibrium between the cytoplasm and various membrane fractions depending on the particular isoform, and recruitment to the membrane is thought to be the primary mechanism of their regulation[51,52]. PLCδ4 is located on the nuclear membrane during the G_1-S phase of the cells cycle and is believed to be regulated by degradation[51,52]. In contrast, PLCδ1 is primarily found at the PM[51,52]. However, some studies have also suggested that it may accumulate at the nuclear membrane during early stages of the cell cycle as well[52,81]. Increased PLCδ1 expression is elevated in the brains of Alzheimer's patients, but its role in the brain and disease is not yet known[82].

As mentioned previously in section 1.3.1.1, the PLCδ PH domain directly binds PIP_2, which contributes to its membrane association and promotes PIP_2 hydrolysis[51]. PIP_2 depletion results in PLCδ1 dissociation from the plasma membrane to the cytosol[83,84]. To achieve optimal

activation, PLCδ also needs Ca^{2+} bound to both its C2 domain and the active site[62]. The presence of Ca^{2+} is also proposed to contribute to the movement of PLCδ from the cytosol to the membrane, allowing for increased PIP_2 hydrolysis.

1.3.2.3 Phospholipase Cε

PLCε is expressed in most cell types, with the highest expression levels found in the heart, liver, and lungs[51,85]. PLCε expression and/or activity plays a role in cardiovascular disease, cancer, and kidney disease[51,52]. PLCε acts downstream of GPCRs coupled to G_q, G_s, G_{12}, and G_i, and receptor tyrosine kinases. In addition to the conserved PLC core domains, PLCε contains an N-terminal cysteine-rich domain, an N-terminal CDC25 domain, and two C-terminal Ras-association (RA) domains. One of the ways in which PLCε is activated is through the binding of GTP-bound H-Ras or Rap1to its RA2 domain[86]. Thus, any of the signaling pathways that activate Ras or Rap result in PLCε activation. The RA1 domain does not interact with activated G proteins and is instead involved in binding to scaffolding proteins[85]. H-Ras and Rap1 have also been shown to recruit PLCε to specific organelles[85,87]. Rap1 recruits PLCε to the Golgi, while H-Ras promotes translocation of PLCε to the plasma membrane[85,87]. The CDC25 domain of PLCε also acts as a GEF, resulting in the exchange of GTP for GDP on the Rap1 subfamily of GTPases[52,88,89]. This suggests that PLCε may have the ability to prolong its own activation through a feed-forward mechanism. Additionally, Rho GTPases also bind and activate PLCε, although the binding site for Rho has not yet been established. The binding site for the Rho family is believed to be different from the binding site for the Ras family, and cell-based assays suggest that additive effects on PLCε activity occur during simultaneous activation by H-Ras and RhoA[52].

1.3.2.4 Phospholipase Cζ

PLCζ is expressed in vertebrate sperm and is the smallest PLC isozyme. PLCζ initiates cytoplasmic Ca^{2+} oscillations that are necessary for the maturation and development of the fertilized egg. Loss of PLCζ expression or activity results in male infertility[90]. The mechanism of PLCζ in cells is not well understood. Calcium binding to the EF hands is thought to regulate lipase activity, and previous studies have shown that removal of the first two EF hands in this PLC isozyme results in decreased affinity for Ca^{2+} and decreased activity[91,92]. It is also the most sensitive to Ca^{2+} out of all of the PLCs and can be activated at Ca^{2+} concentrations as low as 100 nM, which is typically

found in resting cells[91,92]. Ca^{2+} levels in fertilized eggs may be one of the ways the specificity of PLCζ activity is achieved in fertilized eggs. Another way in which PLCζ is thought to be regulated is through the charge of its X-Y linker. As mentioned previously, unlike other PLC subfamilies, the PLCζ X-Y linker is positively charged. This reversal of charges observed in the X-Y linker may increase PLCζ membrane association and/or affinity for its substrate. Movement of PLCζ from the cytoplasm to the pronucleus via a class I nuclear localization signal (NLS) located in the cationic X-Y linker terminates PLCζ-dependent Ca^{2+} oscillations[51,52].

1.3.2.5 Phospholipase Cη

PLCη has two isoforms, PLCη1 and PLCη2, both of which are expressed exclusively in neuron-enriched regions in the brain and are thought to play an essential role in neuronal development[52]. This family of PLCs contains a C-terminal extension after the C-terminal domain comprised of a long carboxy-terminal Ser/Pro-rich sequence with a PDZ-binding motif at the end[93]. The regulation of PLCη has yet to be determined; however, cell-based experiments suggest that PLCη2 may be stimulated by Gβγ subunits[51,93]. Gβγ is thought to interact with the catalytic core of PLCη2, as the PH domain and C-terminal extension are dispensable for Gβγ activation[94]. Similar to PLCδ, the PH domain of PLCη2 is also thought to serve as a localization signal for the PM[51]. In support of this, deletion of the PH domain increased cytosolic PLCη2[94]. However, more studies are needed to determine the role of the PH domain as a membrane anchor in this PLC isozyme and to determine its specificity for phospholipids.

1.3.3 Phospholipase Cβ

The PLCβ subfamily is the among the most extensively studied out of all of the other PLC subfamilies. PLCβ enzymes have low basal activity, but can be activated ~60 fold downstream of G_q and G_i-coupled receptors through direct interactions with $G\alpha_q$ and Gβγ[61]. PLCβ enzymes can also be activated through GPCR-independent mechanisms via direct interactions with the Rho-family of small G proteins, such as Rac isoforms[51,52]. The PLCβ subfamily of enzymes are characterized by an ~400 amino-acid C-terminal extension that is subdivided into a proximal C-terminal domain (CTD) and distal CTD, split by a non-conserved linker. There have been numerous studies that have shown that all or part of this C-terminal extension is required for

membrane binding, $G\alpha_q$ binding, and maximum basal and $G\alpha_q$-mediated activity, however, it is dispensable for $G\beta\gamma$ and Rac activation[59,71,73,95–102].

1.3.3.1 Phospholipase Cβ Isoforms

There are four isoforms of PLCβ: PLCβ1, PLCβ2, PLCβ3, and PLCβ4. Each isoform differs in its expression pattern and regulation. Although the PLCβ isoforms share a conserved structure, they have different subcellular localization[26]. This difference in subcellular localization is thought to be attributed to subtle differences in their amino acid sequences and/or differences in their interactions with scaffolding proteins[26,61].

PLCβ1 is expressed primarily in the hippocampus and is also found in the cardiovascular system[51,103]. Increased PLCβ1 activity in vascular smooth muscle cells is thought to be an underlying mechanism in the development of diabetes[104]. There are also two splice variants of PLCβ1, PLCβ1a, and PLCβ1b, which differ in their C-termini. Both splice variants are found in the nucleus and contribute to the regulation of cell cycle progression[71].

PLCβ2 is almost exclusively expressed in hematopoietic cells and platelets and is involved in chemotaxis[105–107]. Decreased PLCβ2 expression in neutrophils increases their sensitivity to inflammatory agents and chemoattractants[61]. PLCβ2 has also been shown to be essential for thrombin-induced Ca^{2+} release in platelets[108]. There are two splice variants of PLCβ2, PLCβ2a, and PLCβ2b. PLCβ2b is missing 19 residues from the X-Y linker and distal CTD, which is thought to unmask a hydrophobic region on the surface of the enzyme, however, it is currently unknown how this alters its function[61].

The PLCβ3 isoform, which is of most interest in these studies, is expressed in the liver, brain, parotid gland, hemopoietic cells, and the cardiovascular system[109–112]. In the nervous system, PLCβ3 is required for opioid-induced Ca^{2+} release through a $G\beta\gamma$-dependent pathway and has also been shown to mediate Ca^{2+} release in response to noxious stimuli[109,113–115]. This PLCβ isoform also prevents differentiation through interactions with the transcription factor, Stat5, and its regulator SHP1 in the hematopoietic system[110]. Finally, PLCβ3 is most known for its role in cardiovascular disease. It essential for normal cardiovascular function, and mouse studies have shown that increased PLCβ3 expression and/or activation through G_q pathways results in arrhythmias, hypertrophy, and heart failure[111](Figure 1.7).

Finally, PLCβ4 is primarily expressed in the retina, where it is involved in visual processing events that are required for phototransduction[61,107]. It is also highly expressed in the cerebellum and loss of PLCβ4 expression in this region of the brain in mice resulted in motor defects[103]. Two splice variants of this PLCβ isoform have been found in humans, PLCβ4a and PLCβ4b. PLCβ4a is the full-length protein, while PLCβ4b is truncated after the distal CTD[116]. This truncated version of the distal CTD observed in PLCβ4b enzymes is thought result in a loss of membrane association of the protein.

1.3.3.2 Phospholipase Cβ Basal Activity Regulation

1.3.3.2.1 Phospholipase Cβ X-Y Linker

The X-Y linker within the TIM barrel domain of PLCs, mentioned in section 1.3.1.4, serves an autoinhibitory role in PLCβ enzymes. The function of this linker was first identified in reconstruction studies using PLCβ2, where fragments containing the PH, EF hands, and X halve of the TIM barrel domain were combined with fragments containing the Y half of the TIM barrel domain and C2 domain. Reconstitution of these fragments resulted in a 10-fold increase in basal activity relative to the intact protein[117].

The X-Y linker varies in sequence and length between PLCβ isoforms, however it can be broadly divided into an unconserved, disordered N-terminal region, a 10-15 residue highly acidic stretch thought to be important for interfacial activation, and a conserved C-terminal "lid" helix that occludes the active site in all PLCβ crystal structures[54,62,71]. The lid helix is stabilized through interactions with residues adjacent to the active site[71]. Displacement of the lid helix is proposed to occur via electrostatic repulsions between the acidic stretch of the linker and the negatively charged membrane[69,71,73]. In support of this mechanism, deletions within the X-Y linker that include the acidic stretch have been shown to increase basal activity and decrease thermal stability[69,71,73]. However, although electrostatic repulsion plays a role in PLCβ activation, it is insufficient to fully account for interfacial activation, as studies using liposomes with increasing negative charge found PLCβ activity increased only to a sub-maximal threshold.

1.3.3.2.2 Proximal CTD

The proximal CTD contains an autoinhibitory Hα2' helix and the primary $G\alpha_q$ binding site[100]. Under basal conditions, the Hα2' helix binds to a conserved hydrophobic cleft at the

interface of the TIM barrel and C2 domain[100]. Point mutations within the Hα2' helix or its binding site on the catalytic core increase basal activity up to ~50-fold over wild-type PLCβ activity, decrease thermal stability and decrease the efficacy of heterotrimeric G protein-stimulated activity[100,118]. These studies suggest that the Hα2' helix may stabilize the PLCβ catalytic core in a decreased activity state and impair interactions between the core and the membrane. Displacement of Hα2' from the hydrophobic cleft may be facilitated by interfacial activation and occurs in $G\alpha_q$-dependent activation. The Hα2' helix is preceded by the primary $G\alpha_q$ binding site (Hα1/Hα2) which is disordered in the absence of $G\alpha_q$ and is discussed in more detail in section 1.3.3.3.1.

1.3.3.2.3 Distal CTD

As previously discussed, the PH domain of PLCβ lacks the residues required to bind the phosphatidylinositol headgroup with high specificity and/or affinity compared to other PLC subfamilies such as PLCδ[31,57,58]. Instead, the primary membrane binding domain in PLCβ enzymes is the distal CTD[64,73,97,100,101,118]. Crystallographic studies of PLCβ revealed three highly conserved basic clusters located on the same face of the domain, which are thought to interact directly with the negatively charged membrane[64,119]. In support of this, mutation of these basic clusters and/or the entire distal CTD significantly decreased PLCβ membrane association and decreased basal and G protein-stimulated activity[64,69,71,97,101,118]. The distal CTD may also regulate PLCβ membrane association and/or distribution by altering the local structure of the membrane itself, given its similarity to BAR domains, which interact non-specifically with negatively charged phospholipids and sense/induce membrane curvature. It has been proposed that sequence variation between the different PLCβ isoforms may contribute to their differential membrane association, as there is only 30-35% sequence identity in this domain across all PLCβ isoforms[61,119]. For example, PLCβ1 and PLCβ4 are more membrane-associated, while PLCβ2 and PLCβ3 are more cytosolic[71]. One of the reasons why PLCβ3, and likely PLCβ2, may be present primarily in the cytosol is due to interactions between the distal CTD and the hydrophobic ridge in the TIM barrel domain[64]. These interactions may sequester the basic surface of the distal CTD and/or prevent the hydrophobic ridge from inserting into the membrane. Furthermore, cryo-electron microscopy (cryo-EM) studies have shown interactions between the distal CTD and the catalytic core, which may further regulate the distribution between membrane-bound and cytosolic PLCβ[64].

1.3.3.3 Phospholipase Cβ Mechanisms of Activation

1.3.3.3.1 $G\alpha_q$ Activation

The best characterized PLCβ activator is the heterotrimeric G protein subunit $G\alpha_q$. $G\alpha_q$ binds to PLCβ with high affinity, with EC_{50} values ranging between 1-400 nM[64,73,100,120]. However, the ability of $G\alpha_q$ to activate PLCβ varies between the PLCβ isoforms. A ~20-80-fold increase over basal activity is reported for $G\alpha_q$-dependent activation of PLCβ1, while PLCβ2 and PLCβ4 are only activated ~2-4-fold over basal by $G\alpha_q$ [73,121]. Crystallographic studies show that $G\alpha_q$ allosterically activates PLCβ by binding to the disordered Hα1/Hα2 in the proximal CTD via its switch regions, which recognize an ALXXPI binding motif. This binding orders Hα1/Hα2 and displaces Hα2' from the core[64,73,122]. In addition, fusing the PLCβ3 Hα1/Hα2 element to the $G\alpha_q$-insensitive PLCδ enzyme was sufficient to confer modest $G\alpha_q$-dependent activation[73]. The PLCβ C2 domain also interacts with the switch 1 and 2 regions of $G\alpha_q$; however, mutations in this interface only reduce $G\alpha_q$-dependent activation[61,73]. Additionally, a highly conserved loop in between EF hands three and four also contributes to $G\alpha_q$ binding[61]. This loop is involved in intrinsic PLCβ GTPase activating protein (GAP) activity, resulting in the rapid turn-off of $G\alpha_q$-dependent signaling and adding an additional level of complexity to PLCβ regulation by $G\alpha_q$[61]. Similar to RGS proteins, an asparagine (Asp 260) in this loop interacts with the catalytic Gln209 of $G\alpha_q$, stabilizing the transition state of GTP hydrolysis[73,123]. Finally, a hydrophobic patch in the distal CTD interacts with the N-terminus of $G\alpha_q$[64]. $G\alpha_q$ is palmitoylated on its N-terminus at Cys9 and Cys10; however, this lipid modification does not increase membrane association or alter the subcellular distribution of the $G\alpha_q$–PLCβ activation complex[98,124–126]. Furthermore, deletion of the N-terminal region of $G\alpha_q$ or mutations in the hydrophobic patch of the distal CTD decreased the efficacy of $G\alpha_q$ activation but did not alter basal activity or affinity for $G\alpha_q$[127]. This supports a mechanism wherein the N-terminus of $G\alpha_q$ may contribute to activation by potentially bringing the catalytic core into close proximity to the membrane for maximum PIP_2 hydrolysis[64]. It has also been proposed that multivalent interactions between $G\alpha_q$, PLCβ, and the membrane may release autoinhibition by the X-Y linker[71].

1.3.3.3.2 Gβγ Activation

Similar to $G\alpha_q$, each PLCβ isoform is differentially activated upon Gβγ binding. PLCβ2 is the most sensitive to Gβγ activation (EC_{50} of ~30 nM), while PLCβ1 and PLCβ3 are slightly less

sensitive (EC_{50} of ~90-200 nM), and PLCβ4 is unresponsive[69,101,128–130]. Gβγ signaling in cells is primarily generated by G_i-coupled receptors, such as the -δ and -μ opioid receptors, in which Gβγ activation is inhibited by treatment with pertussis toxin[113,128,129]. In addition, Gβγ acts on its effectors, including PLCs, at concentrations at least 10-fold higher than $G\alpha_q$ subunits and G_i-coupled receptors are more abundant than G_q-coupled receptors in cells[52]. Unlike activation by $G\alpha_q$, Gβγ activates PLCβ independently of the proximal and distal CTDs[73,97,101]. Gβγ is also only able to activate PLCβ when the Gγ subunit is prenylated, as loss of prenylation eliminated interactions between PLCβ2 and PLCβ3 with Gβγ[129,131]. However, previous studies have shown that Gβγ does not alter PLCβ membrane affinity or cellular distribution. Instead, Gβγ is proposed to increase the dwell time of the Gβγ-PLCβ complex at the membrane and/or help orient the PLCβ active site in a manner that is more readily accessible to PIP_2 [96,98,124,125,132,133]. The Gβγ binding site on PLCβ is currently unknown; however, it has been proposed that it is the PH domain[61]. Fluorescence resonance energy transfer method studies have shown that Gβγ binds directly to isolated PLCβ2 and PLCβ3 PH domains[133]. In addition, a PLCδ chimera which replaced the PLCδ PH domain with the PH domain from PLCβ2 conferred Gβγ-dependent activation[77,120].

1.3.3.3.3 Regulation by Small G Proteins

PLCβ2 and PLCβ3 are also activated by the small G proteins Cdc42, Rac1, and Rac2 through direct binding, but PLCβ1 and PLCβ4 are unresponsive to these activators[134,135]. These small G proteins only activate PLCβ in their GTP-bound state and must be prenylated at their C-termini for activation[135]. Both crystallographic and functional studies show that the Rac1 binding site is located on the PH domain, and no conformational changes occur within the PLCβ catalytic core upon Rac1 binding[135,136]. Instead, the prenylated C-terminus of activated Rac1 is proposed to increase the dwell time of the Rac1-PLCβ2 complex at the membrane, which may also promote interfacial activation[61,69]. It is unclear whether the Hα2' helix remains associated with the PLCβ catalytic core during Rac1 activation, as the CTDs are dispensable for PLCβ activation.

1.3.3.4 Localization of $G\alpha_q$ in Caveolae and its Effect on PLCβ Activation

One of the most stable lipid raft domains (previously discussed in Section 1.2.3) are caveolae, which are 50-100 nm flask-shaped invaginations, or 'little caves' found in the PM of mammalian cells[137]. Caveolae are similar to canonical lipid rafts in their enrichment of cholesterol,

sphingolipids, and phospholipids. Furthermore, nanoscale labeling techniques have also shown that caveolae are highly concentrated in the PLC substrate PIP_2[138,139]. However, caveolae also contain caveolin-proteins. There are three isoforms of caveolin proteins: caveolin-1, caveolin-2, and caveolin-3[140,141]. Caveolae typically form if cells express either caveolin-1, the predominant isoform, or caveolin-3, the muscle-specific isoform[140,141], caveolin-2 isoforms have not yet been shown to induce caveolae. Aggregation of caveolin proteins at the inner leaflet causes the curved morphology that distinguishes these domains. Caveolin proteins are anchored to the membrane via three palmitoyl groups and interact with various proteins through a scaffolding domain[140,141]. Functionally, caveolae deform and flatten to provide extended surface area when cells are mechanically stretched or osmotically swollen[137,142]. They also serve as scaffolds for proteins that hold actin filaments to the PM and play a role in cell signaling events by scaffolding family members of cell signaling pathways[137].

The lipidation of signaling proteins determines the selectivity of protein targeting to rafts. Because lipid rafts are clusters of ordered phase lipids, only proteins that contain saturated hydrocarbon chains, such as palmitoyl groups, can partition into lipid rafts. Previous studies have shown that palmitoylated and/or myristoylated Gα subunits can partition into lipid rafts, whereas prenylated Gβγ subunits were excluded[143,144]. Furthermore, studies measuring the relative strength of association of different Gα families and caveolae found that only the $G\alpha_q$ subfamily bound to caveolin-1 with high affinity[145–147]. This binding was only observed with GTP-bound $G\alpha_q$, suggesting that $G\alpha_q$ activation promotes translocation into caveolae domains. One potential role for $G\alpha_q$ in caveolae is to prolong the activation of its effectors, including PLCβ[137]. For example, $G\alpha_q$ could preferentially target PLCβ to caveolae domains which are elevated in PIP_2. In support of this mechanism, Förster resonance energy transfer (FRET) studies have shown that $G\alpha_q$-dependent Ca^{2+} signaling is prolonged in cells containing caveolae through a PLCβ-dependent mechanism in myocytes[142].

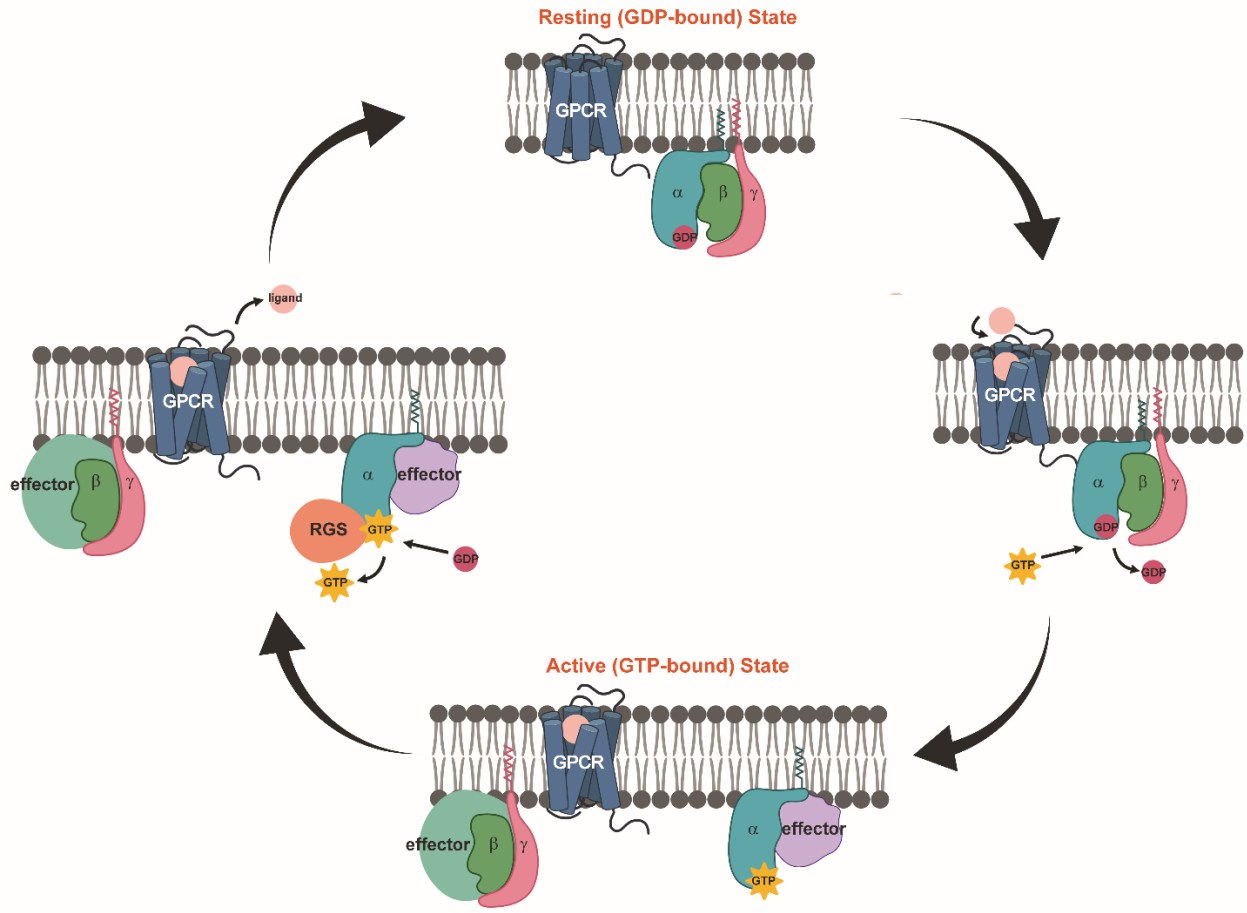

Figure 1.1. Schematic of GPCR-Activation/Deactivation Cycle.
In the inactive resting state, the heterotrimeric G protein subunits, Gα, Gβ, and Gγ interact, and the Gα subunit is bound to GDP. Upon ligand binding, the GPCR undergoes a conformational change, promoting the exchange of GDP for GTP on the Gα subunit. In the active GTP-bound state, Gα and Gβγ subunits dissociate and transmit signals by binding to effector molecules. The GPCR signal is terminated through the binding of RGS to the Gα subunit, and GTP is hydrolyzed to GDP. This results in the re-association of the Gα and Gβγ subunits.

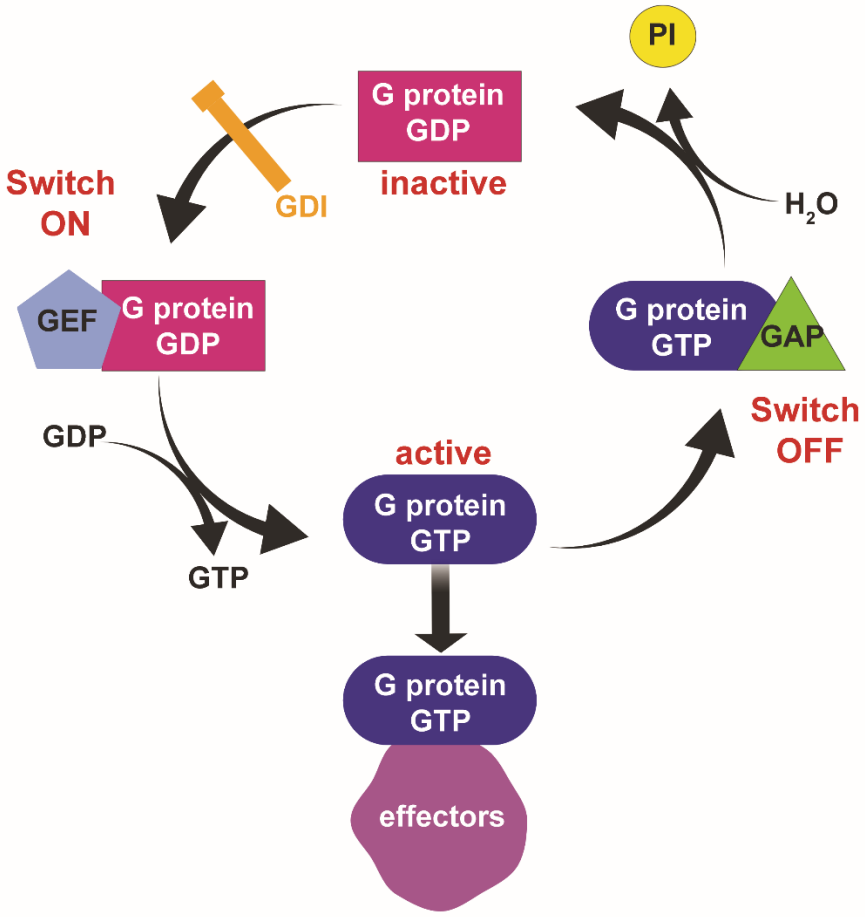

Figure 1.2. Model of GEF/GAP Regulation of G Proteins.
Guanine nucleotide exchange factors (GEFs) and GTPase-activating proteins (GAPs) regulate G proteins to control cellular functions. GEFs activate G proteins by exchanging GDP for GTP. Active G proteins interact with downstream effector molecules to initiate an array of signaling cascades. GEF activity is inhibited by guanine dissociation inhibitors (GDIs). GDIs bind GDP-bound GTPases and inhibit nucleotide exchange and/or sequester GTPases. G proteins are inactivated when GTPase-accelerating proteins (GAPs) stimulate the hydrolysis of the γ-phosphate of GTP.

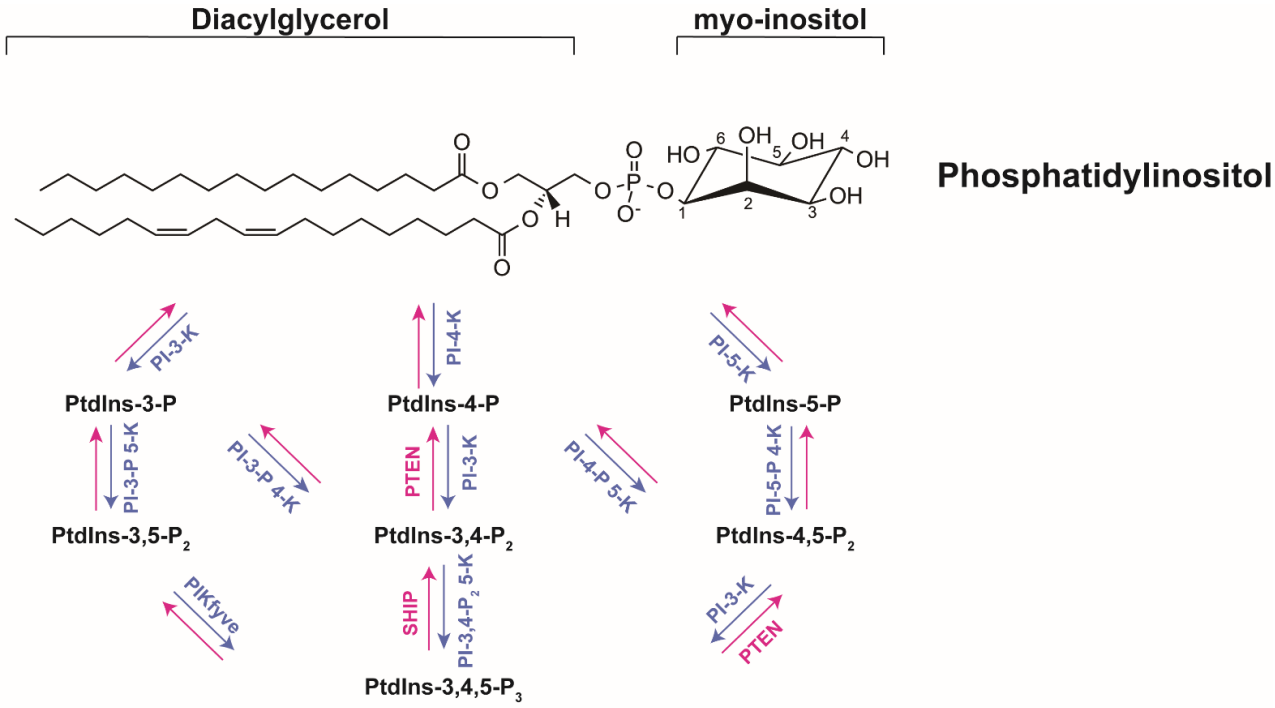

Figure 1.3. Phosphoinositide Metabolism.
Phosphatidylinositol is the precursor for all of the polyphosphoinositide derivatives and is composed of a diacylglycerol backbone attached to a myo-inositol ring. Phosphatidylinositol can be phosphorylated in different combinations by phosphoinositide 3-kinases (shown in purple) which recognize specific hydroxyl groups and transfer the γ-phosphate from ATP to the inositol ring. The removal of specific phosphate groups from the inositol ring is achieved through the lipid phosphatases, phosphatase and tensin homolog deleted on chromosome ten (PTEN) and SH2-containing inositol phosphatase (SHIP) (shown in hot pink).

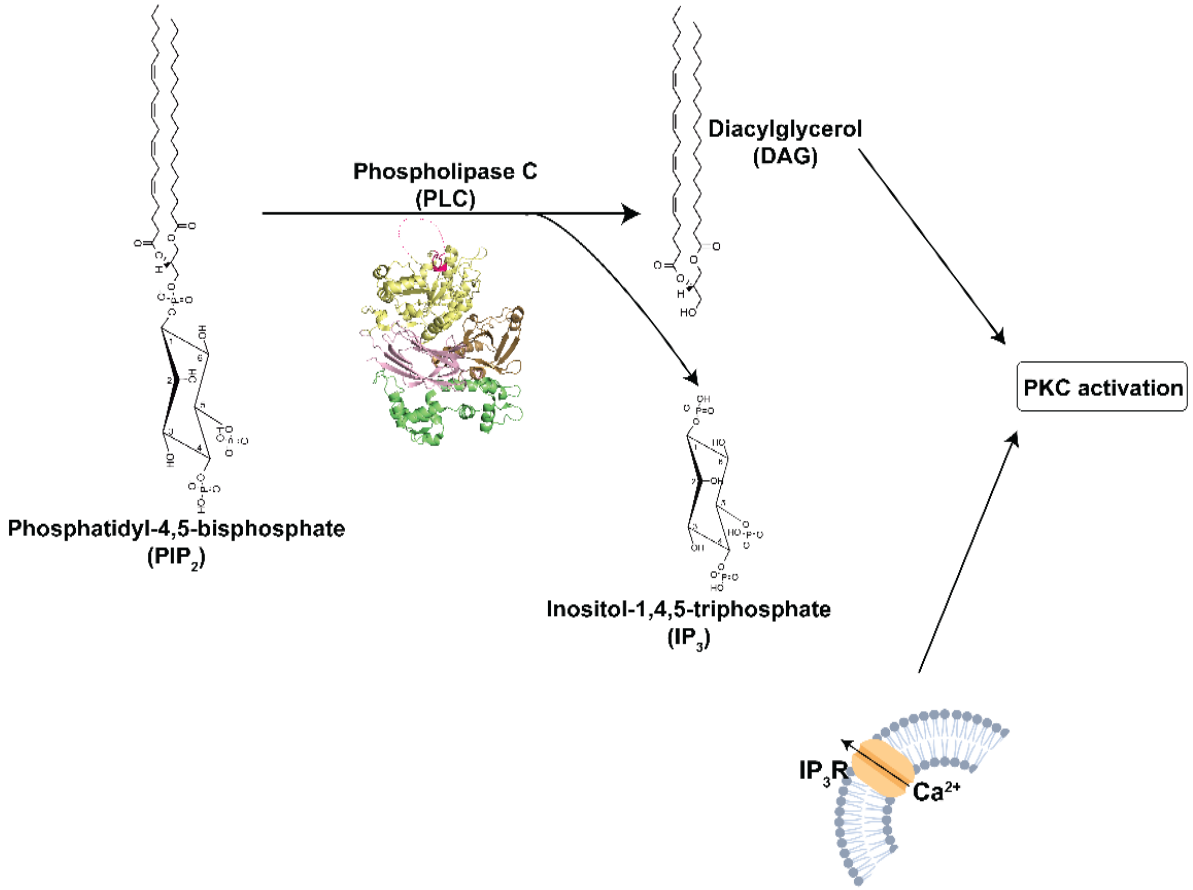

Figure 1.4. General Phospholipase C Enzyme Activity.
All phospholipase C (PLC) enzymes hydrolyze phosphatidylinositol-4,5-bisphosphate (PIP_2) into the two second messengers diacylglycerol (DAG) and inositol-1,4,5-triphosphate (IP_3). DAG remains in the membrane, while IP_3 binds to IP_3 receptors (IP_3R) in the endoplasmic reticulum. This increases intracellular Ca^{2+}, and together, the increase in intracellular Ca^{2+} and DAG activate protein kinase C (PKC). PKC can activate several pathways that are involved in cell proliferation, differentiation, and migration.

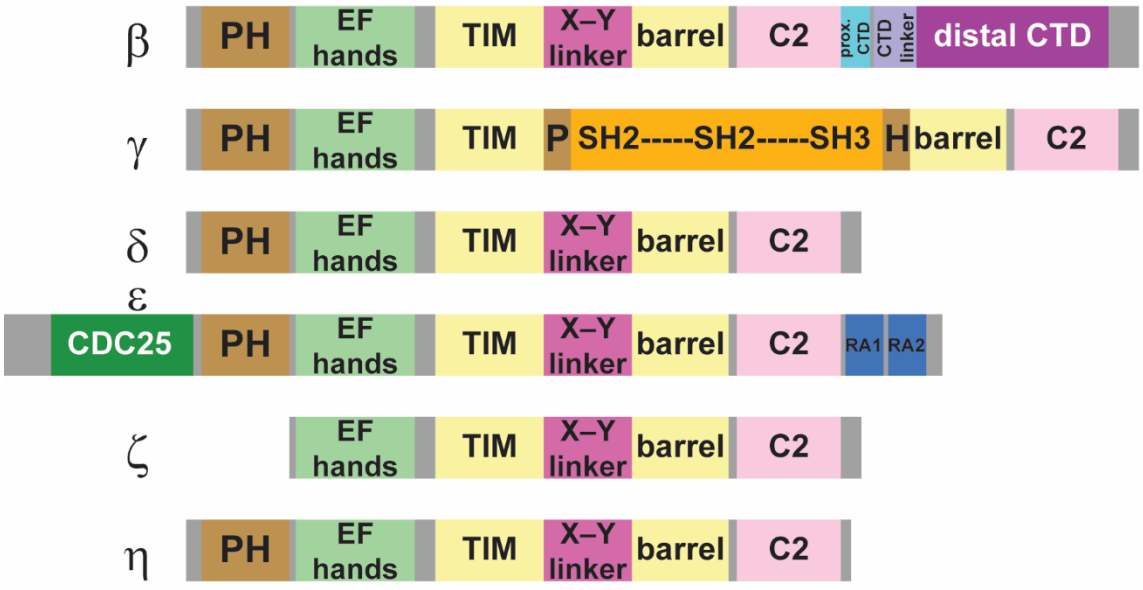

Figure 1.5. Domain Diagrams of Phospholipase C Subfamilies.
All phospholipase C (PLC) subfamilies, with the exception of PLCζ, contain a conserved catalytic core that consists of a pleckstrin homology (PH) domain, four tandem EF hands, a catalytic triose phosphate isomerase (TIM) barrel domain that is split into X and Y halves by the X−Y linker, and a C2 domain. Some subfamilies are flanked by additional domains that are important for regulation of the enzymes. The PLCβ subfamily contains a C-terminal extension that is subdivided into the proximal C-terminal domain (CTD), CTD linker, and distal CTD. This unique C-terminal extension plays a role in regulation, activity, and $G\alpha_q$-mediated activation. The PLCγ subfamily TIM barrel contains a PH domain split by Src-homology (SH) 2 and 3 domains that allow the protein to interact with phosphorylated residues on receptor tyrosine kinases. The PLCε subfamily has an N-terminal cysteine-rich domain and a CDC25 domain, which serves as a guanine nucleotide exchange factor. It also contains two C-terminal Ras association (RA) domains that are thought to be important for PLCε localization and activity.

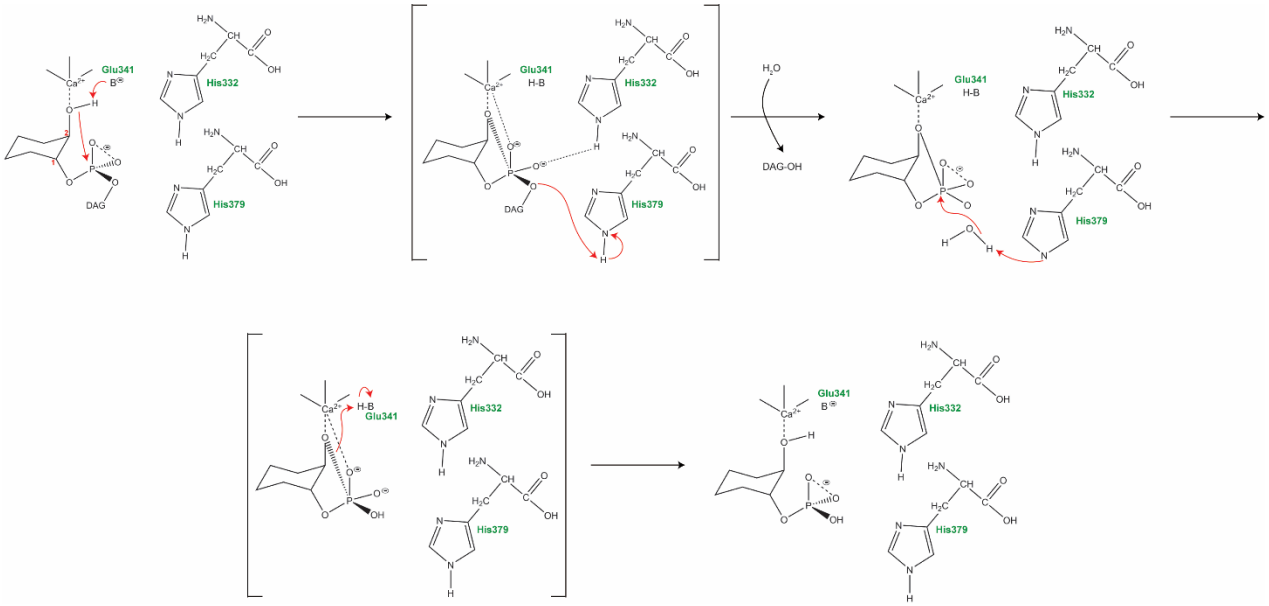

Figure 1.6. Proposed Phospholipase Cβ3 PIP_2 Hydrolysis Mechanism.
The catalytic Ca^{2+} lowers the pKa of the hydroxyl group on the second carbon of the inositol ring (2-hydroxyl). This facilitates the deprotonation of the 2-hydroxyl group by a putative base (Glu 341) before its nucleophilic attack on the 1-phosphate group, resulting in the formation of a 1,2-cyclic monophosphate intermediate and DAG. This intermediate is stabilized by His 332 and Ca^{2+}. In the next step, His 379 utilizes a proton from water to attack the intermediate resulting in the release of IP_3. The transition states for the first and second steps are indicated by brackets.

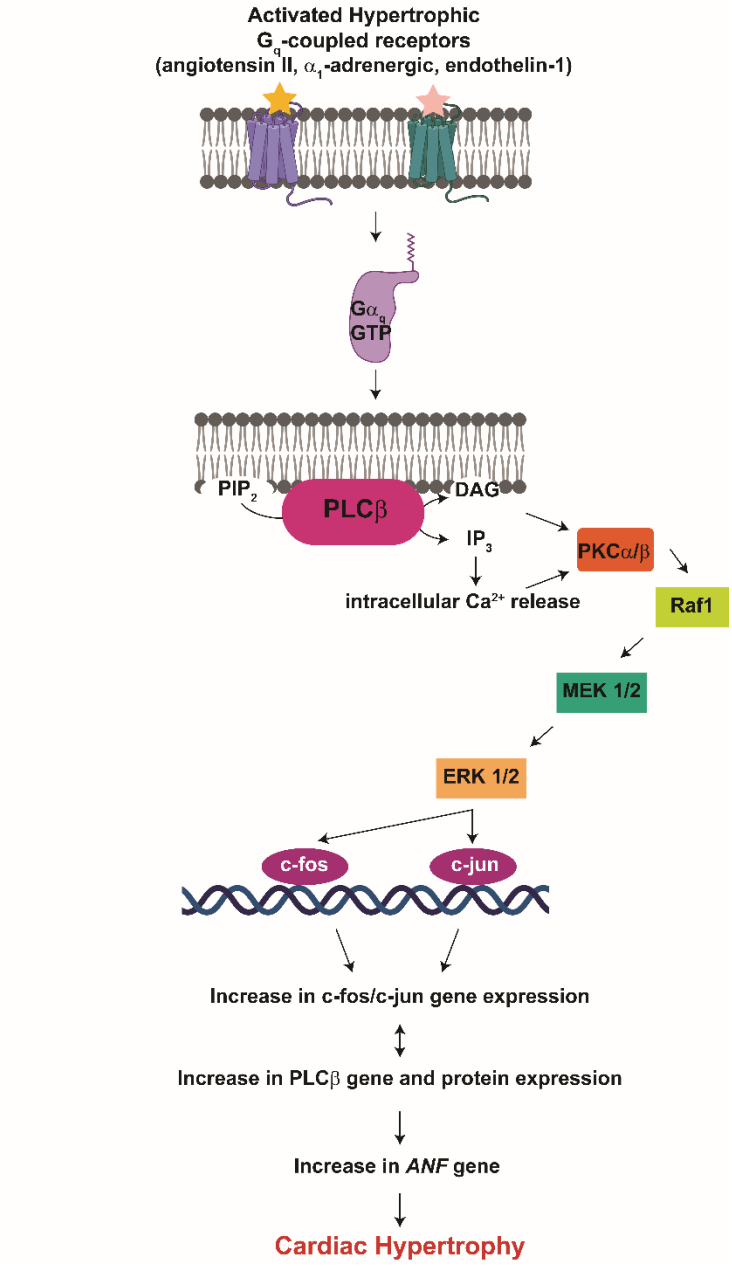

Figure 1.7. Proposed Phospholipase Cβ-Mediated Hypertrophic Pathway.
PLCβ enzymes are essential for normal cardiovascular function and increased protein expression or activity results in the onset and maintenance of cardiac arrhythmias, hypertrophy, and can eventually lead to heart failure. PLCβ has low basal activity and is located predominantly in the cytoplasm. Hypertrophic stimuli such as angiotensin, norepinephrine, and endothelin activate G_q-coupled receptors. Upon receptor activation, $G\alpha_q$ is activated and dissociates from the Gβγ heterodimer. $G\alpha_q$ then binds to PLCβ, increasing its lipase activity and intracellular Ca^{2+}. This results in the activation of PKCα and/or PKCβ. PKCα and/or PKCβ target and activate the Raf1-MEK 1/2-ERK 1/2 mitogen-activated protein cascade, which leads to the phosphorylation of the transcription factors c-fos, and c-jun. These transcription factors regulate several genes in the heart, including atrial natriuretic factor (ANF) and PLC isozymes. Cardiac hypertrophy is characterized by the re-expression of fetal genes like ANF. Thus, increases in PLCβ expression and activity and/or changes in flux through these pathways can result in alterations in cardiac shape and size, and eventually hypertrophy.

1.4 References

(1) Marinissen, M. J.; Gutkind, J. S. G-Protein-Coupled Receptors and Signaling Networks: Emerging Paradigms. *Trends Pharmacol. Sci.* **2001**, *22* (7), 368–376.

(2) Rohrer, D. K.; Kobilka, B. K. G Protein-Coupled Receptors: Functional and Mechanistic Insights through Altered Gene Expression. *Physiol. Rev.* **1998**, *78* (1), 35–52. https://doi.org/10.1152/physrev.1998.78.1.35.

(3) Stoy, H.; Gurevich, V. V. How Genetic Errors in GPCRs Affect Their Function: Possible Therapeutic Strategies. *Genes Dis.* **2015**, *2* (2), 108–132. https://doi.org/10.1016/j.gendis.2015.02.005.

(4) Insel, P. A.; Tang, C.-M.; Hahntow, I.; Michel, M. C. Impact of GPCRs in Clinical Medicine: Genetic Variants and Drug Targets. *Biochim. Biophys. Acta* **2007**, *1768* (4), 994–1005. https://doi.org/10.1016/j.bbamem.2006.09.029.

(5) Hauser, A. S.; Chavali, S.; Masuho, I.; Jahn, L. J.; Martemyanov, K. A.; Gloriam, D. E.; Babu, M. M. Pharmacogenomics of GPCR Drug Targets. *Cell* **2018**, *172* (1–2), 41-54.e19. https://doi.org/10.1016/j.cell.2017.11.033.

(6) Sriram, K.; Insel, P. A. G Protein-Coupled Receptors as Targets for Approved Drugs: How Many Targets and How Many Drugs? *Mol. Pharmacol.* **2018**, *93* (4), 251–258. https://doi.org/10.1124/mol.117.111062.

(7) Rosenbaum, D. M.; Rasmussen, S. G. F.; Kobilka, B. K. The Structure and Function of G-Protein-Coupled Receptors. *Nature* **2009**, *459* (7245), 356–363. https://doi.org/10.1038/nature08144.

(8) Fredriksson, R.; Lagerström, M. C.; Lundin, L.-G.; Schiöth, H. B. The G-Protein-Coupled Receptors in the Human Genome Form Five Main Families. Phylogenetic Analysis, Paralogon Groups, and Fingerprints. *Mol. Pharmacol.* **2003**, *63* (6), 1256–1272. https://doi.org/10.1124/mol.63.6.1256.

(9) Gilman, A. G. G Proteins: Transducers of Receptor-Generated Signals. *Annu. Rev. Biochem.* **1987**, *56*, 615–649. https://doi.org/10.1146/annurev.bi.56.070187.003151.

(10) Kaziro, Y.; Itoh, H.; Kozasa, T.; Nakafuku, M.; Satoh, T. Structure and Function of Signal-Transducing GTP-Binding Proteins. *Annu. Rev. Biochem.* **1991**, *60*, 349–400. https://doi.org/10.1146/annurev.bi.60.070191.002025.

(11) Simon, M. I.; Strathmann, M. P.; Gautam, N. Diversity of G Proteins in Signal Transduction. *Science* **1991**, *252* (5007), 802–808.

(12) Robishaw, J. D.; Berlot, C. H. Translating G Protein Subunit Diversity into Functional Specificity. *Curr. Opin. Cell Biol.* **2004**, *16* (2), 206–209. https://doi.org/10.1016/j.ceb.2004.02.007.

(13) Wettschureck, N.; Offermanns, S. Mammalian G Proteins and Their Cell Type Specific Functions. *Physiol. Rev.* **2005**, *85* (4), 1159–1204. https://doi.org/10.1152/physrev.00003.2005.

(14) Rhee, S. G.; Bae, Y. S. Regulation of Phosphoinositide-Specific Phospholipase C Isozymes. *J. Biol. Chem.* **1997**, *272* (24), 15045–15048.

(15) Kozasa, T.; Jiang, X.; Hart, M. J.; Sternweis, P. M.; Singer, W. D.; Gilman, A. G.; Bollag, G.; Sternweis, P. C. P115 RhoGEF, a GTPase Activating Protein for Galpha12 and Galpha13. *Science* **1998**, *280* (5372), 2109–2111.

(16) Smrcka, A. V. G Protein Bγ Subunits: Central Mediators of G Protein-Coupled Receptor Signaling. *Cell. Mol. Life Sci. CMLS* **2008**, *65* (14), 2191–2214. https://doi.org/10.1007/s00018-008-8006-5.

(17) Syrovatkina, V.; Alegre, K. O.; Dey, R.; Huang, X.-Y. Regulation, Signaling and Physiological Functions of G-Proteins. *J. Mol. Biol.* **2016**, *428* (19), 3850–3868. https://doi.org/10.1016/j.jmb.2016.08.002.

(18) Rajagopal, S.; Shenoy, S. K. GPCR Desensitization: Acute and Prolonged Phases. *Cell. Signal.* **2018**, *41*, 9–16. https://doi.org/10.1016/j.cellsig.2017.01.024.

(19) Gainetdinov, R. R.; Premont, R. T.; Bohn, L. M.; Lefkowitz, R. J.; Caron, M. G. Desensitization of G Protein-Coupled Receptors and Neuronal Functions. *Annu. Rev. Neurosci.* **2004**, *27*, 107–144. https://doi.org/10.1146/annurev.neuro.27.070203.144206.

(20) Eichel, K.; von Zastrow, M. Subcellular Organization of GPCR Signaling. *Trends Pharmacol. Sci.* **2018**, *39* (2), 200–208. https://doi.org/10.1016/j.tips.2017.11.009.

(21) Yang, Z.; Yang, F.; Zhang, D.; Liu, Z.; Lin, A.; Liu, C.; Xiao, P.; Yu, X.; Sun, J.-P. Phosphorylation of G Protein-Coupled Receptors: From the Barcode Hypothesis to the Flute Model. *Mol. Pharmacol.* **2017**, *92* (3), 201–210. https://doi.org/10.1124/mol.116.107839.

(22) Payrastre, B.; Missy, K.; Giuriato, S.; Bodin, S.; Plantavid, M.; Gratacap, M. Phosphoinositides: Key Players in Cell Signalling, in Time and Space. *Cell. Signal.* **2001**, *13* (6), 377–387.

(23) Balla, T. Phosphoinositides: Tiny Lipids with Giant Impact on Cell Regulation. *Physiol. Rev.* **2013**, *93* (3), 1019–1137. https://doi.org/10.1152/physrev.00028.2012.

(24) Viaud, J.; Lagarrigue, F.; Ramel, D.; Allart, S.; Chicanne, G.; Ceccato, L.; Courilleau, D.; Xuereb, J.-M.; Pertz, O.; Payrastre, B.; et al. Phosphatidylinositol 5-Phosphate Regulates Invasion through Binding and Activation of Tiam1. *Nat. Commun.* **2014**, *5*, 4080. https://doi.org/10.1038/ncomms5080.

(25) Godi, A.; Di Campli, A.; Konstantakopoulos, A.; Di Tullio, G.; Alessi, D. R.; Kular, G. S.; Daniele, T.; Marra, P.; Lucocq, J. M.; De Matteis, M. A. FAPPs Control Golgi-to-Cell-Surface Membrane Traffic by Binding to ARF and PtdIns(4)P. *Nat. Cell Biol.* **2004**, *6* (5), 393–404. https://doi.org/10.1038/ncb1119.

(26) Suh, B.-C.; Hille, B. PIP2 Is a Necessary Cofactor for Ion Channel Function: How and Why? *Annu. Rev. Biophys.* **2008**, *37*, 175–195. https://doi.org/10.1146/annurev.biophys.37.032807.125859.

(27) Lahiri, S.; Toulmay, A.; Prinz, W. A. Membrane Contact Sites, Gateways for Lipid Homeostasis. *Curr. Opin. Cell Biol.* **2015**, *33*, 82–87. https://doi.org/10.1016/j.ceb.2014.12.004.

(28) Kim, Y. J.; Guzman-Hernandez, M. L.; Wisniewski, E.; Echeverria, N.; Balla, T. Phosphatidylinositol and Phosphatidic Acid Transport between the ER and Plasma Membrane during PLC Activation Requires the Nir2 Protein. *Biochem. Soc. Trans.* **2016**, *44* (1), 197–201. https://doi.org/10.1042/BST20150187.

(29) Falkenburger, B. H.; Jensen, J. B.; Dickson, E. J.; Suh, B.-C.; Hille, B. Phosphoinositides: Lipid Regulators of Membrane Proteins. *J. Physiol.* **2010**, *588* (Pt 17), 3179–3185. https://doi.org/10.1113/jphysiol.2010.192153.

(30) Leslie, N. R.; Downes, C. P. PTEN: The down Side of PI 3-Kinase Signalling. *Cell. Signal.* **2002**, *14* (4), 285–295.

(31) Lemmon, M. A. Phosphoinositide Recognition Domains. *Traffic Cph. Den.* **2003**, *4* (4), 201–213.

(32) Vanhaesebroeck, B.; Leevers, S. J.; Ahmadi, K.; Timms, J.; Katso, R.; Driscoll, P. C.; Woscholski, R.; Parker, P. J.; Waterfield, M. D. Synthesis and Function of 3-Phosphorylated Inositol Lipids. *Annu. Rev. Biochem.* **2001**, *70*, 535–602. https://doi.org/10.1146/annurev.biochem.70.1.535.

(33) Brown, J. R.; Auger, K. R. Phylogenomics of Phosphoinositide Lipid Kinases: Perspectives on the Evolution of Second Messenger Signaling and Drug Discovery. *BMC Evol. Biol.* **2011**, *11*, 4. https://doi.org/10.1186/1471-2148-11-4.

(34) Jean, S.; Kiger, A. A. Classes of Phosphoinositide 3-Kinases at a Glance. *J. Cell Sci.* **2014**, *127* (5), 923–928. https://doi.org/10.1242/jcs.093773.

(35) Billcliff, P. G.; Lowe, M. Inositol Lipid Phosphatases in Membrane Trafficking and Human Disease. *Biochem. J.* **2014**, *461* (2), 159–175. https://doi.org/10.1042/BJ20140361.

(36) Paolo, G. D.; Camilli, P. D. Phosphoinositides in Cell Regulation and Membrane Dynamics. *Nature* **2006**, *443* (7112), 651. https://doi.org/10.1038/nature05185.

(37) Lietzke, S. E.; Bose, S.; Cronin, T.; Klarlund, J.; Chawla, A.; Czech, M. P.; Lambright, D. G. Structural Basis of 3-Phosphoinositide Recognition by Pleckstrin Homology Domains. *Mol. Cell* **2000**, *6* (2), 385–394.

(38) Neumann, S.; Schmid, S. L. Dual Role of BAR Domain-Containing Proteins in Regulating Vesicle Release Catalyzed by the GTPase, Dynamin-2. *J. Biol. Chem.* **2013**, *288* (35), 25119–25128. https://doi.org/10.1074/jbc.M113.490474.

(39) Hancock, J. F. Lipid Rafts: Contentious Only from Simplistic Standpoints. *Nat. Rev. Mol. Cell Biol.* **2006**, *7* (6), 456–462. https://doi.org/10.1038/nrm1925.

(40) Brown, D. A.; London, E. Functions of Lipid Rafts in Biological Membranes. *Annu. Rev. Cell Dev. Biol.* **1998**, *14*, 111–136. https://doi.org/10.1146/annurev.cellbio.14.1.111.

(41) Koushik, A. B.; Powell, R. R.; Temesvari, L. A. Localization of Phosphatidylinositol 4,5-Bisphosphate to Lipid Rafts and Uroids in the Human Protozoan Parasite Entamoeba Histolytica. *Infect. Immun.* **2013**, *81* (6), 2145–2155. https://doi.org/10.1128/IAI.00040-13.

(42) Brown, D. A.; Rose, J. K. Sorting of GPI-Anchored Proteins to Glycolipid-Enriched Membrane Subdomains during Transport to the Apical Cell Surface. *Cell* **1992**, *68* (3), 533–544.

(43) London, E.; Brown, D. A. Insolubility of Lipids in Triton X-100: Physical Origin and Relationship to Sphingolipid/Cholesterol Membrane Domains (Rafts). *Biochim. Biophys. Acta* **2000**, *1508* (1–2), 182–195.

(44) Brown, D. A.; London, E. Structure of Detergent-Resistant Membrane Domains: Does Phase Separation Occur in Biological Membranes? *Biochem. Biophys. Res. Commun.* **1997**, *240* (1), 1–7. https://doi.org/10.1006/bbrc.1997.7575.

(45) Gao, X.; Lowry, P. R.; Zhou, X.; Depry, C.; Wei, Z.; Wong, G. W.; Zhang, J. PI3K/Akt Signaling Requires Spatial Compartmentalization in Plasma Membrane Microdomains. *Proc. Natl. Acad. Sci. U. S. A.* **2011**, *108* (35), 14509–14514. https://doi.org/10.1073/pnas.1019386108.

(46) Huang, K.-P. The Mechanism of Protein Kinase C Activation. *Trends Neurosci.* **1989**, *12* (11), 425–432. https://doi.org/10.1016/0166-2236(89)90091-X.

(47) Lipp, P.; Reither, G. Protein Kinase C: The "Masters" of Calcium and Lipid. *Cold Spring Harb. Perspect. Biol.* **2011**, *3* (7). https://doi.org/10.1101/cshperspect.a004556.

(48) Spitaler, M.; Cantrell, D. A. Protein Kinase C and Beyond. *Nat. Immunol.* **2004**, *5* (8), 785. https://doi.org/10.1038/ni1097.

(49) Land, M.; Rubin, C. S. A Calcium- and Diacylglycerol-Stimulated Protein Kinase C (PKC), Caenorhabditis Elegans PKC-2, Links Thermal Signals to Learned Behavior by Acting in Sensory Neurons and Intestinal Cells. *Mol. Cell. Biol.* **2017**, *37* (19), e00192-17. https://doi.org/10.1128/MCB.00192-17.

(50) Newton, A. C. Protein Kinase C: Structure, Function, and Regulation. *J. Biol. Chem.* **1995**, *270* (48), 28495–28498. https://doi.org/10.1074/jbc.270.48.28495.

(51) Gresset, A.; Sondek, J.; Harden, T. K. The Phospholipase C Isozymes and Their Regulation. *Subcell. Biochem.* **2012**, *58*, 61–94. https://doi.org/10.1007/978-94-007-3012-0_3.

(52) Kadamur, G.; Ross, E. M. Mammalian Phospholipase C. *Annu. Rev. Physiol.* **2013**, *75* (1), 127–154. https://doi.org/10.1146/annurev-physiol-030212-183750.

(53) Katan, M.; Williams, R. L. Phosphoinositide-Specific Phospholipase C: Structural Basis for Catalysis and Regulatory Interactions. *Semin. Cell Dev. Biol.* **1997**, *8* (3), 287–296. https://doi.org/10.1006/scdb.1997.0150.

(54) Essen, L. O.; Perisic, O.; Cheung, R.; Katan, M.; Williams, R. L. Crystal Structure of a Mammalian Phosphoinositide-Specific Phospholipase C Delta. *Nature* **1996**, *380* (6575), 595–602. https://doi.org/10.1038/380595a0.

(55) Falasca, M.; Logan, S. K.; Lehto, V. P.; Baccante, G.; Lemmon, M. A.; Schlessinger, J. Activation of Phospholipase C Gamma by PI 3-Kinase-Induced PH Domain-Mediated Membrane Targeting. *EMBO J.* **1998**, *17* (2), 414–422. https://doi.org/10.1093/emboj/17.2.414.

(56) Singh, S. M.; Murray, D. Molecular Modeling of the Membrane Targeting of Phospholipase C Pleckstrin Homology Domains. *Protein Sci. Publ. Protein Soc.* **2003**, *12* (9), 1934–1953. https://doi.org/10.1110/ps.0358803.

(57) Tall, E.; Dormán, G.; Garcia, P.; Runnels, L.; Shah, S.; Chen, J.; Profit, A.; Gu, Q. M.; Chaudhary, A.; Prestwich, G. D.; et al. Phosphoinositide Binding Specificity among Phospholipase C Isozymes as Determined by Photo-Cross-Linking to Novel Substrate and Product Analogs. *Biochemistry* **1997**, *36* (23), 7239–7248. https://doi.org/10.1021/bi9702288.

(58) Wang, T.; Pentyala, S.; Rebecchi, M. J.; Scarlata, S. Differential Association of the Pleckstrin Homology Domains of Phospholipases C-Beta 1, C-Beta 2, and C-Delta 1 with Lipid Bilayers and the Beta Gamma Subunits of Heterotrimeric G Proteins. *Biochemistry* **1999**, *38* (5), 1517–1524. https://doi.org/10.1021/bi982008f.

(59) Illenberger, D.; Walliser, C.; Nurnberg, B.; Diaz Lorente, M.; Gierschik, P. Specificity and Structural Requirements of Phospholipase C-Beta Stimulation by Rho GTPases versus G Protein Beta Gamma Dimers. *J. Biol. Chem.* **2003**, *278* (5), 3006–3014. https://doi.org/10.1074/jbc.M208282200.

(60) Kawasaki, H.; Kretsinger, R. H. Calcium-Binding Proteins. 1: EF-Hands. *Protein Profile* **1994**, *1* (4), 343–517.

(61) Lyon, A. M.; Tesmer, J. J. G. Structural Insights into Phospholipase C-β Function. *Mol. Pharmacol.* **2013**, *84* (4), 488–500. https://doi.org/10.1124/mol.113.087403.

(62) Essen, L. O.; Perisic, O.; Katan, M.; Wu, Y.; Roberts, M. F.; Williams, R. L. Structural Mapping of the Catalytic Mechanism for a Mammalian Phosphoinositide-Specific Phospholipase C. *Biochemistry* **1997**, *36* (7), 1704–1718. https://doi.org/10.1021/bi962512p.

(63) Ellis, M. V.; James, S. R.; Perisic, O.; Downes, C. P.; Williams, R. L.; Katan, M. Catalytic Domain of Phosphoinositide-Specific Phospholipase C (PLC). Mutational Analysis of Residues within the Active Site and Hydrophobic Ridge of Plcdelta1. *J. Biol. Chem.* **1998**, *273* (19), 11650–11659.

(64) Lyon, A. M.; Dutta, S.; Boguth, C. A.; Skiniotis, G.; Tesmer, J. J. G. Full-Length Gαq–Phospholipase C-B3 Structure Reveals Interfaces of the C-Terminal Coiled-Coil Domain. *Nat. Struct. Mol. Biol.* **2013**, *20* (3), 355–362. https://doi.org/10.1038/nsmb.2497.

(65) James, S. R.; Paterson, A.; Harden, T. K.; Demel, R. A.; Downes, C. P. Dependence of the Activity of Phospholipase Cβ on Surface Pressure and Surface Composition in Phospholipid Monolayers and Its Implications for Their Regulation. *Biochemistry* **1997**, *36* (4), 848–855. https://doi.org/10.1021/bi962108q.

(66) Ryu, S. H.; Suh, P. G.; Cho, K. S.; Lee, K. Y.; Rhee, S. G. Bovine Brain Cytosol Contains Three Immunologically Distinct Forms of Inositolphospholipid-Specific Phospholipase C. *Proc. Natl. Acad. Sci. U. S. A.* **1987**, *84* (19), 6649–6653. https://doi.org/10.1073/pnas.84.19.6649.

(67) Smrcka, A. V. Regulation of Phosphatidylinositol-Specific Phospholipase C at the Nuclear Envelope in Cardiac Myocytes. *J. Cardiovasc. Pharmacol.* **2015**, *65* (3), 203–210. https://doi.org/10.1097/FJC.0000000000000195.

(68) Malik, S.; deRubio, R. G.; Trembley, M.; Irannejad, R.; Wedegaertner, P. B.; Smrcka, A. V. G Protein Bγ Subunits Regulate Cardiomyocyte Hypertrophy through a Perinuclear Golgi Phosphatidylinositol 4-Phosphate Hydrolysis Pathway. *Mol. Biol. Cell* **2015**, *26* (6), 1188–1198. https://doi.org/10.1091/mbc.E14-10-1476.

(69) Hicks, S. N.; Jezyk, M. R.; Gershburg, S.; Seifert, J. P.; Harden, T. K.; Sondek, J. General and Versatile Autoinhibition of PLC Isozymes. *Mol. Cell* **2008**, *31* (3), 383–394. https://doi.org/10.1016/j.molcel.2008.06.018.

(70) Horstman, D. A.; Chattopadhyay, A.; Carpenter, G. The Influence of Deletion Mutations on Phospholipase C-Gamma 1 Activity. *Arch. Biochem. Biophys.* **1999**, *361* (1), 149–155. https://doi.org/10.1006/abbi.1998.0978.

(71) Lyon, A. M.; Begley, J. A.; Manett, T. D.; Tesmer, J. J. G. Molecular Mechanisms of PLCβ3 Autoinhibition. *Struct. Lond. Engl. 1993* **2014**, *22* (12), 1844–1854. https://doi.org/10.1016/j.str.2014.10.008.

(72) Nomikos, M.; Elgmati, K.; Theodoridou, M.; Georgilis, A.; Gonzalez-Garcia, J. R.; Nounesis, G.; Swann, K.; Lai, F. A. Novel Regulation of PLCζ Activity via Its XY-Linker. *Biochem. J.* **2011**, *438* (3), 427–432. https://doi.org/10.1042/BJ20110953.

(73) Waldo, G. L.; Ricks, T. K.; Hicks, S. N.; Cheever, M. L.; Kawano, T.; Tsuboi, K.; Wang, X.; Montell, C.; Kozasa, T.; Sondek, J.; et al. Kinetic Scaffolding Mediated by a Phospholipase C–β and Gq Signaling Complex. *Science* **2010**, *330* (6006), 974–980. https://doi.org/10.1126/science.1193438.

(74) Homma, Y.; Takenawa, T.; Emori, Y.; Sorimachi, H.; Suzuki, K. Tissue- and Cell Type-Specific Expression of MRNAs for Four Types of Inositol Phospholipid-Specific Phospholipase C. *Biochem. Biophys. Res. Commun.* **1989**, *164* (1), 406–412.

(75) Ji, Q.; Winnier, G. E.; Niswender, K. D.; Horstman, D.; Wisdom, R.; Magnuson, M. A.; Carpenter, G. Essential Role of the Tyrosine Kinase Substrate Phospholipase C-Γ1 in Mammalian Growth and Development. *Proc. Natl. Acad. Sci. U. S. A.* **1997**, *94* (7), 2999–3003.

(76) Liao, H.-J.; Kume, T.; McKay, C.; Xu, M.-J.; Ihle, J. N.; Carpenter, G. Absence of Erythrogenesis and Vasculogenesis in Plcg1-Deficient Mice. *J. Biol. Chem.* **2002**, *277* (11), 9335–9341. https://doi.org/10.1074/jbc.M109955200.

(77) Wang, D.; Feng, J.; Wen, R.; Marine, J. C.; Sangster, M. Y.; Parganas, E.; Hoffmeyer, A.; Jackson, C. W.; Cleveland, J. L.; Murray, P. J.; et al. Phospholipase Cgamma2 Is Essential in the Functions of B Cell and Several Fc Receptors. *Immunity* **2000**, *13* (1), 25–35.

(78) Hubbard, S. R.; Till, J. H. Protein Tyrosine Kinase Structure and Function. *Annu. Rev. Biochem.* **2000**, *69*, 373–398. https://doi.org/10.1146/annurev.biochem.69.1.373.

(79) Bae, Y. S.; Cantley, L. G.; Chen, C. S.; Kim, S. R.; Kwon, K. S.; Rhee, S. G. Activation of Phospholipase C-Gamma by Phosphatidylinositol 3,4,5-Trisphosphate. *J. Biol. Chem.* **1998**, *273* (8), 4465–4469. https://doi.org/10.1074/jbc.273.8.4465.

(80) Harden, T. K.; Sondek, J. Regulation of Phospholipase C Isozymes by Ras Superfamily GTPases. *Annu. Rev. Pharmacol. Toxicol.* **2006**, *46*, 355–379. https://doi.org/10.1146/annurev.pharmtox.46.120604.141223.

(81) Stallings, J. D.; Tall, E. G.; Pentyala, S.; Rebecchi, M. J. Nuclear Translocation of Phospholipase C-Delta1 Is Linked to the Cell Cycle and Nuclear Phosphatidylinositol 4,5-Bisphosphate. *J. Biol. Chem.* **2005**, *280* (23), 22060–22069. https://doi.org/10.1074/jbc.M413813200.

(82) Shimohama, S.; Homma, Y.; Suenaga, T.; Fujimoto, S.; Taniguchi, T.; Araki, W.; Yamaoka, Y.; Takenawa, T.; Kimura, J. Aberrant Accumulation of Phospholipase C-Delta in Alzheimer Brains. *Am. J. Pathol.* **1991**, *139* (4), 737–742.

(83) Stauffer, T. P.; Ahn, S.; Meyer, T. Receptor-Induced Transient Reduction in Plasma Membrane PtdIns(4,5)P2 Concentration Monitored in Living Cells. *Curr. Biol. CB* **1998**, *8* (6), 343–346.

(84) Raucher, D.; Stauffer, T.; Chen, W.; Shen, K.; Guo, S.; York, J. D.; Sheetz, M. P.; Meyer, T. Phosphatidylinositol 4,5-Bisphosphate Functions as a Second Messenger That Regulates Cytoskeleton-Plasma Membrane Adhesion. *Cell* **2000**, *100* (2), 221–228.

(85) Kelley, G. G.; Reks, S. E.; Ondrako, J. M.; Smrcka, A. V. Phospholipase C(Epsilon): A Novel Ras Effector. *EMBO J.* **2001**, *20* (4), 743–754. https://doi.org/10.1093/emboj/20.4.743.

(86) Boguski, M. S.; McCormick, F. Proteins Regulating Ras and Its Relatives. *Nature* **1993**, *366* (6456), 643–654. https://doi.org/10.1038/366643a0.

(87) Song, C.; Hu, C. D.; Masago, M.; Kariyai, K.; Yamawaki-Kataoka, Y.; Shibatohge, M.; Wu, D.; Satoh, T.; Kataoka, T. Regulation of a Novel Human Phospholipase C, PLCepsilon, through Membrane Targeting by Ras. *J. Biol. Chem.* **2001**, *276* (4), 2752–2757. https://doi.org/10.1074/jbc.M008324200.

(88) Lopez, I.; Mak, E. C.; Ding, J.; Hamm, H. E.; Lomasney, J. W. A Novel Bifunctional Phospholipase c That Is Regulated by Galpha 12 and Stimulates the Ras/Mitogen-Activated Protein Kinase Pathway. *J. Biol. Chem.* **2001**, *276* (4), 2758–2765. https://doi.org/10.1074/jbc.M008119200.

(89) Jin, J.; Lian, T.; Gu, C.; Yu, K.; Gao, Y. Q.; Su, X.-D. The Effects of Cytosine Methylation on General Transcription Factors. *Sci. Rep.* **2016**, *6*. https://doi.org/10.1038/srep29119.

(90) Saunders, C. M.; Larman, M. G.; Parrington, J.; Cox, L. J.; Royse, J.; Blayney, L. M.; Swann, K.; Lai, F. A. PLC Zeta: A Sperm-Specific Trigger of Ca(2+) Oscillations in Eggs and Embryo Development. *Dev. Camb. Engl.* **2002**, *129* (15), 3533–3544.

(91) Kouchi, Z.; Shikano, T.; Nakamura, Y.; Shirakawa, H.; Fukami, K.; Miyazaki, S. The Role of EF-Hand Domains and C2 Domain in Regulation of Enzymatic Activity of Phospholipase Czeta. *J. Biol. Chem.* **2005**, *280* (22), 21015–21021. https://doi.org/10.1074/jbc.M412123200.

(92) Kashir, J.; Jones, C.; Lee, H. C.; Rietdorf, K.; Nikiforaki, D.; Durrans, C.; Ruas, M.; Tee, S. T.; Heindryckx, B.; Galione, A.; et al. Loss of Activity Mutations in Phospholipase C Zeta (PLCζ) Abolishes Calcium Oscillatory Ability of Human Recombinant Protein in Mouse Oocytes. *Hum. Reprod. Oxf. Engl.* **2011**, *26* (12), 3372–3387. https://doi.org/10.1093/humrep/der336.

(93) Zhou, Y.; Wing, M. R.; Sondek, J.; Harden, T. K. Molecular Cloning and Characterization of PLC-Eta2. *Biochem. J.* **2005**, *391* (Pt 3), 667–676. https://doi.org/10.1042/BJ20050839.

(94) Nakahara, M.; Shimozawa, M.; Nakamura, Y.; Irino, Y.; Morita, M.; Kudo, Y.; Fukami, K. A Novel Phospholipase C, PLC(Eta)2, Is a Neuron-Specific Isozyme. *J. Biol. Chem.* **2005**, *280* (32), 29128–29134. https://doi.org/10.1074/jbc.M503817200.

(95) Park, D.; Jhon, D. Y.; Lee, C. W.; Lee, K. H.; Rhee, S. G. Activation of Phospholipase C Isozymes by G Protein Beta Gamma Subunits. *J. Biol. Chem.* **1993**, *268* (7), 4573–4576.

(96) Schnabel, P.; Camps, M.; Carozzi, A.; Parker, P. J.; Gierschik, P. Mutational Analysis of Phospholipase C-B2. *Eur. J. Biochem.* **1993**, *217* (3), 1109–1115. https://doi.org/10.1111/j.1432-1033.1993.tb18343.x.

(97) Kim, C. G.; Park, D.; Rhee, S. G. The Role of Carboxyl-Terminal Basic Amino Acids in Gqα-Dependent Activation, Particulate Association, and Nuclear Localization of Phospholipase C-B1. *J. Biol. Chem.* **1996**, *271* (35), 21187–21192. https://doi.org/10.1074/jbc.271.35.21187.

(98) Jenco, J. M.; Becker, K. P.; Morris, A. J. Membrane-Binding Properties of Phospholipase C-Beta1 and PhospholipaseC-Beta2: Role of the C-Terminus and Effects of Polyphosphoinositides, G-Proteins and Ca2+. *Biochem. J.* **1997**, *327* (Pt 2), 431–437.

(99) Adjobo-Hermans, M. J. W.; Goedhart, J.; Gadella, T. W. J. Regulation of PLCβ1a Membrane Anchoring by Its Substrate Phosphatidylinositol (4,5)-Bisphosphate. *J. Cell Sci.* **2008**, *121* (22), 3770–3777. https://doi.org/10.1242/jcs.029785.

(100) Lyon, A. M.; Tesmer, V. M.; Dhamsania, V. D.; Thal, D. M.; Gutierrez, J.; Chowdhury, S.; Suddala, K. C.; Northup, J. K.; Tesmer, J. J. G. An Autoinhibitory Helix in the C-Terminal Region of Phospholipase C-β Mediates Gαq Activation. *Nat. Struct. Mol. Biol.* **2011**, *18* (9), 999–1005. https://doi.org/10.1038/nsmb.2095.

(101) Lee, S. B.; Shin, S. H.; Hepler, J. R.; Gilman, A. G.; Rhee, S. G. Activation of Phospholipase C-Beta 2 Mutants by G Protein Alpha q and Beta Gamma Subunits. *J. Biol. Chem.* **1993**, *268* (34), 25952–25957.

(102) Wu, D.; Katz, A.; Lee, C. H.; Simon, M. I. Activation of Phospholipase C by Alpha 1-Adrenergic Receptors Is Mediated by the Alpha Subunits of Gq Family. *J. Biol. Chem.* **1992**, *267* (36), 25798–25802.

(103) Kim, D.; Jun, K. S.; Lee, S. B.; Kang, N. G.; Min, D. S.; Kim, Y. H.; Ryu, S. H.; Suh, P. G.; Shin, H. S. Phospholipase C Isozymes Selectively Couple to Specific Neurotransmitter Receptors. *Nature* **1997**, *389* (6648), 290–293. https://doi.org/10.1038/38508.

(104) Descorbeth, M.; Anand-Srivastava, M. B. Role of Growth Factor Receptor Transactivation in High Glucose-Induced Increased Levels of Gq/11alpha and Signaling in Vascular Smooth Muscle Cells. *J. Mol. Cell. Cardiol.* **2010**, *49* (2), 221–233. https://doi.org/10.1016/j.yjmcc.2009.12.010.

(105) Mao, G. F.; Kunapuli, S. P.; Koneti Rao, A. Evidence for Two Alternatively Spliced Forms of Phospholipase C-Beta2 in Haematopoietic Cells. *Br. J. Haematol.* **2000**, *110* (2), 402–408.

(106) Sun, L.; Mao, G.; Kunapuli, S. P.; Dhanasekaran, D. N.; Rao, A. K. Alternative Splice Variants of Phospholipase C-Beta2 Are Expressed in Platelets: Effect on Galphaq-Dependent Activation and Localization. *Platelets* **2007**, *18* (3), 217–223. https://doi.org/10.1080/09537100601016133.

(107) Suh, P.-G.; *; Park, J.-I.; Manzoli, L.; Cocco, L.; Peak, J. C.; Katan, M.; Fukami, K.; Kataoka, T.; Ryu, S. Y. & S. H. Multiple Roles of Phosphoinositide-Specific Phospholipase C Isozymes. *BMB Rep.* **2008**, *41* (6), 415–434.

(108) Vaidyula, V. R.; Rao, A. K. Role of Galphaq and Phospholipase C-Beta2 in Human Platelets Activation by Thrombin Receptors PAR1 and PAR4: Studies in Human Platelets Deficient in Galphaq and Phospholipase C-Beta2. *Br. J. Haematol.* **2003**, *121* (3), 491–496.

(109) Bianchi, E.; Norcini, M.; Smrcka, A.; Ghelardini, C. Supraspinal Gβγ-Dependent Stimulation of PLCβ3 Originating from G Inhibitory Protein-μ Opioid Receptor-Coupling Is Necessary for Morphine Induced Acute Hyperalgesia. *J. Neurochem.* **2009**, *111* (1), 171–180. https://doi.org/10.1111/j.1471-4159.2009.06308.x.

(110) Xiao, W.; Hong, H.; Kawakami, Y.; Kato, Y.; Wu, D.; Yasudo, H.; Kimura, A.; Kubagawa, H.; Bertoli, L. F.; Davis, R. S.; et al. Tumor Suppression by Phospholipase C-Beta3 via SHP-1-Mediated Dephosphorylation of Stat5. *Cancer Cell* **2009**, *16* (2), 161–171. https://doi.org/10.1016/j.ccr.2009.05.018.

(111) Mende, U.; Kagen, A.; Meister, M.; Neer, E. J. Signal Transduction in Atria and Ventricles of Mice with Transient Cardiac Expression of Activated G Protein Alpha(q). *Circ. Res.* **1999**, *85* (11), 1085–1091.

(112) Arthur, J. F.; Matkovich, S. J.; Mitchell, C. J.; Biden, T. J.; Woodcock, E. A. Evidence for Selective Coupling of Alpha 1-Adrenergic Receptors to Phospholipase C-Beta 1 in Rat Neonatal Cardiomyocytes. *J. Biol. Chem.* **2001**, *276* (40), 37341–37346. https://doi.org/10.1074/jbc.M106572200.

(113) Xie, W.; Samoriski, G. M.; McLaughlin, J. P.; Romoser, V. A.; Smrcka, A.; Hinkle, P. M.; Bidlack, J. M.; Gross, R. A.; Jiang, H.; Wu, D. Genetic Alteration of Phospholipase C B3 Expression Modulates Behavioral and Cellular Responses to μ Opioids. *Proc. Natl. Acad. Sci. U. S. A.* **1999**, *96* (18), 10385–10390.

(114) Han, S.-K.; Mancino, V.; Simon, M. I. Phospholipase Cbeta 3 Mediates the Scratching Response Activated by the Histamine H1 Receptor on C-Fiber Nociceptive Neurons. *Neuron* **2006**, *52* (4), 691–703. https://doi.org/10.1016/j.neuron.2006.09.036.

(115) Mathews, J. L.; Smrcka, A. V.; Bidlack, J. M. A Novel Gβγ-Subunit Inhibitor Selectively Modulates μ-Opioid-Dependent Antinociception and Attenuates Acute Morphine-Induced Antinociceptive Tolerance and Dependence. *J. Neurosci.* **2008**, *28* (47), 12183–12189. https://doi.org/10.1523/JNEUROSCI.2326-08.2008.

(116) Adamski, F. M.; Timms, K. M.; Shieh, B. H. A Unique Isoform of Phospholipase Cbeta4 Highly Expressed in the Cerebellum and Eye. *Biochim. Biophys. Acta* **1999**, *1444* (1), 55–60.

(117) Zhang, W.; Neer, E. J. Reassembly of Phospholipase C-Beta2 from Separated Domains: Analysis of Basal and G Protein-Stimulated Activities. *J. Biol. Chem.* **2001**, *276* (4), 2503–2508. https://doi.org/10.1074/jbc.M003562200.

(118) Hudson, B. N.; Hyun, S.-H.; Thompson, D. H.; Lyon, A. M. Phospholipase Cβ3 Membrane Adsorption and Activation Are Regulated by Its C-Terminal Domains and Phosphatidylinositol 4,5-Bisphosphate. *Biochemistry* **2017**, *56* (41), 5604–5614. https://doi.org/10.1021/acs.biochem.7b00547.

(119) Singer, A. G.; Ghomashchi, F.; Calvez, C. L.; Bollinger, J.; Bezzine, S.; Rouault, M.; Sadilek, M.; Nguyen, E.; Lazdunski, M.; Lambeau, G.; et al. Interfacial Kinetic and Binding Properties of the Complete Set of Human and Mouse Groups I, II, V, X, and XII Secreted Phospholipases A2. *J. Biol. Chem.* **2002**, *277* (50), 48535–48549. https://doi.org/10.1074/jbc.M205855200.

(120) Runnels, L. W.; Scarlata, S. F. Determination of the Affinities between Heterotrimeric G Protein Subunits and Their Phospholipase C-Beta Effectors. *Biochemistry* **1999**, *38* (5), 1488–1496. https://doi.org/10.1021/bi9821519.

(121) Berstein, G.; Blank, J. L.; Jhon, D. Y.; Exton, J. H.; Rhee, S. G.; Ross, E. M. Phospholipase C-Beta 1 Is a GTPase-Activating Protein for Gq/11, Its Physiologic Regulator. *Cell* **1992**, *70* (3), 411–418.

(122) Adjobo-Hermans, M. J. W.; Crosby, K. C.; Putyrski, M.; Bhageloe, A.; van Weeren, L.; Schultz, C.; Goedhart, J.; Gadella Jr., T. W. J. PLCβ Isoforms Differ in Their Subcellular Location and Their CT-Domain Dependent Interaction with Gαq. *Cell. Signal.* **2013**, *25* (1), 255–263. https://doi.org/10.1016/j.cellsig.2012.09.022.

(123) Tesmer, J. J.; Berman, D. M.; Gilman, A. G.; Sprang, S. R. Structure of RGS4 Bound to AlF4--Activated G(i Alpha1): Stabilization of the Transition State for GTP Hydrolysis. *Cell* **1997**, *89* (2), 251–261.

(124) Runnels, L. W.; Jenco, J.; Morris, A.; Scarlata, S. Membrane Binding of Phospholipases C-Beta 1 and C-Beta 2 Is Independent of Phosphatidylinositol 4,5-Bisphosphate and the Alpha and Beta Gamma Subunits of G Proteins. *Biochemistry* **1996**, *35* (51), 16824–16832. https://doi.org/10.1021/bi961606w.

(125) Scarlata, S. Regulation of the Lateral Association of Phospholipase Cbeta2 and G Protein Subunits by Lipid Rafts. *Biochemistry* **2002**, *41* (22), 7092–7099.

(126) Gutman, O.; Walliser, C.; Piechulek, T.; Gierschik, P.; Henis, Y. I. Differential Regulation of Phospholipase C-Beta2 Activity and Membrane Interaction by Galphaq, Gbeta1gamma2, and Rac2. *J. Biol. Chem.* **2010**, *285* (6), 3905–3915. https://doi.org/10.1074/jbc.M109.085100.

(127) Hepler, J. R.; Biddlecome, G. H.; Kleuss, C.; Camp, L. A.; Hofmann, S. L.; Ross, E. M.; Gilman, A. G. Functional Importance of the Amino Terminus of G. *J. Biol. Chem.* **1996**, *271* (1), 496–504. https://doi.org/10.1074/jbc.271.1.496.

(128) Camps, M.; Carozzi, A.; Schnabel, P.; Scheer, A.; Parker, P. J.; Gierschik, P. Isozyme-Selective Stimulation of Phospholipase C-B2 by G Protein Bγ-Subunits. *Nature* **1992**, *360* (6405), 684–686. https://doi.org/10.1038/360684a0.

(129) Katz, A.; Wu, D.; Simon, M. I. Subunits Beta Gamma of Heterotrimeric G Protein Activate Beta 2 Isoform of Phospholipase C. *Nature* **1992**, *360* (6405), 686–689. https://doi.org/10.1038/360686a0.

(130) Smrcka, A. V.; Sternweis, P. C. Regulation of Purified Subtypes of Phosphatidylinositol-Specific Phospholipase C Beta by G Protein Alpha and Beta Gamma Subunits. *J. Biol. Chem.* **1993**, *268* (13), 9667–9674.

(131) Dietrich, A.; Brazil, D.; Jensen, O. N.; Meister, M.; Schrader, M.; Moomaw, J. F.; Mann, M.; Illenberger, D.; Gierschik, P. Isoprenylation of the G Protein γ Subunit Is Both Necessary and Sufficient for Bγ Dimer-Mediated Stimulation of Phospholipase C. *Biochemistry* **1996**, *35* (48), 15174–15182. https://doi.org/10.1021/bi960305j.

(132) Romoser, V.; Ball, R.; Smrcka, A. V. Phospholipase C B2 Association with Phospholipid Interfaces Assessed by Fluorescence Resonance Energy Transfer G Protein Bγ Subunit-Mediated Translocation Is Not Required for Enzyme Activation. *J. Biol. Chem.* **1996**, *271* (41), 25071–25078. https://doi.org/10.1074/jbc.271.41.25071.

(133) Wang, T.; Pentyala, S.; Elliott, J. T.; Dowal, L.; Gupta, E.; Rebecchi, M. J.; Scarlata, S. Selective Interaction of the C2 Domains of Phospholipase C-B1 and -B2 with Activated Gαq Subunits: An Alternative Function for C2-Signaling Modules. *Proc. Natl. Acad. Sci. U. S. A.* **1999**, *96* (14), 7843–7846.

(134) Camps, M.; Hou, C. F.; Jakobs, K. H.; Gierschik, P. Guanosine 5'-[Gamma-Thio]Triphosphate-Stimulated Hydrolysis of Phosphatidylinositol 4,5-Bisphosphate in HL-60 Granulocytes. Evidence That the Guanine Nucleotide Acts by Relieving Phospholipase C from an Inhibitory Constraint. *Biochem. J.* **1990**, *271* (3), 743–748. https://doi.org/10.1042/bj2710743.

(135) Illenberger, D.; Schwald, F.; Pimmer, D.; Binder, W.; Maier, G.; Dietrich, A.; Gierschik, P. Stimulation of Phospholipase C-Beta2 by the Rho GTPases Cdc42Hs and Rac1. *EMBO J.* **1998**, *17* (21), 6241–6249. https://doi.org/10.1093/emboj/17.21.6241.

(136) Jezyk, M. R.; Snyder, J. T.; Gershberg, S.; Worthylake, D. K.; Harden, T. K.; Sondek, J. Crystal Structure of Rac1 Bound to Its Effector Phospholipase C-Beta2. *Nat. Struct. Mol. Biol.* **2006**, *13* (12), 1135–1140. https://doi.org/10.1038/nsmb1175.

(137) Golebiewska, U.; Scarlata, S. The Effect of Membrane Domains on the G Protein – Phospholipase Cβ Signaling Pathway. *Crit. Rev. Biochem. Mol. Biol.* **2010**, *45* (2), 97–105. https://doi.org/10.3109/10409231003598812.

(138) Fujita, A.; Cheng, J.; Tauchi-Sato, K.; Takenawa, T.; Fujimoto, T. A Distinct Pool of Phosphatidylinositol 4,5-Bisphosphate in Caveolae Revealed by a Nanoscale Labeling Technique. *Proc. Natl. Acad. Sci.* **2009**, *106* (23), 9256–9261. https://doi.org/10.1073/pnas.0900216106.

(139) Lanzafame, A. A.; Turnbull, L.; Amiramahdi, F.; Arthur, J. F.; Huynh, H.; Woodcock, E. A. Inositol Phospholipids Localized to Caveolae in Rat Heart Are Regulated by Alpha1-Adrenergic Receptors and by Ischemia-Reperfusion. *Am. J. Physiol. Heart Circ. Physiol.* **2006**, *290* (5), H2059-2065. https://doi.org/10.1152/ajpheart.01210.2005.

(140) Thomas, C. M.; Smart, E. J. Caveolae Structure and Function. *J. Cell. Mol. Med.* **2008**, *12* (3), 796–809. https://doi.org/10.1111/j.1582-4934.2008.00295.x.

(141) Bastiani, M.; Parton, R. G. Caveolae at a Glance. *J. Cell Sci.* **2010**, *123* (Pt 22), 3831–3836. https://doi.org/10.1242/jcs.070102.

(142) Qifti, A.; Garwain, O.; Scarlata, S. Mechanical Stretch Redefines Membrane Gαq–Calcium Signaling Complexes. *J. Membr. Biol.* **2019**. https://doi.org/10.1007/s00232-019-00063-8.

(143) Levental, I.; Grzybek, M.; Simons, K. Greasing Their Way: Lipid Modifications Determine Protein Association with Membrane Rafts. *Biochemistry* **2010**, *49* (30), 6305–6316. https://doi.org/10.1021/bi100882y.

(144) Pike, L. J. Lipid Rafts Bringing Order to Chaos. *J. Lipid Res.* **2003**, *44* (4), 655–667. https://doi.org/10.1194/jlr.R200021-JLR200.

(145) Digby, G. J.; Lober, R. M.; Sethi, P. R.; Lambert, N. A. Some G Protein Heterotrimers Physically Dissociate in Living Cells. *Proc. Natl. Acad. Sci. U. S. A.* **2006**, *103* (47), 17789–17794. https://doi.org/10.1073/pnas.0607116103.

(146) Hein, P.; Rochais, F.; Hoffmann, C.; Dorsch, S.; Nikolaev, V. O.; Engelhardt, S.; Berlot, C. H.; Lohse, M. J.; Bünemann, M. Gs Activation Is Time-Limiting in Initiating Receptor-Mediated Signaling. *J. Biol. Chem.* **2006**, *281* (44), 33345–33351. https://doi.org/10.1074/jbc.M606713200.

(147) Hughes, T. E.; Zhang, H.; Logothetis, D. E.; Berlot, C. H. Visualization of a Functional Galpha Q-Green Fluorescent Protein Fusion in Living Cells. Association with the Plasma Membrane Is Disrupted by Mutational Activation and by Elimination of Palmitoylation Sites, but Not Be Activation Mediated by Receptors or AlF4-. *J. Biol. Chem.* **2001**, *276* (6), 4227–4235. https://doi.org/10.1074/jbc.M007608200.

(148) Filtz, T. M.; Grubb, D. R.; McLeod-Dryden, T. J.; Luo, J.; Woodcock, E. A. Gq-Initiated Cardiomyocyte Hypertrophy Is Mediated by Phospholipase Cβ1b. *FASEB J.* **2009**, *23* (10), 3564–3570. https://doi.org/10.1096/fj.09-133983.

(149) Grubb, D. R.; Luo, J.; Woodcock, E. A. Phospholipase Cβ1b Directly Binds the SH3 Domain of Shank3 for Targeting and Activation in Cardiomyocytes. *Biochem. Biophys. Res. Commun.* **2015**, *461* (3), 519–524. https://doi.org/10.1016/j.bbrc.2015.04.060.

(150) Atef, M. E.; Anand-Srivastava, M. B. Oxidative Stress Contributes to the Enhanced Expression of Gqα/PLCβ1 Proteins and Hypertrophy of VSMC from SHR: Role of Growth Factor Receptor Transactivation. *Am. J. Physiol. - Heart Circ. Physiol.* **2016**, *310* (5), H608–H618. https://doi.org/10.1152/ajpheart.00659.2015.

(151) Woodcock, E. A.; Grubb, D. R.; Filtz, T. M.; Marasco, S.; Luo, J.; McLeod-Dryden, T. J.; Kaye, D. M.; Sadoshima, J.; Du, X.-J.; Wong, C.; et al. Selective Activation of the "b" Splice Variant of Phospholipase Cβ1 in Chronically Dilated Human and Mouse Atria. *J. Mol. Cell. Cardiol.* **2009**, *47* (5), 676–683. https://doi.org/10.1016/j.yjmcc.2009.08.020.

(152) Dent, M. R.; Dhalla, N. S.; Tappia, P. S. Phospholipase C Gene Expression, Protein Content, and Activities in Cardiac Hypertrophy and Heart Failure Due to Volume Overload. *Am. J. Physiol. - Heart Circ. Physiol.* **2004**, *287* (2), H719–H727. https://doi.org/10.1152/ajpheart.01107.2003.

(153) Charpentier, T. H.; Waldo, G. L.; Barrett, M. O.; Huang, W.; Zhang, Q.; Harden, T. K.; Sondek, J. Membrane-Induced Allosteric Control of Phospholipase C-β Isozymes. *J. Biol. Chem.* **2014**, *289* (43), 29545–29557. https://doi.org/10.1074/jbc.M114.586784.

(154) Singer, A. U.; Waldo, G. L.; Harden, T. K.; Sondek, J. A Unique Fold of Phospholipase C-Beta Mediates Dimerization and Interaction with G Alpha q. *Nat. Struct. Biol.* **2002**, *9* (1), 32–36. https://doi.org/10.1038/nsb731.

(155) Illenberger, D.; Walliser, C.; Strobel, J.; Gutman, O.; Niv, H.; Gaidzik, V.; Kloog, Y.; Gierschik, P.; Henis, Y. I. Rac2 Regulation of Phospholipase C-Beta 2 Activity and Mode of Membrane Interactions in Intact Cells. *J. Biol. Chem.* **2003**, *278* (10), 8645–8652. https://doi.org/10.1074/jbc.M211971200.

(156) Park, D.; Jhon, D. Y.; Lee, C. W.; Ryu, S. H.; Rhee, S. G. Removal of the Carboxyl-Terminal Region of Phospholipase C-Beta 1 by Calpain Abolishes Activation by G Alpha q. *J. Biol. Chem.* **1993**, *268* (5), 3710–3714.

(157) Ilkaeva, O.; Kinch, L. N.; Paulssen, R. H.; Ross, E. M. Mutations in the Carboxyl-Terminal Domain of Phospholipase C-B1 Delineate the Dimer Interface and a Potential GαqInteraction Site. *J. Biol. Chem.* **2002**, *277* (6), 4294–4300. https://doi.org/10.1074/jbc.M109612200.

(158) Sahu, S.; Philip, F.; Scarlata, S. Hydrolysis Rates of Different Small Interfering RNAs (SiRNAs) by the RNA Silencing Promoter Complex, C3PO, Determines Their Regulation by Phospholipase Cβ. *J. Biol. Chem.* **2014**, *289* (8), 5134–5144. https://doi.org/10.1074/jbc.M113.531467.

(159) Sahu, S.; Williams, L.; Perez, A.; Philip, F.; Caso, G.; Zurawsky, W.; Scarlata, S. Regulation of the Activity of the Promoter of RNA- induced Silencing, C3PO. *Protein Sci. Publ. Protein Soc.* **2017**, *26* (9), 1807–1818. https://doi.org/10.1002/pro.3219.

(160) Yerramilli, V. S.; Scarlata, S. The Breast Cancer Susceptibility Gene Product (γ-Synuclein) Alters Cell Behavior through It Interaction with Phospholipase Cβ. *Cell. Signal.* **2016**, *28* (1), 91–99. https://doi.org/10.1016/j.cellsig.2015.10.018.

(161) Narayanan, V.; Guo, Y.; Scarlata, S. Fluorescence Studies Suggest a Role for α-Synuclein in the Phosphatidylinositol Lipid Signaling Pathway. *Biochemistry* **2005**, *44* (2), 462–470. https://doi.org/10.1021/bi0487140.

(162) Guo, Y.; Rosati, B.; Scarlata, S. α–Synuclein Increases the Cellular Level of Phospholipase Cβ1. *Cell. Signal.* **2012**, *24* (5), 1109–1114. https://doi.org/10.1016/j.cellsig.2012.01.007.

(163) Kan, W.; Adjobo-Hermans, M.; Burroughs, M.; Faibis, G.; Malik, S.; Tall, G. G.; Smrcka, A. V. M3 Muscarinic Receptor Interaction with Phospholipase C B3 Determines Its Signaling Efficiency. *J. Biol. Chem.* **2014**, *289* (16), 11206–11218. https://doi.org/10.1074/jbc.M113.538546.

(164) Grubb, D. R.; Luo, J.; Yu, Y. L.; Woodcock, E. A. Scaffolding Protein Homer 1c Mediates Hypertrophic Responses Downstream of Gq in Cardiomyocytes. *FASEB J. Off. Publ. Fed. Am. Soc. Exp. Biol.* **2012**, *26* (2), 596–603. https://doi.org/10.1096/fj.11-190330.

(165) Hwang, J.-I.; Kim, H. S.; Lee, J. R.; Kim, E.; Ryu, S. H.; Suh, P.-G. The Interaction of Phospholipase C-Beta3 with Shank2 Regulates MGluR-Mediated Calcium Signal. *J. Biol. Chem.* **2005**, *280* (13), 12467–12473. https://doi.org/10.1074/jbc.M410740200.

(166) Suh, P. G.; Hwang, J. I.; Ryu, S. H.; Donowitz, M.; Kim, J. H. The Roles of PDZ-Containing Proteins in PLC-Beta-Mediated Signaling. *Biochem. Biophys. Res. Commun.* **2001**, *288* (1), 1–7. https://doi.org/10.1006/bbrc.2001.5710.

(167) Cocco, L.; Faenza, I.; Follo, M. Y.; Billi, A. M.; Ramazzotti, G.; Papa, V.; Martelli, A. M.; Manzoli, L. Nuclear Inositides: PI-PLC Signaling in Cell Growth, Differentiation and Pathology. *Adv. Enzyme Regul.* **2009**, *49* (1), 2–10. https://doi.org/10.1016/j.advenzreg.2008.12.001.

(168) Faenza, I.; Matteucci, A.; Manzoli, L.; Billi, A. M.; Aluigi, M.; Peruzzi, D.; Vitale, M.; Castorina, S.; Suh, P. G.; Cocco, L. A Role for Nuclear Phospholipase Cbeta 1 in Cell Cycle Control. *J. Biol. Chem.* **2000**, *275* (39), 30520–30524. https://doi.org/10.1074/jbc.M004630200.

(169) Böhm, D.; Schwegler, H.; Kotthaus, L.; Nayernia, K.; Rickmann, M.; Köhler, M.; Rosenbusch, J.; Engel, W.; Flügge, G.; Burfeind, P. Disruption of PLC-Beta 1-Mediated Signal Transduction in Mutant Mice Causes Age-Dependent Hippocampal Mossy Fiber Sprouting and Neurodegeneration. *Mol. Cell. Neurosci.* **2002**, *21* (4), 584–601.

(170) Aisiku, O. R.; Runnels, L. W.; Scarlata, S. Identification of a Novel Binding Partner of Phospholipase Cβ1: Translin-Associated Factor X. *PLoS ONE* **2010**, *5* (11). https://doi.org/10.1371/journal.pone.0015001.

(171) Demel, R. A.; Geurts van Kessel, W. S. M.; Zwaal, R. F. A.; Roelofsen, B.; van Deenen, L. L. M. Relation between Various Phospholipase Actions on Human Red Cell Membranes and the Interfacial Phospholipid Pressure in Monolayers. *Biochim. Biophys. Acta BBA - Biomembr.* **1975**, *406* (1), 97–107. https://doi.org/10.1016/0005-2736(75)90045-0.

(172) Boguslavsky, V.; Rebecchi, M.; Morris, A. J.; Jhon, D. Y.; Rhee, S. G.; McLaughlin, S. Effect of Monolayer Surface Pressure on the Activities of Phosphoinositide-Specific Phospholipase C-.Beta.1, -.Gamma.1, and -.Delta.1. *Biochemistry* **1994**, *33* (10), 3032–3037. https://doi.org/10.1021/bi00176a036.

(173) James, S. R.; Demel, R. A.; Downes, C. P. Interfacial Hydrolysis of Phosphatidylinositol 4-Phosphate and Phosphatidylinositol 4,5-Bisphosphate by Turkey Erythrocyte Phospholipase C. *Biochem. J.* **1994**, *298* (2), 499–506. https://doi.org/10.1042/bj2980499.

(174) Arduin, A.; Gaffney, P. R. J.; Ces, O. Regulation of PLCβ2 by the Electrostatic and Mechanical Properties of Lipid Bilayers. *Sci. Rep.* **2015**, *5*. https://doi.org/10.1038/srep12628.

(175) Kates, M. Techniques of Lipidology. 2. Rev. Ed. **1986**.

(176) Georgiev, G. A.; Kutsarova, E.; Jordanova, A.; Krastev, R.; Lalchev, Z. Interactions of Meibomian Gland Secretion with Polar Lipids in Langmuir Monolayers. *Colloids Surf. B Biointerfaces* **2010**, *78* (2), 317–327. https://doi.org/10.1016/j.colsurfb.2010.03.024.

(177) Levental, I.; Cēbers, A.; Janmey, P. A. Combined Electrostatics and Hydrogen Bonding Determine Intermolecular Interactions Between Polyphosphoinositides. *J. Am. Chem. Soc.* **2008**, *130* (28), 9025–9030. https://doi.org/10.1021/ja800948c.

(178) Mezzasalma, T. M.; Kranz, J. K.; Chan, W.; Struble, G. T.; Schalk-Hihi, C.; Deckman, I. C.; Springer, B. A.; Todd, M. J. Enhancing Recombinant Protein Quality and Yield by Protein Stability Profiling. *J. Biomol. Screen.* **2007**, *12* (3), 418–428. https://doi.org/10.1177/1087057106297984.

(179) Liu, X.; Villalta, P. W.; Sturla, S. J. Simultaneous Determination of Inositol and Inositol Phosphates in Complex Biological Matrices: Quantitative Ion-Exchange Chromatography/Tandem Mass Spectrometry. *Rapid Commun. Mass Spectrom.* **2009**, *23* (5), 705–712. https://doi.org/10.1002/rcm.3923.

(180) Ghosh, M.; Smrcka, A. V. Assay for G Protein-Dependent Activation of Phospholipase C Beta Using Purified Protein Components. *Methods Mol. Biol. Clifton NJ* **2004**, *237*, 67–75.

(181) Redfern, D. A.; Gericke, A. Domain Formation in Phosphatidylinositol Monophosphate/Phosphatidylcholine Mixed Vesicles. *Biophys. J.* **2004**, *86* (5), 2980–2992.

(182) Redfern, D. A.; Gericke, A. PH-Dependent Domain Formation in Phosphatidylinositol Polyphosphate/Phosphatidylcholine Mixed Vesicles. *J. Lipid Res.* **2005**, *46* (3), 504–515. https://doi.org/10.1194/jlr.M400367-JLR200.

(183) Qualmann, B.; Koch, D.; Kessels, M. M. Let's Go Bananas: Revisiting the Endocytic BAR Code. *EMBO J.* **2011**, *30* (17), 3501–3515. https://doi.org/10.1038/emboj.2011.266.

(184) Peter, B. J.; Kent, H. M.; Mills, I. G.; Vallis, Y.; Butler, P. J. G.; Evans, P. R.; McMahon, H. T. BAR Domains as Sensors of Membrane Curvature: The Amphiphysin BAR Structure. *Science* **2004**, *303* (5657), 495–499. https://doi.org/10.1126/science.1092586.

(185) Pykäläinen, A.; Boczkowska, M.; Zhao, H.; Saarikangas, J.; Rebowski, G.; Jansen, M.; Hakanen, J.; Koskela, E. V.; Peränen, J.; Vihinen, H.; et al. Pinkbar Is an Epithelial-Specific BAR Domain Protein That Generates Planar Membrane Structures. *Nat. Struct. Mol. Biol.* **2011**, *18* (8), 902–907. https://doi.org/10.1038/nsmb.2079.

(186) Zhao, H.; Michelot, A.; Koskela, E. V.; Tkach, V.; Stamou, D.; Drubin, D. G.; Lappalainen, P. Membrane-Sculpting BAR Domains Generate Stable Lipid Microdomains. *Cell Rep.* **2013**, *4* (6), 1213–1223. https://doi.org/10.1016/j.celrep.2013.08.024.

(187) McCullar, J. S.; Malencik, D. A.; Vogel, W. K.; Crofoot, K. M.; Anderson, S. R.; Filtz, T. M. Calmodulin Potentiates Gβγ Activation of Phospholipase C-B3. *Biochem. Pharmacol.* **2007**, *73* (2), 270–278. https://doi.org/10.1016/j.bcp.2006.10.004.

(188) Hammond, G. R. V.; Fischer, M. J.; Anderson, K. E.; Holdich, J.; Koteci, A.; Balla, T.; Irvine, R. F. PI4P and PI(4,5)P2 Are Essential but Independent Lipid Determinants of Membrane Identity. *Science* **2012**, *337* (6095), 727–730. https://doi.org/10.1126/science.1222483.

(189) Willars, G. B.; Nahorski, S. R.; Challiss, R. A. Differential Regulation of Muscarinic Acetylcholine Receptor-Sensitive Polyphosphoinositide Pools and Consequences for Signaling in Human Neuroblastoma Cells. *J. Biol. Chem.* **1998**, *273* (9), 5037–5046. https://doi.org/10.1074/jbc.273.9.5037.

(190) Yadav, S.; Garner, K.; Georgiev, P.; Li, M.; Gomez-Espinosa, E.; Panda, A.; Mathre, S.; Okkenhaug, H.; Cockcroft, S.; Raghu, P. RDGBα, a PtdIns-PtdOH Transfer Protein, Regulates G-Protein-Coupled PtdIns(4,5)P2 Signalling during Drosophila Phototransduction. *J. Cell Sci.* **2015**, *128* (17), 3330–3344. https://doi.org/10.1242/jcs.173476.

(191) Kim, S.; Kedan, A.; Marom, M.; Gavert, N.; Keinan, O.; Selitrennik, M.; Laufman, O.; Lev, S. The Phosphatidylinositol-Transfer Protein Nir2 Binds Phosphatidic Acid and Positively Regulates Phosphoinositide Signalling. *EMBO Rep.* **2013**, *14* (10), 891–899. https://doi.org/10.1038/embor.2013.113.

(192) Zhang, H.; Craciun, L. C.; Mirshahi, T.; Rohács, T.; Lopes, C. M. B.; Jin, T.; Logothetis, D. E. PIP(2) Activates KCNQ Channels, and Its Hydrolysis Underlies Receptor-Mediated Inhibition of M Currents. *Neuron* **2003**, *37* (6), 963–975.

(193) Whorton, M. R.; MacKinnon, R. X-Ray Structure of the Mammalian GIRK2-Bγ G-Protein Complex. *Nature* **2013**, *498* (7453), 190–197. https://doi.org/10.1038/nature12241.

(194) Suh, B.-C.; Hille, B. Regulation of Ion Channels by Phosphatidylinositol 4,5-Bisphosphate. *Curr. Opin. Neurobiol.* **2005**, *15* (3), 370–378. https://doi.org/10.1016/j.conb.2005.05.005.

(195) Zhang, Y.; Vogel, W. K.; McCullar, J. S.; Greenwood, J. A.; Filtz, T. M. Phospholipase C-Beta3 and -Beta1 Form Homodimers, but Not Heterodimers, through Catalytic and Carboxyl-Terminal Domains. *Mol. Pharmacol.* **2006**, *70* (3), 860–868. https://doi.org/10.1124/mol.105.021923.

CHAPTER 2. PHOSPHOLIPASE C BETA 3 MEMBRANE ADSORPTION AND ACTIVATION IS REGULATED BY ITS C-TERMINAL DOMAINS AND PHOSPHATIDYLINOSITOL-4,5-BISPHOSPHATE

Adapted with permission from Hudson, B. N.; Hyun, S.-H.; Thompson, D. H.; Lyon, A. M. *Biochemistry* 2017, 56 (41), 5604–5614. https://doi.org/10.1021/acs.biochem.7b00547. Copyright 2017 American Chemical Society.

2.1 Abstract

Phospholipase Cβ (PLCβ) enzymes hydrolyze phosphatidylinositol-4,5-bisphosphate to produce second messengers that regulate intracellular Ca^{2+}, cell proliferation, and survival. Their activity is dependent upon interfacial activation that occurs upon localization to cell membranes. However, the molecular basis for how these enzymes productively interact with the membrane is poorly understood. Herein, atomic force microscopy demonstrates that the ~300 residue C-terminal domain promotes adsorption to monolayers and is required for the spatial organization of the protein on the monolayer surface. PLCβ variants lacking this C-terminal domain display differences in their distribution on the surface. In addition, a previously identified autoinhibitory helix that binds to the PLCβ catalytic core negatively impacts membrane binding, providing an additional level of regulation for membrane adsorption. Lastly, defects in PIP_2 hydrolysis also alter monolayer adsorption, reflecting a role for the active site in membrane binding. Together, these findings support a model in which multiple elements of PLCβ modulate adsorption, distribution, and catalysis at the cell membrane.

2.2 Introduction

Phospholipase C (PLC) enzymes hydrolyze the inner plasma membrane lipid phosphatidylinositol-4,5-bisphosphate (PIP_2) to produce inositol-1,4,5-triphosphate (IP_3) and diacylglycerol (DAG). These second messengers promote Ca^{2+} release and protein kinase C (PKC) activation, resulting in numerous downstream effects such as cell survival and proliferation[1]. The PLCβ subfamily has very low basal activity, but are stimulated up to ~60-fold through direct interactions with the heterotrimeric G protein subunits $G\alpha_q$ and $G\beta\gamma$ downstream of G_q- and G_i-coupled receptors,

respectively[1,2]. Dysregulation of PLCβ expression or activity is associated with arrhythmias[3,4], hypertrophy[3,5,6], heart failure[3,7], and opioid tolerance[8,9].

The catalytic cores of PLC enzymes are typically flanked by domains that regulate activity in response to extracellular signals. These domains control membrane targeting, mediate autoinhibition, contribute to allosteric regulation, and bind activating proteins. In PLCβ enzymes, these regulatory domains are thought to influence the stability of an autoinhibitory lid that blocks the active site known as the X–Y linker, which contains a highly conserved acidic stretch that is proposed to be displaced from the active site via electrostatic interactions with the membrane[10–13]. The defining regulatory domain of PLCβ is a ~400 amino acid C-terminal extension, which is subdivided into proximal and distal C-terminal domains (CTDs) (Figure 2.1)[1,2]. The proximal CTD contains the primary $G\alpha_q$ binding site followed by an autoinhibitory helix (Hα2') that docks to a cleft adjacent to the active site in the absence of $G\alpha_q$[14,15]. Hα2' is also anticipated to regulate interactions between the PLCβ active site and the membrane. Mutations that disrupt its binding site on the catalytic core increase basal activity decrease thermal stability and decrease the efficacy of heterotrimeric G protein-dependent activation[15]. One possible mechanism by which Hα2' achieves autoinhibition may be to prevent the active site from optimally engaging PIP_2. Displacement of Hα2' from its bound conformation on the catalytic core could be achieved through an interfacial activation process[10–13] and/or via $G\alpha_q$-dependent activation[11]. The distal CTD is a coiled-coil domain with highly conserved clusters of lysines and arginines arrayed along one face that function as a major membrane binding determinant[16,17]. Deletion of the entire distal CTD or perturbation of basic clusters decreases membrane association[18–21] and dramatically lowers basal and heterotrimeric G protein-stimulated activity[22–25]. The PLCβ3 distal CTD has also been reported to interact with the catalytic core or $G\alpha_q$ in solution, potentially representing autoinhibitory and activating modes, respectively[16]. Finally, the CTDs have emerged as protein interaction sites. The proximal CTD interacts with the RNA silencing complex C3PO[26,27] and synucleins[28–30]. The distal CTD is reported to interact with numerous proteins, including the M3 muscarinic receptor[31], the translin-associated factor-X[33], and scaffolding proteins[32–34]. These protein-protein interactions are likely to perturb intramolecular interactions within PLCβ, in addition to its interactions with $G\alpha_q$ and potentially the cell membrane. These PLCβ binding

partners may impose an additional level of regulation on the membrane association of PLCβ, alone or in complex with its G protein activators, its subcellular distribution, and its lipase activity.

Despite the importance of the distal CTD in membrane association and maximum lipase activity, it is not sufficient to target PLCβ to the membrane. For example, the PLCβ1 and PLCβ4 isoforms are typically associated with the plasma membrane, whereas PLCβ2 and PLCβ3 are found predominantly in the cytoplasm[35,36]. These differences are attributed in part to sequence differences within the distal CTD, which shares only 30-35% identity between isoforms[2]. In addition, the subcellular distribution of PLCβ proteins is highly dependent on the isoform[37–39], cell type[40–42], cell cycle stage[38,39], interaction partners[34,40], and phosphorylation state[43].

Our knowledge of how the lipid composition and physical properties of the membrane regulate PLCβ binding and activation is limited. Early studies using compressed lipid monolayers found that lipase activity is highly dependent upon surface pressure, with maximum PIP_2 hydrolysis observed at a surface pressure of ~30-35 mN/m, consistent with that of the plasma membrane[44–47]. It was recently shown that liposomes with increasingly negative surface charge only increased PLCβ basal activity up to a sub-maximal threshold, indicating that other membrane-dependent processes are involved in stimulating lipase activity. Furthermore, liposomes that contained minimal curvature elastic stress were unable to support PLC-dependent PIP_2 hydrolysis, suggesting that PLCβ must also insert into the membrane for its activation[48]. These results are consistent with interfacial activation, given the dependence upon surface charge and the need for the enzyme to penetrate the membrane for its activity[44,46,47].

In this study, we sought to directly evaluate the roles of the catalytic core and proximal and distal CTDs in regulating membrane binding using atomic force microscopy to characterize adsorption of PLCβ3 variants on compressed lipid monolayers containing PIP_2. Introduction of a point mutant that significantly decreases lipase activity was used to differentiate whether changes in the appearance and topography of the monolayer upon addition of protein to the subphase were due to adsorption versus PIP_2 hydrolysis. We confirm that the distal CTD is a key regulator of adsorption, and demonstrate that the proximal CTD impairs adsorption in the absence of the distal CTD, which may fine-tune interactions between the membrane and active site. Furthermore, we find that the distal CTD can promote adsorption to specific regions of the monolayer, suggesting that there is a spatial contribution to activity. These findings support a model in which the membrane association of PLCβ3 is dictated by multivalent interactions within the protein.

2.3 Materials and Methods

2.3.1 Cloning, Expression, and Mutagenesis of Human PLCβ3

cDNAs encoding N-terminally His-tagged human PLCβ3 (UniProt ID Q01970 and residues 10-1234) and C-terminally truncated variants PLCβ3-Δ847 (residues 10-847) and PLCβ3-Δ892 (residues 10-892) were cloned into the pFastBac Dual vector. The H332A point mutation was introduced using QuikChange Site-Directed Mutagenesis (Stratagene, San Diego, CA, USA), and sequenced over the open reading frame. High Five cells were infected with baculovirus encoding PLCβ3 variants for 40 h. Cells were harvested and resuspended in 20 mM HEPES pH 8, 200 mM NaCl, 10 mM β-mercaptoethanol (BME), 0.1 mM EDTA, 0.1 mM EGTA, and Roche EDTA-free protease inhibitor tablets at one-third concentration. Cells were homogenized and lysed by dounce on ice. The lysate was clarified by centrifugation and the supernatant was filtered twice through a 0.2 μm glass fiber filter (Millipore, Billerica, MA, USA), and applied to an Ni-NTA column (Roche, Basel, Switzerland) pre-equilibrated with Buffer A (20 mM HEPES pH 8, 100 mM NaCl, 10 mM BME, 0.1 mM EDTA, 0.1 mM EGTA). The column was washed with 10 column volumes of Buffer A, followed by ten column volumes of buffer A supplemented with 10 mM imidazole and 300 mM NaCl. PLCβ3 variants were eluted with 200 mM imidazole in Buffer A, concentrated to 500 μL and filtered through a 0.2 μm filter (Millipore, Billerica, MA, USA). The sample was then applied to tandem Superdex S200 columns (GE Healthcare) pre-equilibrated with S200 buffer (20 mM HEPES pH 8, 200 mM NaCl, 2 mM DTT, 0.1 mM EDTA, 0.1 mM EGTA). Fractions containing the protein of interest were pooled, concentrated, and flash frozen in liquid nitrogen[15].

2.3.2 Formation of Compressed Lipid Monolayers

Chicken egg white phosphatidylethanolamine (PE) and porcine brain phosphatidylinositol-4,5-bisphosphate (PIP_2) were purchased from Avanti Polar Lipids (Alabaster, AL, USA) and mixed in a 7:3 molar ratio in chloroform at a total lipid concentration of 1 mg/mL, and dried as 10 μl aliquots under nitrogen prior to storage at -20 °C.

A small Langmuir-Blodgett microtrough (Kibron, Helsinki, Finland) equipped with a computer-controlled microbalance (Kibron) was used to prepare all compressed monolayers. Surface pressure was monitored via the Wilhelmy method[49] by an alloy wire DyneProbe (Kibron) with a

sensitivity of ± 0.01 mN/m. The DyneProbe was cleaned by flame before and after each measurement. The microtrough was rinsed three times with ethanol and distilled water before and after each experiment and dried using compressed air. The subphase used in all experiments was 30 mL of 0.2 μm-filtered 20 mM HEPES (pH 8.0) passed through a 0.2 μM filter (Millipore, VWR, United States). The PE:PIP_2 lipid mixture used to form the monolayer was resuspended in chloroform and deposited drop-wise onto the air-water interface using a 25 μL Hamilton microsyringe (Hamilton, Bonaduz, Switzerland) until the surface pressure reached 7.0 ± 3 mN/m. The monolayer equilibrated for 5 min to allow for solvent evaporation and was then compressed to maintain a constant surface pressure of 30 mN/m at a rate of 9.847 $Å^2$/chain/min. Once the surface pressure reached 30mN/m, PLCβ3 variants in S200 buffer were added to the subphase gradually to prevent perturbation of the monolayer and incubated for 20 min. For the control experiments, buffer alone was added to the subphase. The surface pressure and molecular area of the monolayer were monitored throughout the experiment (Figures 2.2 and 2.3). The molecular area per molecule was automatically determined by the control software by monitoring the barrier motion (FilmWare 3.61; Kibron)[50,51] (Figures 2.2, 2.3, Table 2.1). After the 20 min incubation period, samples of each monolayer were transferred to freshly cleaved, highly ordered pyrolytic graphite (HOPG) (SPI Supplies, West Chester, PA, USA) by Langmuir-Schaefer transfer. The samples were dried for one hour in a 50 x 9mm petri dish (Falcon, MA, USA) and rinsed three times with 1 mL of ultrapure water. Samples were dried for an additional 24 h at room temperature in a covered 50 x 9 mm petri dish prior to imaging by atomic force microscopy. All experiments were carried out at 20 °C and repeated at least three times. At least two independent preparations of protein were also used for each experiment. For the molecular area measurements, data from at least two independent experiments were used to calculate the molecular area per molecule mean values.

2.3.3 Atomic Force Microscopy

All AFM imaging was performed using a Veeco MultiMode AFM equipped with a Nanoscope V controller. Monolayers were imaged in tapping mode using aluminum cantilevers with a force constant of 5 N/m (MikroMasch, Watsonville, CA, USA) and a scan rate of 1.00 Hz. At least five images were taken per film. All scanning was performed in air at room temperature (22 °C). Images were flattened and analyzed by section using the Nanoscope Analysis 1.5 software.

Langmuir-Schaefer transfer of the monolayer to the HOPG substrate was confirmed by measuring the change in sample height relative to the bare substrate. For these measurements, contact mode AFM was used to excavate a region of the sample down to the HOPG surface. The change in height was determined by sectional analysis using Nanoscope Analysis 1.5 **(**Figure 2.4**)**. For cross-sectional analysis of the monolayer surfaces alone and following incubation with PLCβ3 variants, at least five distinct topographical features were chosen from each monolayer sample, and at least three independently prepared monolayers were sampled. The criterion imposed on sampling was the selection of regions containing both peaks and valleys (clear separation between light and dark colors on the false-colored AFM image) in a single line-scan profile. The relative height of surface features was also measured for twenty surface features from at least three independently prepared monolayer samples. The change in height was measured from a valley to a peak, and the frequencies of the feature heights were quantified and plotted in histograms for each PLCβ3 variant using GraphPad Prism 7.0. The lowest bin for each histogram was set to the average of the five lowest height measurements in each data set, which also established the bin width and the total number of bins.

2.3.4 Differential Scanning Fluorimetry Assays

The melting temperatures (T_m) of PLCβ3 variants were determined by monitoring the change in fluorescence of SYPRO Orange (Molecular Probes, Eugene, OR, USA) due to protein denaturation as a function of temperature[11,15,52]. PLCβ3 variants purified in S200 buffer (0.5 mg/mL) were incubated with 5X SYPRO Orange dye and 5 mM $CaCl_2$ in a final volume of 20 μL. For experiments with IP_3, 5 mM inositol-1,4,5-triphosphate (IP_3) (Cayman Chemical, Ann Arbor, MI, USA) was included. All samples were loaded in triplicate in a MicroAmp Optical 96-well reaction Plate and sealed with MicroAmp Optical Adhesive Film (Applied Biosystems, Waltham, MA, USA), and centrifuged for 1 min. Thermal shift assays were carried out using a ViiA7 qPCR machine (Thermo Fisher, Foster City, CA, USA). The change in fluorescence was measured at 0.2 °C intervals between 25-95 °C. At least three experiments were carried out, with samples measured in triplicate from two independent preparations. The T_m is calculated by fitting the increase in fluorescence as a function of temperature to a Boltzmann sigmoid (GraphPad Prism 7.0).

2.3.5 IP_3 Quantification by Mass Spectrometry

The subphases from all monolayer experiments were collected and immediately transferred to storage at -80 °C for four hours, terminating the reaction. The samples were then thawed in lukewarm water, and 13 mL of each sample was evaporated to dryness at 20 °C on a Speed Vac concentration system (~18 hours) (Thermo Fisher, MA, USA). The dry residue was reconstituted in 200 μL of a 30% methanol:70% water solution. Inositol triphosphate (IP_3) levels were quantitated by HPLC/MS-MS, based on the procedure established by Liu, et al[53]. Separation of IP_3 was performed with an Agilent Rapid Res 1200 HPLC system using a Thermo Biobasic anion-exchange 0.5 x 150 mm, 5 μm column. Mobile phase A was comprised of 200 mM $(NH_4)_2CO_3$ (pH 9.0) in ultrapure H_2O and mobile phase B, used to equilibrate the column, contained 95% H_2O and 5% methanol. A linear gradient elution was used to isolate the IP_3 as follows: 100% B from 0-3 min; 50% B at 8 min; 25% B at 28 min; 100% B at 33 min; 100% B until 43 min. A column flow rate of 10 μL/min was used, and the retention time of IP_3 was found to be 5 minutes with a sample injection volume of 3 μL.

Analytes were quantified using MS/MS utilizing an Agilent 6410 triple quadrupole mass spectrometer with electrospray ionization (ESI). Quantitation was based on Multiple Reaction Monitoring (MRM). ESI negative mode was used with a transition of 418.9 to 321.0 and a collision energy (CE) of 9 V, a fragmentor energy of 135 V, and a dwell time of 200 ms. Source parameters were as follows: nitrogen gas temperature and flow rate: 300 °C and 5 L/min, respectively, nebulizer pressure: 17 psi, and capillary potential: 4,000 V. The limit of detection was 2.5 ng/mL, as defined as a signal-to-noise ratio (RMS) of 3:1, respectively, determined using authentic standards.

2.3.6 Liposome-based Phosphatidylinositol-4,5-bisphosphate Hydrolysis Assays

Hen egg white phosphatidylethanolamine (200 μM) and 50 μM porcine brain phosphatidylinositol-4,5-bisphosphate (Avanti Polar Lipids, Alabaster, AL, USA) were combined with 4000-8000 cpm [^{3}H]-labeled PIP_2 (Perkin-Elmer, Waltham, MA, USA) and dried under nitrogen. Lipids were resuspended in sonication buffer (50 mM HEPES pH 7, 80 mM KCl, 2 mM EGTA, and 1 mM DTT) to form liposomes using a bath sonicator (Avanti Polar Lipids, Alabaster, AL USA). Activity assays contained 50 mM HEPES pH 7, 80 mM KCl, 15 mM NaCl, 0.83 mM $MgCl_2$, 3 mM DTT, 1 mg/ml BSA, 2.5 mM EGTA, 0.2 mM EDTA, 200 mM free Ca^{2+}, and varying

amounts of PLCβ3 variants. PLCβ3 variants were used at concentrations to produce activity in the linear range over the time course of the experiment. The final protein concentrations were: PLCβ3 at 0.5 ng/μL, PLCβ3-Δ892 at 12 ng/μL, PLCβ3-Δ847 at 4 or 5 ng/μL, PLCβ3 H332A at 0.5 and 2.5 ng/μL, PLCβ3-Δ892 H332A at 12 and 60 ng/μL, and PLCβ3-Δ847 H332A at 4 and 20 ng/μL. Reactions were initiated by addition of liposomes and transfer to 30 °C. Control reactions to measure background contained all the components except free Ca^{2+}. Samples were incubated for times ranging from 2-10 min and terminated by the addition of 200 μL 10% (w/v) ice-cold trichloroacetic acid and 100 μL 10 mg/mL BSA, followed by centrifugation to pellet the protein and liposomes. 200 μL of the supernatant was removed and free [^{3}H]-IP_3 was quantified by liquid scintillation counting[15,54]. All experiments were carried out at least three times with samples measured in duplicate from two independent protein purifications.

2.4 Results

2.4.1 Phosphatidylinositol-4,5-bisphosphate Forms Clusters on Compressed Lipid Monolayers

PLC proteins have not previously been characterized by compressed lipid monolayers using atomic force microscopy (AFM). We generated PE and PE:PIP_2 monolayers containing 10-30% PIP_2 and compressed each monolayer to a final surface pressure of 30 mN/m. Monolayer samples were then transferred to HOPG using the Langmuir-Schaefer transfer method and imaged by atomic force microscopy (AFM). Monolayer transfer was confirmed by measuring the height of the sample relative to the HOPG surface (Figure 2.4). The PE monolayer does not have any clear surface features, as evidenced by the uniform appearance and color of the surface, where increases in surface height are shown as lighter colors (Figure 2.5A). Incorporation of 10% or 20% PIP_2 within the PE monolayer results in the formation of well-defined elevated regions on the monolayer surface (Figure 2.5B, C). For monolayers containing 30% PIP_2, the clustered regions are still present, but smaller and more dispersed (Figure 2.5D). The 7:3 PE:PIP_2 ratio is similar to the conditions used in a well-established liposome-based activity assay routinely used for measuring in vitro PLC activity[11,16,54]. As the elevated regions are only present when PIP_2 is incorporated within the monolayer, these clusters likely represent regions enriched in PIP_2. Similar clusters have been reported in other model membrane systems[44,51,55,56].

2.4.2 Adsorption is Regulated by the Proximal and Distal CTDs

The distal CTD is a major membrane binding determinant in PLCβ enzymes, but the catalytic core and proximal CTD are also expected to modulate this process (Figure 2.1A, B)[1,2]. In a first step towards deconvoluting the roles of these elements in membrane binding, PLCβ3 variants differing in their C-termini (Figure 2.1A) were assessed for their ability to adsorb to PIP_2-containing monolayers and visualized using AFM. For these experiments, the surface pressure of the monolayer was maintained at 30 mN/m, and the molecular area per molecule was recorded as a function of time.

Full-length PLCβ3 has the highest reported basal activity of the three variants under study, which has been attributed to the ability of the distal CTD to enhance membrane association of the protein[1]. PLCβ3 was added to the subphase of the PE:PIP_2 monolayer and incubated prior to Langmuir-Schaefer transfer to HOPG for visualization by AFM. Addition of 10 nM PLCβ3 to the system results in larger and taller surface features than observed in the monolayer alone, consistent with protein adsorption (Figure 2.6A,B and Figure 2.7). Protein adsorption can also be detected by cross-sectional analysis of selected sample regions, which provides information on surface topography. Topographical changes appear as peaks and valleys, with larger surface features resulting in the appearance of wider peaks and valleys, relative to the no protein control (Figure 2.6A,B, Figure 2.7, and Figure 2.8A). These surface features are similar in their distribution and shape to the PIP_2 clusters observed in the monolayer alone. Addition of increasing amounts of PLCβ3, up to 50 nM, to the subphase causes a further increase in the relative height of large, raised elements on the monolayer surface, which is confirmed by the broadening of the surface features in the cross-sectional analysis (Figure 2.6, Figure 2.7, Figure 2.8A, and Table 2.1). Even with 50 nM PLCβ3, the monolayer still displays clear surface features, suggesting that adsorption is targeted to specific regions.

We next compared the ability of two PLCβ3 C-terminal truncations to adsorb to the monolayer. PLCβ3-Δ847 lacks both the proximal and distal CTDs, whereas PLCβ3-Δ892 lacks only the distal CTD (Figure 2.1A). Consequently, PLCβ3-Δ847 has higher basal activity than PLCβ3-Δ892 because the latter variant retains the autoinhibitory Hα2' helix[11,14,15]. As both proteins exhibit some degree of basal activity, they are able to partition to the membrane at least part of the time[15,21,22,57]. Addition of 10 nM of PLCβ3-Δ847 to the subphase results in a more

uniform appearance of the monolayer surface, as shown by the consistent color and fewer topographical features relative to the PE:PIP_2 monolayer alone (Figure 2.6D and Figure 2.7). The trend towards a uniform surface continues as the concentration of PLCβ3-Δ847 increases, and at 50 nM protein, there are no clear surface features on the monolayer (Figure 2.6E and Figure 2.7). Cross-sectional analysis of selected regions of these samples and their quantification provides further confirmation that the surface is increasingly uniform and its topographical features obscured.

Similar trends are observed for PLCβ3-Δ892, which contains the catalytic core and proximal CTD (Figure 2.1A). At 10 nM PLCβ3-Δ892, the surface of the monolayer is similar to those incubated with PLCβ3-Δ847. Some clustered features on the surface are visible for monolayers incubated with low concentrations of PLCβ3-Δ892 relative to those incubated with PLCβ3-Δ847 (Figure 2.4D-G and Figure 2.7). Similar to the monolayers incubated with 50 nM PLCβ3-Δ847, the addition of 50 nM PLCβ3-Δ892 minimizes the appearance of clustered regions of the monolayer. These changes are further confirmed by cross-sectional analysis of the surfaces (Figure 2.6F, G and Figure 2.7).

Comparison of monolayers incubated with PLCβ3 to those incubated with the C-terminal truncations reveals clear differences in the appearance of the surface. Monolayers containing PLCβ3 have elevated surface features that are taller relative to the PE:PIP_2 monolayer alone, whereas monolayers incubated with PLCβ3-Δ847 and PLCβ3-Δ892 show an overall loss of surface features. These differences can be attributed to the presence of the distal CTD, which appears to preferentially target the enzyme to specific regions of the monolayer. These regions could potentially be enriched in PIP_2, given the similarities in the surface features of the monolayers. The differences observed in the monolayers incubated with PLCβ3-Δ847 and PLCβ3-Δ892 are likely due to the presence of the proximal CTD, which is predicted to hinder adsorption of the catalytic core to the monolayer.

2.4.3 Disruption of Phosphatidylinositol-4,5-bisphosphate Hydrolysis Does Not Alter Protein Fold or Stability

PIP_2 has been previously reported to contribute to membrane association and/or increase the affinity of PLCβ for the membrane[20,35], but these findings are controversial[19,58]. All the PLCβ3 variants must at least transiently adsorb to the monolayer, as they all have activity. However,

PLCβ3-Δ892 showed the lowest degree of adsorption and has the lowest activity of the three variants[11,15]. These differences could either reflect true differences in the affinity for the membrane of each variant or the influence of PIP_2 hydrolysis by the catalytic domain. Previous studies of the related enzyme PLCδ identified an active site histidine, His311, as critical for PIP_2 hydrolysis. This residue, equivalent to human PLCβ3 H332, binds the 1-phosphate group and stabilizes the transition state (Figure 2.9). Mutation of PLCδ His311 to alanine decreased basal activity ~20,000-fold relative to wild-type, confirming its functional importance in PIP_2 hydrolysis[59]. We, therefore, generated the PLCβ3 H332A, PLCβ3-Δ847 H332A, and PLCβ3-Δ892 H332A variants for use in our monolayer analysis.

To ensure the mutant proteins were folded properly, differential scanning fluorimetry (DSF) was used to determine the thermal stability of each variant[52]. Introduction of the H332A mutation caused a small ~1.5-2 °C change in the background of each PLCβ3 variants (Figure 2.10 and Table 2.2). We used the same technique to determine whether the H332A variants were still able to bind PIP_2 by using IP_3 as a probe to determine the integrity and accessibility of the active site[11]. For each of the wild-type and the H332A variants, the addition of 5 mM IP_3 caused a ~2-3 °C increase in thermal stability (Table 2.2 and Figure 2.10), consistent with ligand-induced stabilization[71]. Thus, the H332A mutation does not seem to disrupt protein fold, stability, or substrate binding in PLCβ3.

To assess whether the PLCβ3 variants are active under the monolayer assay conditions, we used mass spectrometry to quantify the production of IP_3. For these experiments, the subphase from a monolayer incubated with a PLCβ3 variant was collected, concentrated, and dried under vacuum. The remaining residue, containing IP_3 and buffer components, was then resuspended and further purified via high-performance liquid chromatography, and the eluent analyzed by electrospray ionization mass spectrometry[53]. Under these conditions, we find that PLCβ3 is able to robustly hydrolyze PIP_2 at all concentrations tested (Figure 2.11A and Table 2.3). The difference in IP_3 detected for monolayers incubated with either 10 or 50 nM PLCβ3 is modest (4500 ± 200 ng/mL IP_3 versus 7400 ± 800 ng/mL IP_3), perhaps due to the manner in which the protein adsorbs to the monolayer, which may confine its activity to only regions enriched in PIP_2. However, this hypothesis is contingent upon the formation of stable, slowly diffusing PIP_2 clusters. Importantly, these conditions do not result in the complete depletion of PIP_2 from the monolayer. For

monolayers incubated with PLCβ3, only ~2% of the PIP_2 in the monolayer is hydrolyzed for the time course used. Thus, the changes in the monolayer upon protein addition are unlikely due to PIP_2 depletion.

In contrast, monolayers incubated with PLCβ3 H332A produced very little IP_3 relative to the wild-type protein, even at the highest protein concentration tested (460 ± 30 ng/mL IP_3 for monolayers incubated with 50 nM PLCβ3 H332A). The subphases from monolayers incubated with PLCβ3-Δ847 also had greater amounts of IP_3 than those incubated with PLCβ3-Δ892 (Figure 2.11B, C and Table 2.3), consistent with their relative basal activities using a liposome substrate[11,15]. Introduction of the H332A mutations in the background of PLCβ3-Δ847 or PLCβ3-Δ892 decreases or eliminates IP_3 production, respectively (Figure 2.11B,C and Table 2.3). For example, the subphase of monolayers incubated with 50 nM PLCβ3-Δ847 H334A contained only 30 ± 8 ng/mL IP_3, a ~7.5-fold decrease relative to wild-type. IP_3 was not detected in the subphase from monolayers incubated with any concentration of PLCβ3-Δ892 H332A. However, given the very low amounts of IP_3 produced by PLCβ3-Δ847 and PLCβ3-Δ892 and their respective H332A variants, it is not clear whether the observed differences are meaningful under these conditions.
As an additional control, the specific activities of all PLCβ3 variants were assessed using a liposome-based activity assay, which has been used extensively to quantify PLC activity in vitro (Figure 2.12 and Table 2.4)[11,15,54]. Consistent with the IP_3 quantitation by mass spectrometry (Figure 2.11) and previously published results, PLCβ3 has the highest specific activity (37 ± 6 nmol IP_3/min/nmol PLCβ3) relative to PLCβ3-Δ847 (30 ± 2 nmol IP_3/min/nmol PLCβ3-Δ847) and PLCβ3-Δ892 (3 ± 0.6 nmol IP_3/min/nmol PLCβ3-Δ892). PLCβ3 H332A had no detectable activity at any concentration tested, whereas the specific activity of PLCβ3-Δ847 H332A and PLCβ3-Δ892 H332A decreased 47-fold and 4.5-fold respectively (Figure 2.12 and Table 2.4). For PLCβ3-Δ847 H332A and PLCβ3-Δ892 H332A, the specific activity is at the limit of detection.

2.4.4 Phosphatidylinositol-4,5-bisphosphate Turnover Contributes to Monolayer Adsorption

All three PLCβ3 H332A variants are able to bind IP_3 but are impaired in PIP_2 hydrolysis. To determine whether the rate of PIP_2 hydrolysis contributes to adsorption and distribution at the monolayer interface, the H332A variants were assessed for monolayer adsorption using the same strategy previously described for PLCβ3, PLCβ3-Δ847, and PLCβ3-Δ892. Addition of 10 nM

PLCβ3 H332A to the compressed PE:PIP_2 monolayer does not have a substantial impact on the appearance of the monolayer, and clustered surface features are still observed (Figure 2.8B, 2.13A, B, Figure 2.14, and Table 2.1). This is supported by the cross-sectional analyses of the surface, which show minimal changes in the topographical features relative to the monolayer incubated with the same concentration of wild-type protein (Figure 2.6). Monolayers incubated with increasing concentrations of PLCβ3 H332A, up to 50 nM protein, more strongly resemble monolayers incubated with wild-type PLCβ3 (Figure 2.13C and Figure 2.5C, respectively). These PLCβ3 H332A monolayers feature an increase in light puncta dispersed across the surface. Cross-sectional analysis confirms these regions correspond to surface features of increased height, and there is an overall increase in the number of these features. Comparing monolayers incubated with PLCβ3 or PLCβ3 H332A suggests that the reduced ability of the H332A variant to hydrolyze PIP_2 does not profoundly alter the distribution of PLCβ3 and that the distal CTD alone appears to be sufficient for targeting the enzyme to specific regions of the monolayer.

We next tested whether the H332A mutant perturbed monolayer adsorption in the background of PLCβ3-Δ847 or PLCβ3-Δ892. Addition of 10 nM PLCβ3-Δ847 H332A to the subphase had minimal effect on the appearance of the monolayer, which retains surface features of comparable height to the monolayer alone (Figure 2.13A, E). Addition of up to 50 nM PLCβ3-Δ847 H332A caused the formation of elevated, extended regions on the monolayer surface. These regions are similar in relative height to those observed for PLCβ3 H332A, and they appear to cover a greater surface. The surface of monolayers incubated with PLCβ3-Δ847 H332A also differs from those incubated with wild-type PLCβ3-Δ847, where incubation with the latter protein results in a more uniform surface (Figure 2.13E and Figure 2.6E, respectively).

Addition of low concentrations of PLCβ3-Δ892 H332A to the subphase of the monolayer results in minimal changes to the surface, which is similar to the monolayer alone or upon addition of PLCβ3-Δ847 H332A. This is supported by cross-sectional analyses of the monolayer, which show few changes in topographical features upon protein addition (Figure 2.13). Addition of 50 nM PLCβ3-Δ892 H332A results in a more uniform appearance for the monolayer surface, most similar to monolayers incubated with wild-type PLCβ3-Δ892 (Figure 2.13 and Figure 2.6, respectively). Cross-sectional analyses confirm these samples feature extended plateaus (Figure 2.13G). These results contrast with monolayers incubated with PLCβ3 H332A or PLCβ3-Δ847

H332A, where the surface features are clearly defined as elevated peaks on the surface. These differences may be due to the impaired catalysis of the PLCβ3-Δ892 H332A variant, which could not be detected in the monolayer experiment, and the proximal CTD, which further inhibits activity and appears to hinder interactions between the catalytic core and the monolayer.

2.4.5 Discussion

PLCβ enzymes are thought to bind the membrane via multivalent interactions for efficient PIP_2 hydrolysis. Under basal conditions, these proteins have very low activity but are dramatically activated through interactions with G proteins[1]. The distal CTD has emerged as an important modulator of membrane binding, as loss of the domain or perturbation of its basic surface decreases association and activity. However, it is not required for membrane binding, as C-terminal truncations of PLCβ3 retain lipase activity and therefore must bind to the membrane[16,22–24,26,58]. Localization of PLCβ to the membrane also plays an allosteric role in activation through interfacial mechanisms[10,11,13] and/or release of steric constraints[11,15]. Thus, in order to more fully understand PLCβ regulation under basal conditions, it is essential to understand the molecular interactions between PLCβ and the membrane.

AFM provides a method to image molecules adsorbed to a stable surface and provides information about the appearance, organization, and topography of the resulting sample. To the best of our knowledge, this study is the first to use this technique to begin elucidating the interactions between PLCβ3 and a model membrane system. We find that the compressed PE:PIP_2 monolayers alone have clear surface features, most likely due to the spontaneous formation of PIP_2 clusters, as has been reported for other model systems (Figure 2.5)[51,55,56]. Addition of PLCβ3 does not eliminate these features; instead, its adsorption to the monolayer increases the relative height of clustered surface features, suggesting the distal CTD may regulate the spatial distribution of the enzyme on the monolayer (Figure 2.6 and Figure 2.7). The distal CTD itself has structural similarity to BAR (Bin-Amphiphysin-RVS) domains. These domains are extended coiled-coil structures which are involved in recognizing and/or inducing membrane curvature[60,61]. Indeed, some BAR domains specifically bind to PIP_2-containing microdomains within the membrane, providing an additional level of control in regulating downstream signaling events reliant on PIP_2[62,63]. Whether the PLCβ distal CTD has similar properties is not known.

In contrast, PLCβ3-Δ847 and PLCβ3-Δ892 adsorb uniformly across the surface of the monolayer, and high concentrations of these proteins result in monolayers that lack the distinctive peaks observed for the monolayer alone or upon addition of PLCβ3 (Figures 2.6 and Figure 2.7). This provides further support for the role of the distal CTD in targeting the enzyme to specific regions of the monolayer. PLCβ3-Δ847 and PLCβ3-Δ892 also have low basal activity relative to PLCβ3 (Figure 2.11, Figure 2.12, Table 2.3, and Table 2.4), and these differences in PIP_2 turnover may also contribute to the observed differences in the monolayer surface. In the case of PLCβ3-Δ892, these differences may be further explained by the presence of the proximal CTD, which we propose regulates activity, at least in part, by impairing binding of the catalytic core to the membrane[11].

The role of PIP_2 itself in promoting monolayer adsorption is ambiguous and difficult to assess, as it is also the canonical PLC substrate[19,20,58,64]. To greatly reduce the catalytic activity of our variants without compromising their ability to bind PIP_2, we introduced the H332A mutation within the PLCβ3 active site (Figure 2.9). PLCβ3 variants with the H332A mutation all adsorbed to the monolayer, and at low protein concentrations, had minimal effect on the appearance or topographical features of the monolayer (Figure 2.8B, Figure 2.13B, Figure 2.14, and Table 2.1). At higher protein concentrations, monolayers incubated with PLCβ3 H332A and PLCβ3-Δ847 H332A had clear, elevated peaks on the surface, similar to monolayers incubated with wild-type PLCβ3. However, monolayers incubated PLCβ3-Δ892 H332A had a more uniform appearance and a loss of topographical features, consistent with monolayers incubated with wild-type PLCβ3-Δ892. This could be due to the decrease in catalytic activity caused by the H332A mutation, in addition to the autoinhibition and regulation of catalytic core–membrane interactions imposed by the proximal CTD (Figure 2.13 and Figure 2.14).

The results herein suggest PLCβ3 could be preferentially adsorbed to regions of the membrane enriched in PIP_2. In cells, PIP_2 clusters could be generated through local synthesis, followed by the rapid recruitment of effectors, which include PLC enzymes[35,65–69]. PLCβ3 adsorption to these regions and subsequent PIP_2 hydrolysis could result in inhibition of second messenger signaling downstream of PLCβ, and would negatively regulate other signaling processes that rely on these same pools of PIP_2. For example, many ion channels, including KCNQ and GIRK channels, are regulated in part by the local concentration of PIP_2[69–72]. Another

possibility is that PIP_2-enriched regions may promote dimerization or oligomerization of PLCβ enzymes at the membrane[17,25,72]. By acting to increase the local PLCβ concentration at specific membrane microdomains, its activity could be further stimulated. Although there is little evidence to support dimerization of PLCβ in solution, the formation of oligomers at the membrane remains a possibility. Finally, the contributions of heterotrimeric G proteins in stimulating PLCβ activity and/or increasing its residence time at the membrane interface remain to be fully addressed. Thus, future AFM studies that integrate heterotrimeric G proteins, PLCβ, and the membrane will provide novel and more comprehensive insights into how PLCβ is regulated and how its activity may influence downstream signaling pathways.

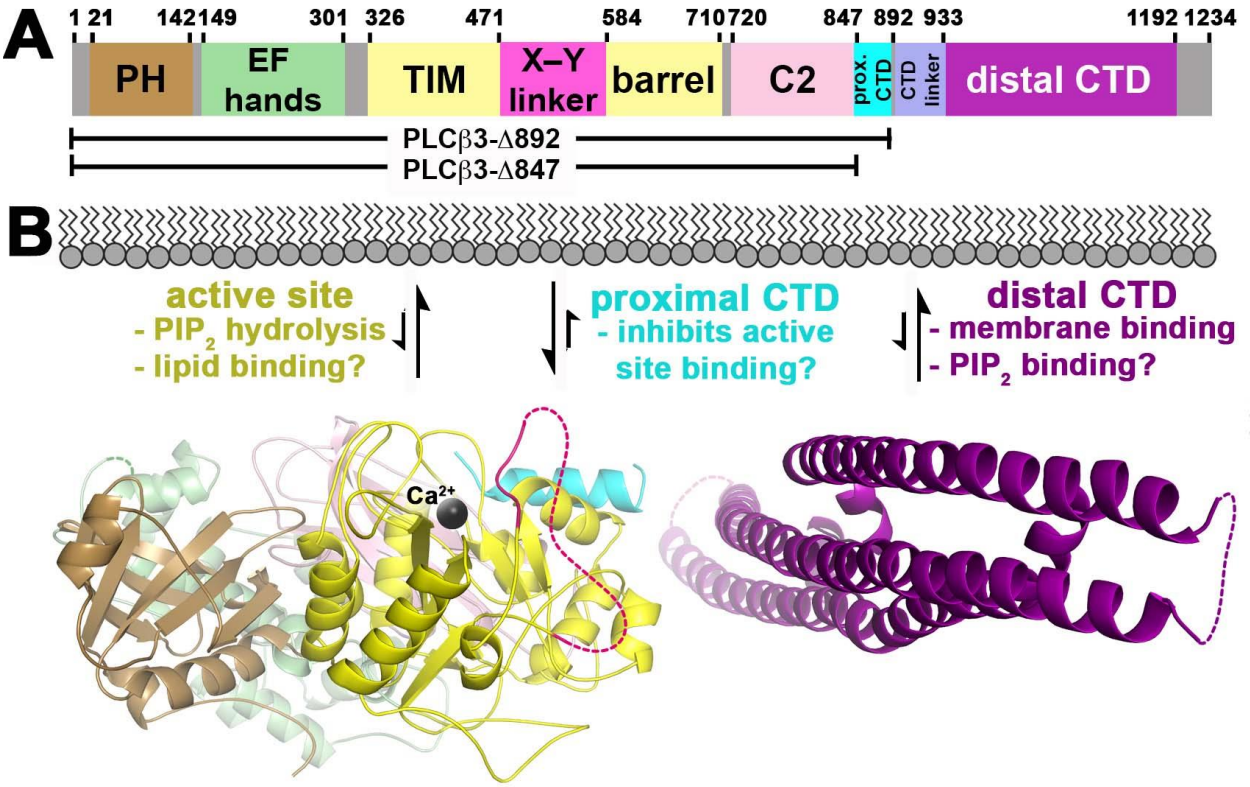

Figure 2.1. Primary Structure and Membrane Interactions of PLCβ3.
(A) Domain architecture of human PLCβ3. The numbers above correspond to amino acids at domain boundaries. The C-terminal truncations used in this study are shown below. PLCβ3-Δ847 corresponds to the catalytic core of the enzyme. (B) Model of full-length PLCβ3 at the membrane and the structural elements proposed to regulate membrane binding. In this model, PLCβ3 is oriented such that the active site, pleckstrin homology (PH), and the conserved basic surface of the distal CTD are in line with the membrane plane. The predicted contributions of the active site, proximal CTD, and distal CTD to membrane association are reflected in the relative size of the equilibrium arrows. Domains are colored as in (A). The disordered region of the X–Y linker is shown as a dashed hot pink line and disordered loops within the distal CTD as dashed purple lines. The active site Ca^{2+} is shown as a black sphere. The CTD linker, which connects the proximal and distal CTDs, is disordered in all structures and is not shown for clarity. This model is based on PDB ID 3OHM[14], 3QR0[15], and 4GNK[16].

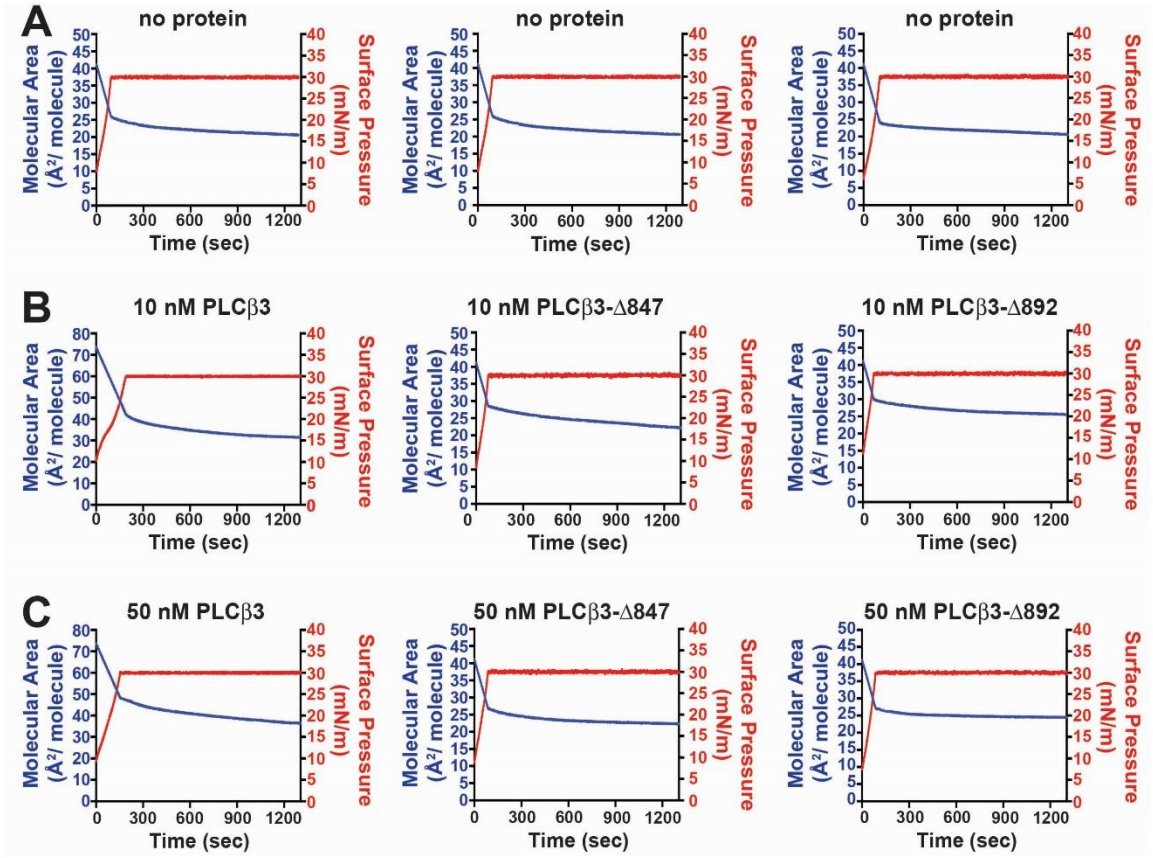

Figure 2.2. Representative Surface Area and Molecular Area versus Time Plots for PE:PIP_2 Monolayer Deposition in a Langmuir-Blodgett Trough.

(A) PE:PIP_2 monolayers alone or incubated with (B) 10 nM or (C) 50 nM PLCβ3, PLCβ3-Δ847, or PLCβ3-Δ892 at 20°C prior to Langmuir-Schaefer transfer of the film to HOPG. The blue and red traces show the molecular area and surface pressure, respectively, of the monolayer over time. The zero-time point reflects the molecular area and surface pressure of the system following the addition of the PE:PIP_2 mixture to the subphase. The barriers forming the monolayer were closed at a rate of 9.8 $Å^2$/chain/min, resulting in a gradual increase in surface pressure and a gradual decrease in molecular area until the desired surface pressure of 30 mN/m was achieved. The PLCβ3 variants were then added to the aqueous subphase, and incubated for 20 min. For each PLCβ3 variant tested, the molecular area at the time of protein addition for each independent monolayer varied by 5-10 $Å^2$/molecule. Protein adsorption to the monolayer, PIP_2 hydrolysis, and/or lipid peroxidation are detected as changes in the molecular area over the incubation period.

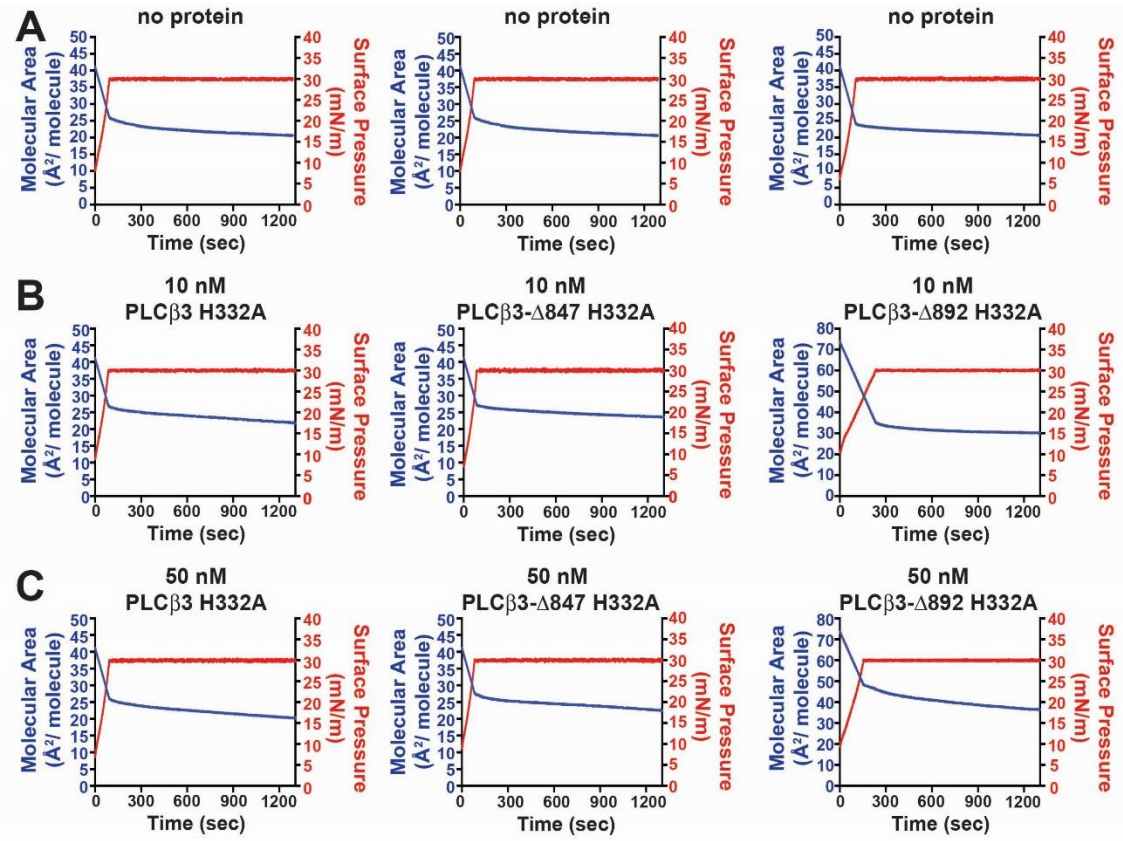

Figure 2.3. Representative Surface Area and Molecular Area versus Time Plots for PE:PIP_2 Monolayer Deposition in a Langmuir-Blodgett Trough.

(A) PE:PIP_2 monolayers alone or incubated with (B) 10 nM or (C) 50 nM PLCβ3 H332A, PLCβ3-Δ847 H332A, or PLCβ3-Δ892 H332A at 20°C prior to Langmuir-Schaefer transfer of the film to HOPG. Blue and red traces show the molecular area and surface pressure, respectively, of the monolayer as a function of time. Experiments were performed as described in Figure 2.2.

Table 2.1. Molecular Area Prior to Langmuir-Schaefer Transfer.

Variant	0 nM Protein	10 nM Protein	50 nM Protein
no protein	20.6 ± 0.15	24.0 ± 1.5	24.0 ± 0.96
PLCβ3		32.7 ± 1.3	36.3 ± 0.12
PLCβ3 H332A		21.3 ± 0.54	21.0 ± 0.73
-Δ847		22.5 ± 0.24	22.3 ± 0.10
-Δ847 H332A		23.9 ± 1.2	21.0 ± 1.4
-Δ892		24.0 ± 1.5	24.0 ± 0.96
-Δ892 H332A		30.4 ± 0.59	22.2 ± 0.34

The molecular area for the monolayer alone or incubated with PLCβ3 variants at 1200 s, immediately prior to Langmuir-Schaefer transfer of the monolayer. The data shown represent the average ± SEM from at least two independent monolayer adsorption experiments, with protein from two independent preparations.

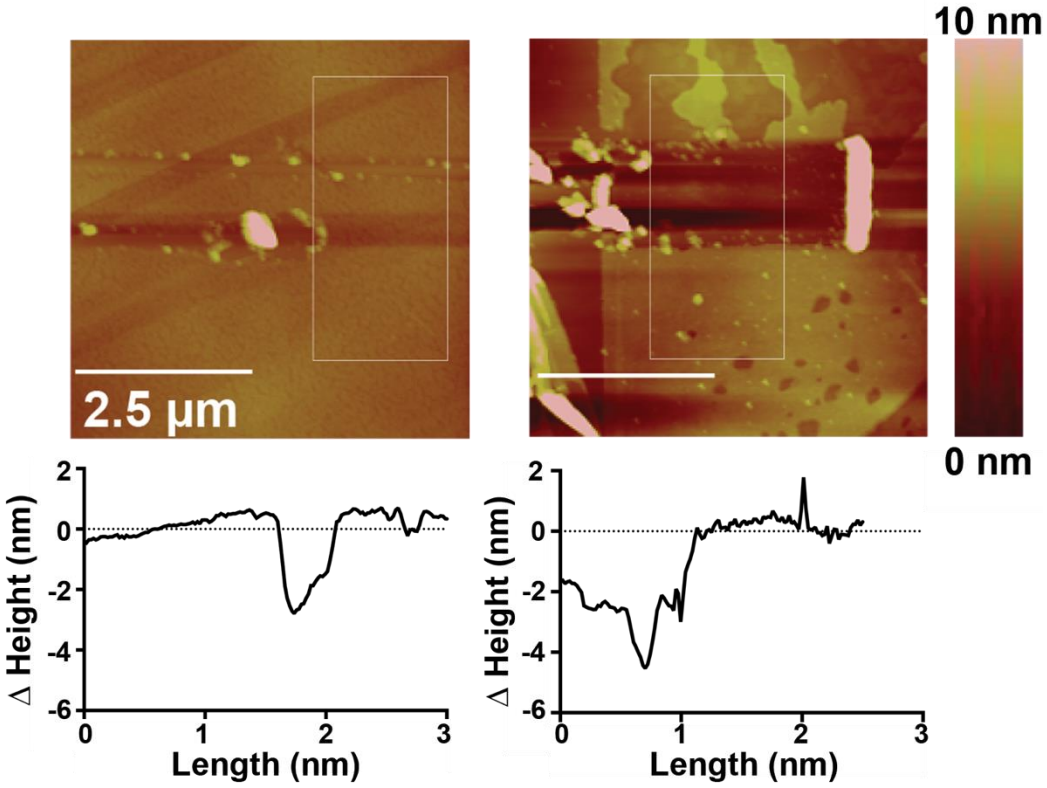

Figure 2.4. PE:PIP_2 Monolayers Can Be Transferred to HOPG by Langmuir-Schaefer Transfer. Two representative AFM tapping mode micrographs of PE:PIP_2 (7:3) monolayers compressed to 30 mN/m. The samples were etched using contact mode AFM to reveal the HOPG surface, and the change in height was determined by measuring the step height of the sample. The boxed area, outlined in white, shows the region of the monolayer used in the height measurement. The height of the monolayer (~2-3 nm) is consistent with the height of other previously characterized phospholipid monolayers.

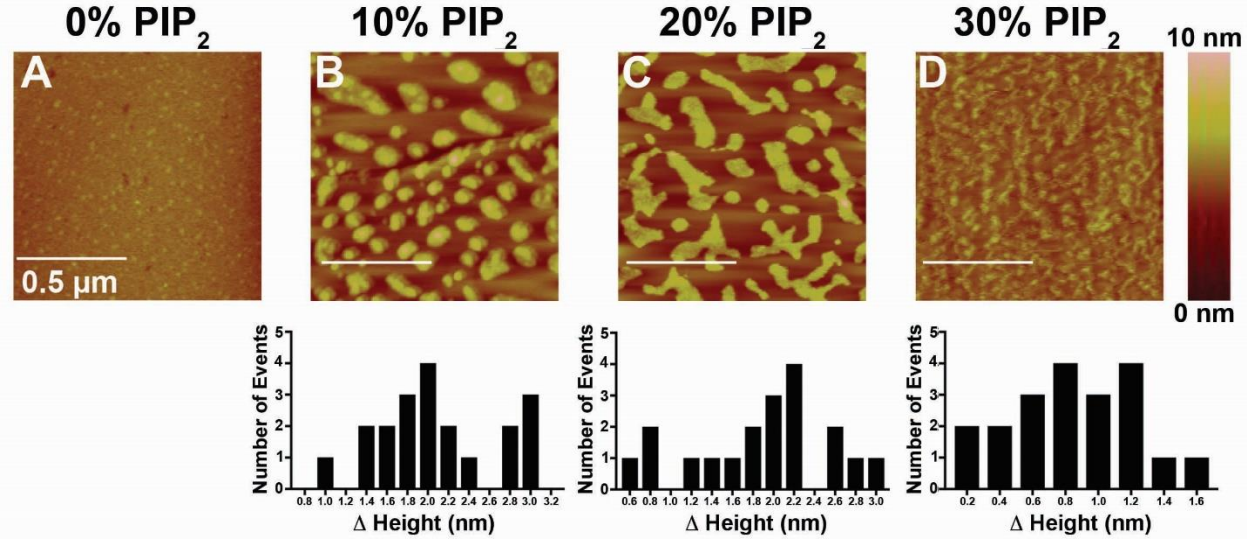

Figure 2.5. PIP_2 Promotes Formation of Surface Features in Compressed Lipid Monolayers. PE or PE:PIP_2 monolayers were spread and compressed to 30 mN/m using a Langmuir trough. Monolayer samples were then transferred to HOPG using the Langmuir-Schaefer method and imaged using tapping mode AFM. Surfaces are colored such that lighter colors correspond to regions elevated in height with respect to the monolayer surface. Representative images for each monolayer composition are shown. (A) The PE monolayer displays a relatively uniform surface. Addition of (B) 10% PIP_2 or (C) 20% PIP_2 yields clustered regions elevated in height with respect to the rest of the monolayer. (D) Addition of 30% PIP_2 results in the formation of smaller dispersed clusters across the monolayer surface. Shown below each PE:PIP_2 monolayer are histograms quantifying the height and frequency of twenty surface features from at least two independent monolayers. At low PIP_2 concentrations, the monolayer features taller clusters, whereas the clustered regions are on average shorter in monolayers containing 30% PIP_2.

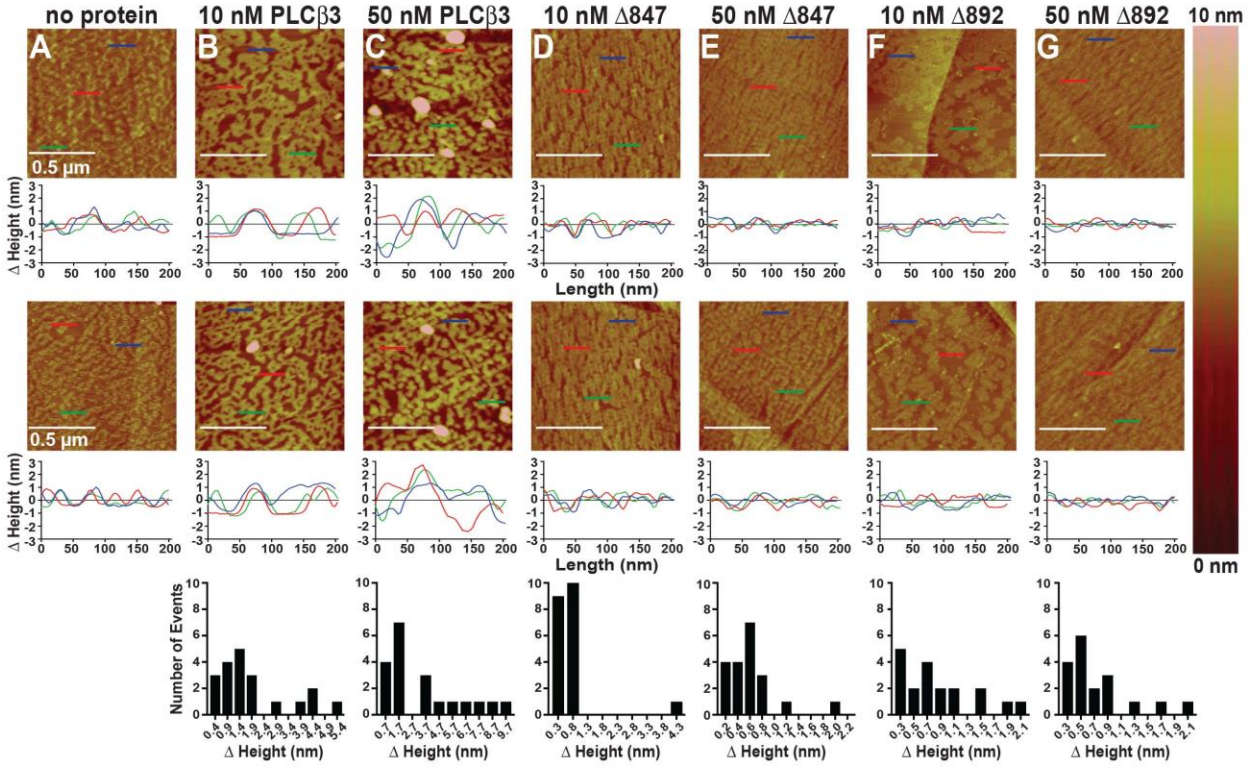

Figure 2.6. Representative AFM Tapping Mode Height Images of PE:PIP_2 Monolayers Alone or Incubated with PLCβ3 Variants for 20 min at Room Temperature.

Two representative images for each condition are shown, with sample variation most likely due to differences in the HOPG surface used in the Langmuir-Schaefer transfer. Protein adsorption is reflected by relative increases in height across the monolayer surface, shown in lighter colors. Below each micrograph are cross-sectional analyses from three representative scans across the surface. The color of the cross-section corresponds to the region of the monolayer depicted. Relative changes in topography are detected as changes in the height and appearance of the monolayer surface. For each monolayer, the change in height for twenty surface features was measured from at least two independent monolayer samples, and the frequencies of each height range were quantified. This data is shown as histograms below each protein concentration. (A) Monolayer in the absence of protein or incubated with (B) 10 nM PLCβ3, (C) 50 nM PLCβ3, (D) 10 nM PLCβ3-Δ847, (E) 50 nM PLCβ3-Δ847, (F) 10 nM PLCβ3-Δ892, and (G) 50 nM PLCβ3-Δ892 for 20 min at 20 °C prior to Langmuir-Schaefer transfer of the film.

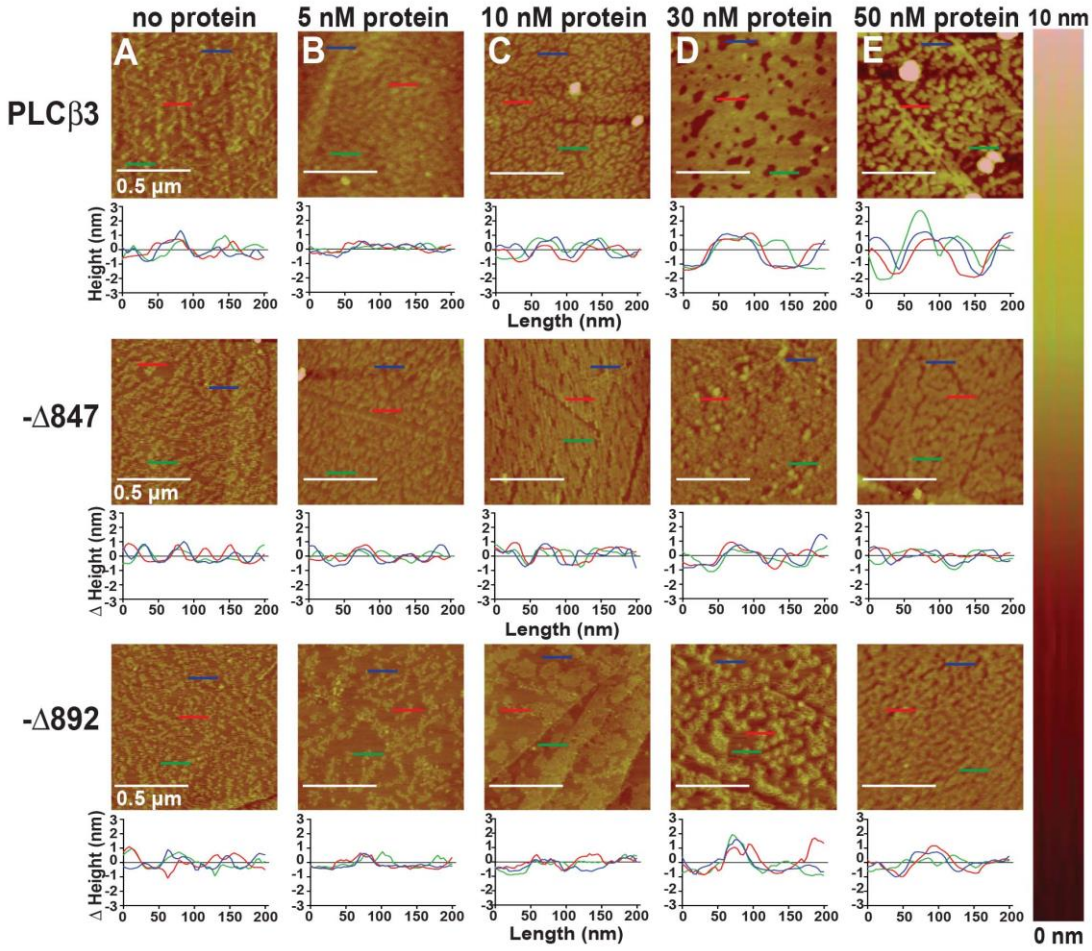

Figure 2.7. Representative AFM Tapping Mode Micrographs of PE:PIP_2 Monolayers Compressed to 30 mN/m Alone or Incubated with Increasing Concentrations of PLCβ3, PLCβ3-Δ847, or PLCβ3-Δ892.

(A) Monolayers in the absence of protein or incubated for 20 min at 20°C with (B) 5 nM PLCβ3 variant, (C) 10 nM PLCβ3 variant, (D) 30 nM PLCβ3 variant, and (E) 50 nM PLCβ3 variant. After 20 min, samples were collected via Langmuir-Schaefer transfer of the film to HOPG. Protein adsorption is reflected by increases in the relative height of the monolayer surface, which are shown in the lighter colors. Below each micrograph are representative cross-sectional plots from three distinct regions of the surface, depicted as colored lines on the micrograph. The color of the trace corresponds to the representative regions of the monolayer depicted. Changes in topography are detected as changes in the relative height of surface features along the cross-section. These trends are observed across at least three independently prepared monolayers and represent at least two independent protein preparations.

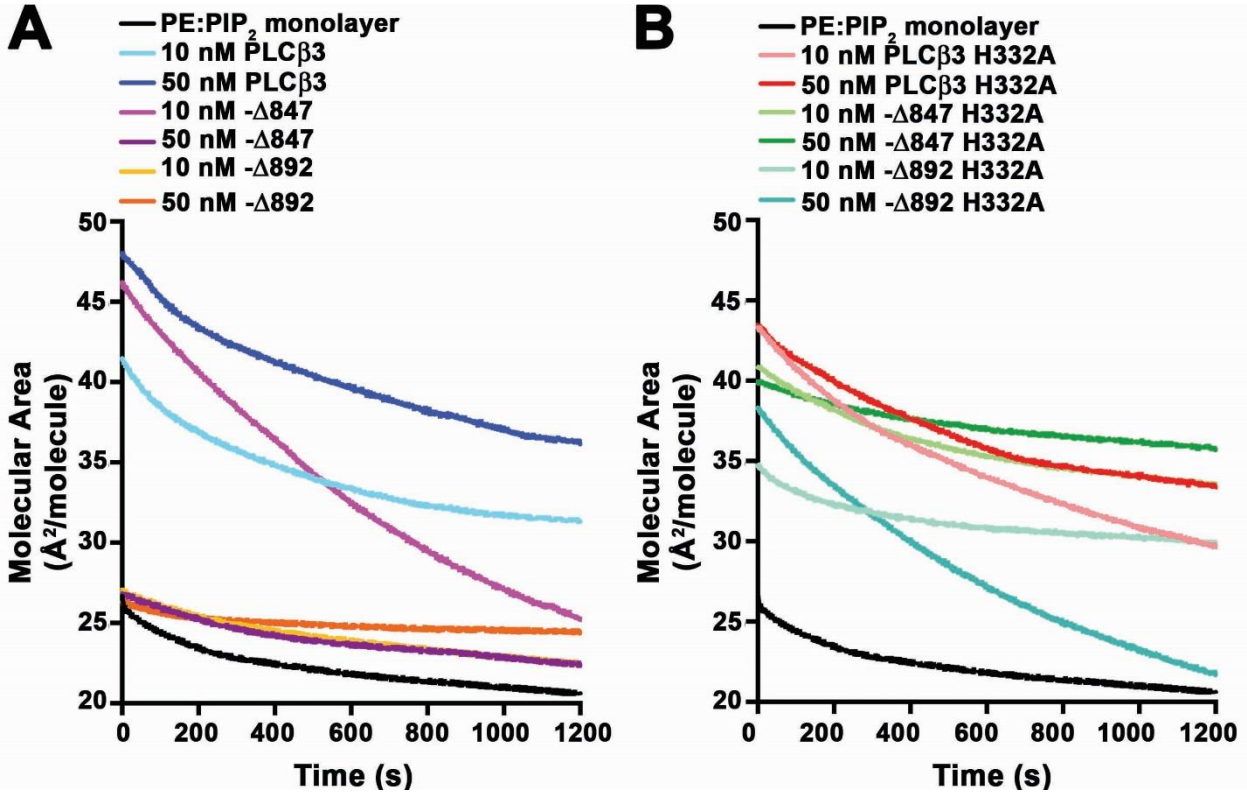

Figure 2.8. Representative Plots for the Decrease in the Molecular Area of the Monolayer Alone and Upon Addition of PLCβ3 Variants.

In all experiments, the monolayer was first compressed to a surface pressure of 30 mN/m, followed by addition of the PLCβ3 variants to the subphase. The zero time point corresponds to the molecular area of the monolayer immediately following the addition of the PLCβ3 variant to the subphase. All experiments were performed at 20 ˚C, and the surface pressure maintained at 30 mN/m. At 1200 s, Langmuir-Schaefer transfer of representative monolayer samples to HOPG was carried out, followed by AFM analysis. In the absence of protein, the decrease in the molecular area of the monolayer is due to spontaneous lipid oxidation over the incubation period. Changes in the molecular area of the monolayer in the presence of protein are due to spontaneous oxidation, protein adsorption to the monolayer, and PIP_2 hydrolysis over the 20 min incubation period. For each protein and each protein concentration assessed, at least two independent monolayers were prepared, with protein from at least two independent preparations. (A) Changes in the molecular area of the monolayer upon addition of PLCβ3, PLCβ3-Δ847, and PLCβ3-Δ892. (B) Changes in the molecular area of the monolayer upon addition of PLCβ3 H332A, PLCβ3-Δ847 H332A, and PLCβ3-Δ892 H332A.

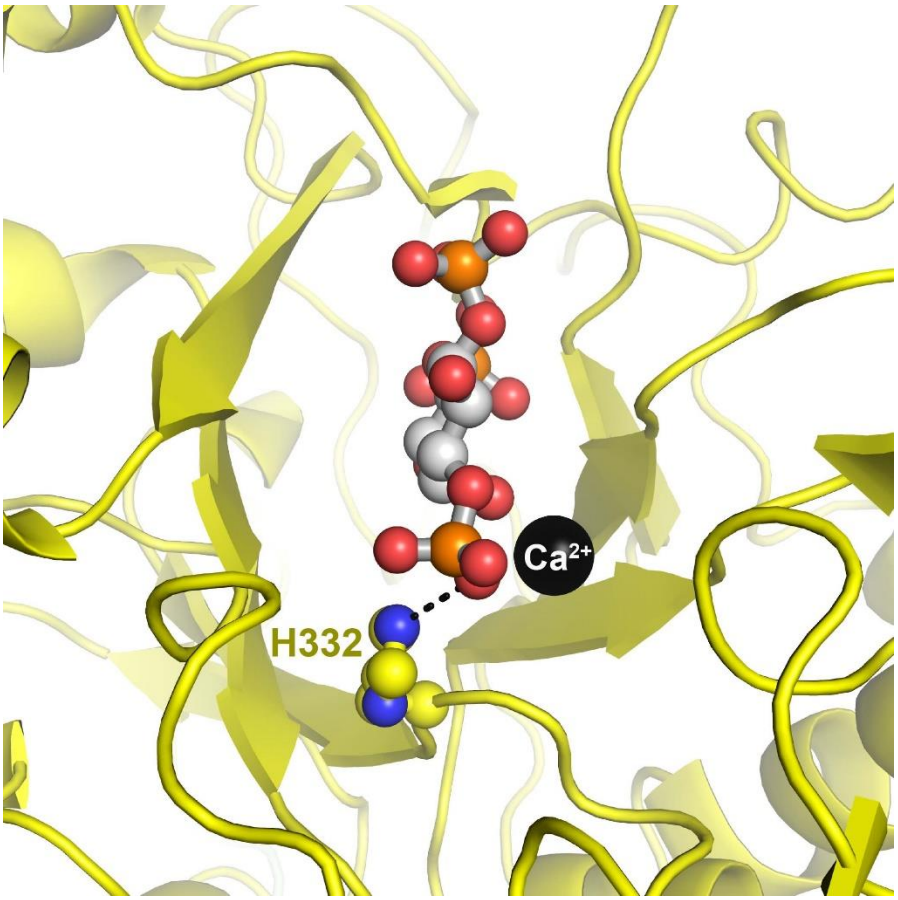

Figure 2.9. View of the PLCβ3 Active Site Bound to IP_3.
IP_3 (shown in gray ball and stick representation) is the product of the PIP_2 hydrolysis reaction (PDB ID 4QJ4).[15] The calcium ion required for catalysis is shown as a black sphere. His332 (side chain shown in ball and stick representation) forms a hydrogen bond with the 1-phosphate group of IP_3. This interaction is proposed to stabilize the transition state of the reaction.

Table 2.2. Thermal Stability of PLCβ3 Variants.

PLCβ3 Variant	Protein T_m ± SEM (°C)	Protein + 5 mM IP_3 T_m ± SEM (°C)
PLCβ3	52 ± 2.1	53 ± 0.96
PLCβ3 H332A	54.9 ± 0.80	59.4 ± 0.12[1]
-Δ847	54.5 ± 0.53	57.4 ± 0.14[2]
-Δ847 H332A	52.6 ± 0.35	54.5 ± 0.28
- Δ892	60.1 ± 0.32	63.0 ± 0.20[3]
-Δ892 H332A	60.2 ± 0.08	62.3 ± 0.07

The data represent at least 3 experiments performed in triplicate from at least two purifications (Figure 2.10). [1]Significant relative to PLCβ3 H332A, $p \leq 0.01$. [2]Significant relative to –Δ847, $p \leq 0.5$. [3]Significant relative to –Δ892, $p \leq 0.5$.

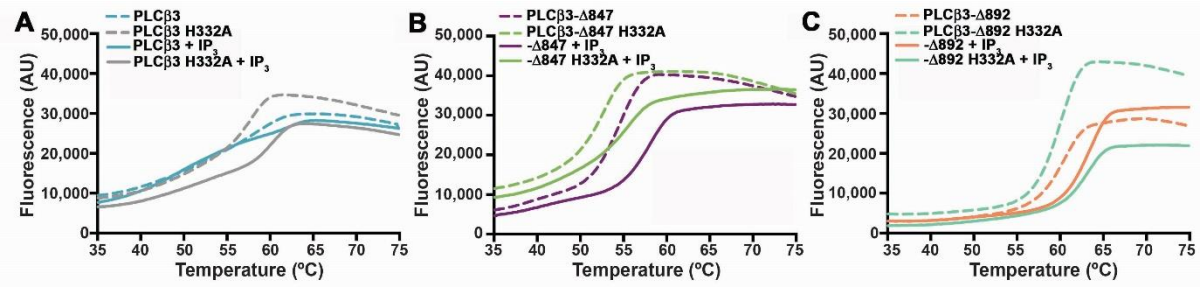

Figure 2.10. Representative DSF Curves of PLCβ3 Variants Alone and in the Presence of IP_3. In these experiments, PLCβ3 variants alone (dashed lines) or in the presence of IP_3 (solid lines) are incubated with a fluorescent dye, and the change in fluorescence is monitored as a function of temperature. The inflection point corresponds to the melting temperature T_m of the protein. IP_3 binding is detected as an increase in thermal stability, as evidenced by a rightward shift in the curve.[15] (A) PLCβ3 (blue lines) and PLCβ3 H332A (gray lines) are stabilized by the addition of IP_3, as are (B) PLCβ3-Δ847 (purple lines) and PLCβ3-Δ847 H332A and (C) PLCβ3-Δ892 (orange lines) and PLCβ3-Δ892 H332A (teal lines).

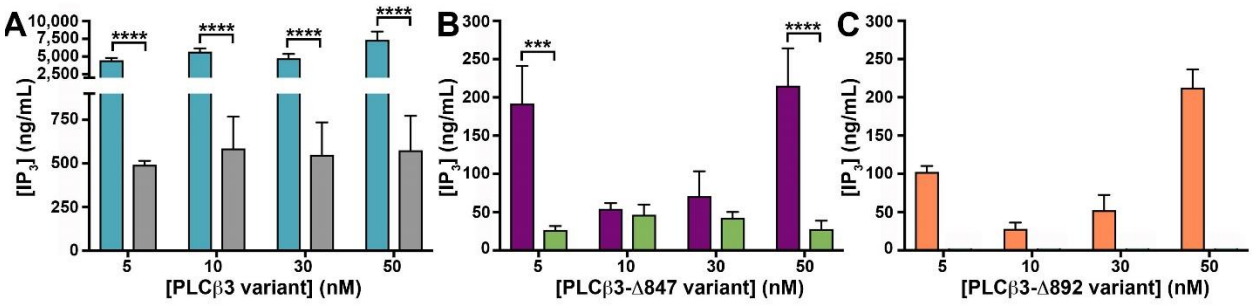

Figure 2.11. PLCβ3 Variants Hydrolyze PIP_2 at the Monolayer as Detected by Mass Spectrometry.

(A) PLCβ3 (cyan bars) is significantly more active than PLCβ3 H332A (grey) at all protein concentrations tested (****, $p \leq 0.0001$). (B) PLCβ3-Δ847 (purple) and PLCβ3-Δ847 H332A (green) hydrolyze PIP_2 to a lesser extent than PLCβ3. PLCβ3-Δ847 H332A is less active than PLCβ3-Δ847 (at 5 nM protein, ***, $p = 0.0001$, at 50 nM protein, **** $p \leq 0.0001$). (C) PLCβ3-Δ892 (orange) exhibits a further decrease in PIP_2 hydrolysis at the monolayer with respect to PLCβ3-Δ847, but IP_3 was not detected in the subphase for monolayers incubated at any PLCβ3-Δ892 H332A concentration tested. Data shown are the mean ± SEM of IP_3 from at least two independent monolayers and two separate protein preparations. Statistical significance was determined using 2-way ANOVA analysis.

Table 2.3. Quantitation of IP_3 from Monolayer Subphases.

	PLCβ3 (nM)	IP_3 (ng/mL)	Activity (nmol IP_3/min/nmol PLCβ3 variant)
PLCβ3	5[1]	4500 ± 190	0.02 ± 0.001
	10[1]	5700 ± 260	0.02 ± 0.0007
	30[1]	4800 ± 350	0.004 ± 0.0003
	50[1]	7400 ± 820	0.004 ± 0.0004
PLCβ3 H332A	5	490 ± 13	0.003 ± 0.00007
	10	590 ± 130	0.002 ± 0.0004
	30	460 ± 100	0.0004 ± 0.00009
	50	460 ± 26	0.0003 ± 0.00001
-Δ847[2]	5[2]	190 ± 30	0.0007 ± 0.0001
	10	54 ± 6	0.0001 ± 0.00001
	30	71 ± 23	0.00004 ± 0.00001
	50[3]	220 ± 30	0.00008 ± 0.00001
-Δ847 H332A	5	30 ± 3	0.0001 ± 0.00001
	10	50 ± 8	0.00009 ± 0.00002
	30	40 ± 5	0.00002 ± 0.000003
	50	30 ± 8	0.00001 ± 0.000003
-Δ892	5	100 ± 6	0.0004 ± 0.00002
	10	30 ± 6	0.00006 ± 0.00001
	30	50 ± 14	0.00003 ± 0.000009
	50	210 ± 13	0.00008 ± 0.000005
-Δ892 H332A	5	ND	ND
	10	ND	ND
	30	ND	ND
	50	ND	ND

The data represent subphases collected from at least two independent monolayers for each protein variant, and concentration tested. Values shown are the mean ± SEM. Significance was determined using a 2-way ANOVA for each PLCβ3 variant and its corresponding H332A point mutant. [1]Significant relative to PLCβ3 H332A $p \leq 0.0001$. [2]Significant relative to 5 nM PLCβ3-Δ847 H332A, $p \leq 0.0001$, [3]Significant relative to 50 nM PLCβ3-Δ847 H332A, $p \leq 0.0001$. ND, not detected.

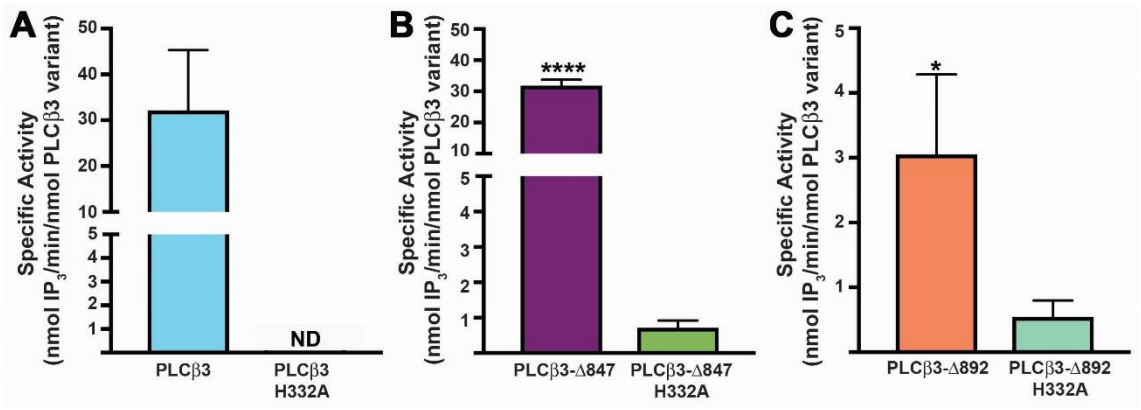

Figure 2.12. The Basal Activities of the PLCβ3 Variants and Their Respective H332A Mutants. (A) PLCβ3, (B) PLCβ3-Δ847, (C) PLCβ3-Δ892 and their respective H332A mutants were determined using a liposome-based activity assay. Proteins were incubated with [^{3}H]-PIP_2-containing liposomes for increasing times, and free [^{3}H]-IP_3 was detected by scintillation counting. Assays contained ~200 nM free Ca^{2+} relative to controls that lacked Ca^{2+}. PLCβ3 variants were compared to their respective H332A mutant and assessed using an unpaired t-test. Significance is denoted as follows: ****, $p \leq 0.0001$ and *, $p \leq 0.4$.

Table 2.4. Specific Activity of PLCβ3 variants.

	Specific Activity (nmol IP_3/min/nmol PLCβ3 Variant)
PLCβ3	37 ± 6
PLCβ3 H332A (0.5 ng/μL)	ND
PLCβ3 H332A (2.5 ng/μL)	ND
PLCβ3-Δ847[1]	33 ± 2
PLCβ3-Δ847 H332A (4 ng/μL)	ND
PLCβ3-Δ847 H332A (20 ng/μL)	0.7 ± 0.1
PLCβ3-Δ892[2,3]	3.0 ± 0.6
PLCβ3-Δ892 (12 ng/μL)	ND
PLCβ3-Δ892 (60 ng/μL)	0.7 ± 0.3

The data represent at least three independent assays performed in duplicate from at least two protein preparations. Values shown represent the mean ± SEM. For comparisons of the PLCβ3 variant specific activity to their respective H332A mutant, unpaired t-tests were performed. [1]Significant relative to PLCβ3-Δ847 H332A, $p \leq 0.0001$. [2]Significant relative to 12 ng/μL PLCβ3-Δ892 H332A, $p \leq 0.04$. [3]Significant relative to 60 ng/μL PLCβ3-Δ892 H332A, $p \leq 0.08$. ND, not detected.

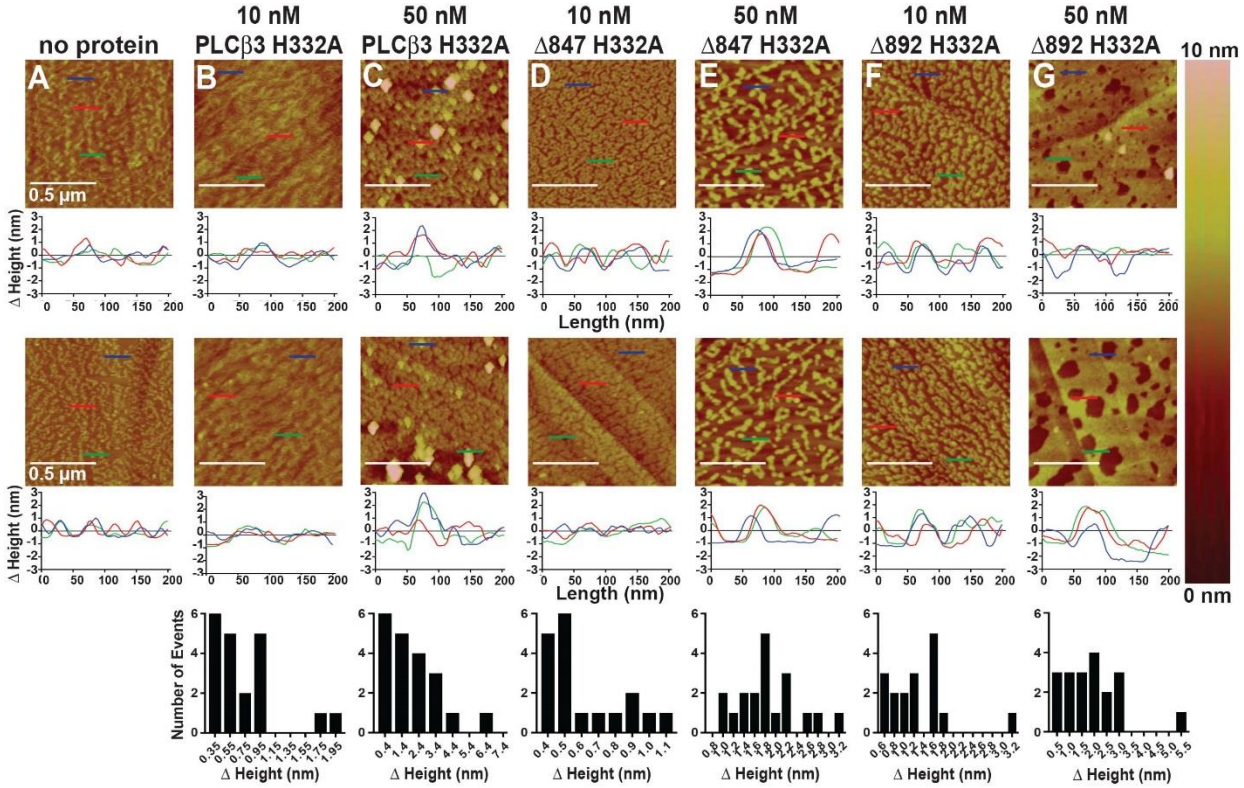

Figure 2.13. Representative AFM Tapping Mode Height Images of PE:PIP_2 Monolayers Alone or Incubated with PLCβ3 H332A Variants.

Two representative images for each condition are shown. Protein adsorption is reflected by relative increases in height across the monolayer surface, shown in lighter colors. Below each micrograph are cross-sectional analyses from three representative regions from the surface. The color of the cross-section corresponds to the region of the monolayer depicted. Relative changes in topography are detected as changes in the height and appearance of the monolayer surface. For each monolayer, the change in height for twenty surface features was measured from at least two independent monolayer samples, and the frequencies of each height range were quantified. This data is shown as histograms below each protein concentration. (A) Monolayer in the absence of protein or incubated with (B) 10 nM PLCβ3 H332A, (C) 50 nM PLCβ3 H332A, (D) 10 nM PLCβ3-Δ847 H332A, (E) 50 nM PLCβ3-Δ847 H332A, (F) 10 nM PLCβ3-Δ892 H332A, and (G) 50 nM PLCβ3-Δ892 H332A for 20 min at 20 °C prior to Langmuir-Schaefer transfer of the film.

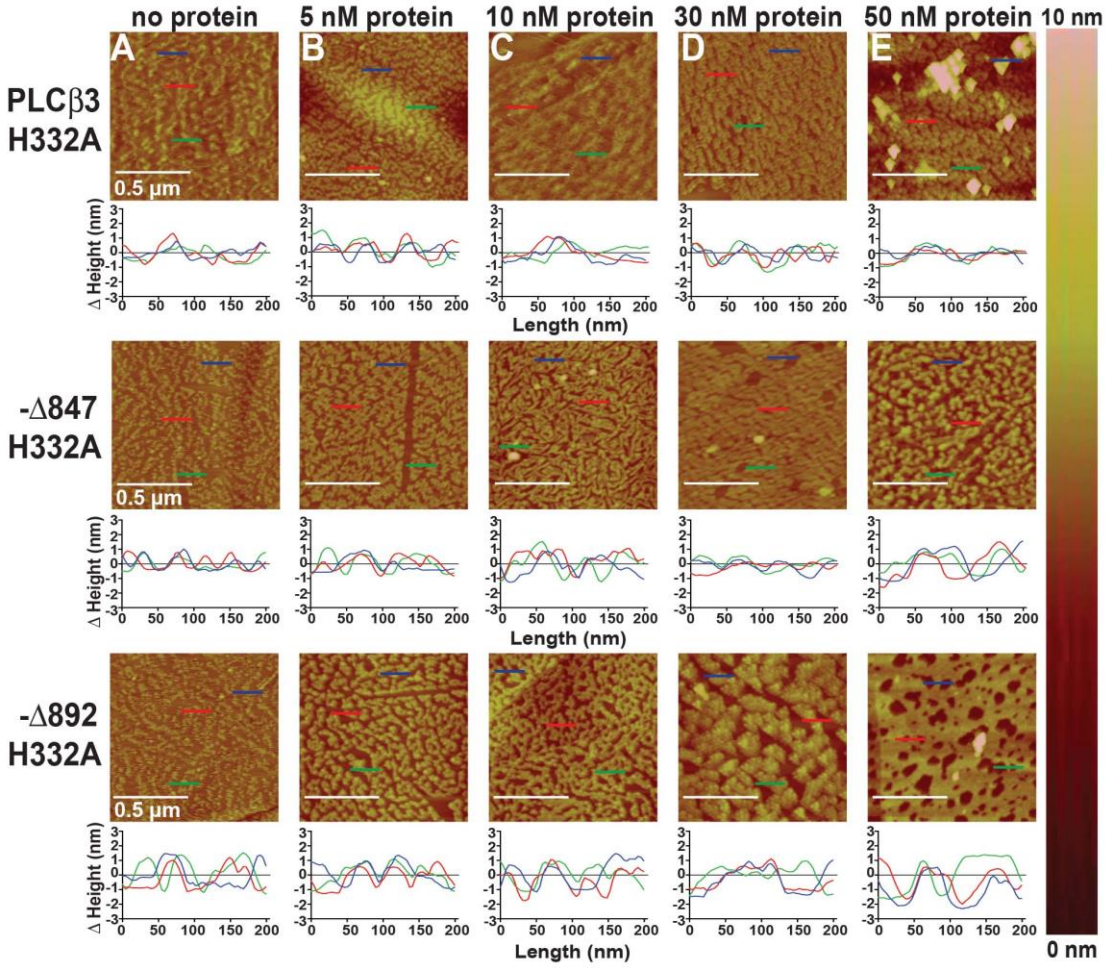

Figure 2.14. Representative AFM Tapping Mode Micrographs of PE:PIP_2 Monolayers Compressed to 30 mN/m Alone or Incubated for 20 min at 20°C with Increasing Concentrations of PLCβ3 H332A Mutants.

Monolayers incubated alone (A) or in the presence of (B) 5 nM PLCβ3 H332A variant, (C) 10 nM PLCβ3 H332A variant, (D) 30 nM PLCβ3 H332A variant, and (E) 50 nM PLCβ3 H332A variant. After 20 minutes, samples were collected via Langmuir-Schaefer transfer of the film to HOPG. Protein adsorption is reflected by increases in the relative height of the monolayer surface, which are shown in the lighter colors. Below each micrograph are representative cross-sectional plots from three distinct regions of the surface, depicted as colored lines on the micrograph. The color of the trace corresponds to the region of the monolayer depicted. Changes in topography are detected as changes in the relative height of surface features along the cross-section. These trends are observed across at least three independently prepared monolayers and represent at least two independent protein preparations.

2.5 References

(1) Kadamur, G.; Ross, E. M. Mammalian Phospholipase C. *Annu. Rev. Physiol.* **2013**, *75* (1), 127–154. https://doi.org/10.1146/annurev-physiol-030212-183750.

(2) Lyon, A. M.; Tesmer, J. J. G. Structural Insights into Phospholipase C-β Function. *Mol. Pharmacol.* **2013**, *84* (4), 488–500. https://doi.org/10.1124/mol.113.087403.

(3) Filtz, T. M.; Grubb, D. R.; McLeod-Dryden, T. J.; Luo, J.; Woodcock, E. A. Gq-Initiated Cardiomyocyte Hypertrophy Is Mediated by Phospholipase Cβ1b. *FASEB J.* **2009**, *23* (10), 3564–3570. https://doi.org/10.1096/fj.09-133983.

(4) Grubb, D. R.; Luo, J.; Woodcock, E. A. Phospholipase Cβ1b Directly Binds the SH3 Domain of Shank3 for Targeting and Activation in Cardiomyocytes. *Biochem. Biophys. Res. Commun.* **2015**, *461* (3), 519–524. https://doi.org/10.1016/j.bbrc.2015.04.060.

(5) Atef, M. E.; Anand-Srivastava, M. B. Oxidative Stress Contributes to the Enhanced Expression of Gαq/PLCβ1 Proteins and Hypertrophy of VSMC from SHR: Role of Growth Factor Receptor Transactivation. *Am. J. Physiol. - Heart Circ. Physiol.* **2016**, *310* (5), H608–H618. https://doi.org/10.1152/ajpheart.00659.2015.

(6) Woodcock, E. A.; Grubb, D. R.; Filtz, T. M.; Marasco, S.; Luo, J.; McLeod-Dryden, T. J.; Kaye, D. M.; Sadoshima, J.; Du, X.-J.; Wong, C.; et al. Selective Activation of the "b" Splice Variant of Phospholipase Cβ1 in Chronically Dilated Human and Mouse Atria. *J. Mol. Cell. Cardiol.* **2009**, *47* (5), 676–683. https://doi.org/10.1016/j.yjmcc.2009.08.020.

(7) Dent, M. R.; Dhalla, N. S.; Tappia, P. S. Phospholipase C Gene Expression, Protein Content, and Activities in Cardiac Hypertrophy and Heart Failure Due to Volume Overload. *Am. J. Physiol. - Heart Circ. Physiol.* **2004**, *287* (2), H719–H727. https://doi.org/10.1152/ajpheart.01107.2003.

(8) Bianchi, E.; Norcini, M.; Smrcka, A.; Ghelardini, C. Supraspinal Gβγ-Dependent Stimulation of PLCβ3 Originating from G Inhibitory Protein-μ Opioid Receptor-Coupling Is Necessary for Morphine Induced Acute Hyperalgesia. *J. Neurochem.* **2009**, *111* (1), 171–180. https://doi.org/10.1111/j.1471-4159.2009.06308.x.

(9) Mathews, J. L.; Smrcka, A. V.; Bidlack, J. M. A Novel Gβγ-Subunit Inhibitor Selectively Modulates μ-Opioid-Dependent Antinociception and Attenuates Acute Morphine-Induced Antinociceptive Tolerance and Dependence. *J. Neurosci.* **2008**, *28* (47), 12183–12189. https://doi.org/10.1523/JNEUROSCI.2326-08.2008.

(10) Hicks, S. N.; Jezyk, M. R.; Gershburg, S.; Seifert, J. P.; Harden, T. K.; Sondek, J. General and Versatile Autoinhibition of PLC Isozymes. *Mol. Cell* **2008**, *31* (3), 383–394. https://doi.org/10.1016/j.molcel.2008.06.018.

(11) Lyon, A. M.; Begley, J. A.; Manett, T. D.; Tesmer, J. J. G. Molecular Mechanisms of PLCβ3 Autoinhibition. *Struct. Lond. Engl. 1993* **2014**, *22* (12), 1844–1854. https://doi.org/10.1016/j.str.2014.10.008.

(12) Zhang, W.; Neer, E. J. Reassembly of Phospholipase C-Beta2 from Separated Domains: Analysis of Basal and G Protein-Stimulated Activities. *J. Biol. Chem.* **2001**, *276* (4), 2503–2508. https://doi.org/10.1074/jbc.M003562200.

(13) Charpentier, T. H.; Waldo, G. L.; Barrett, M. O.; Huang, W.; Zhang, Q.; Harden, T. K.; Sondek, J. Membrane-Induced Allosteric Control of Phospholipase C-β Isozymes. *J. Biol. Chem.* **2014**, *289* (43), 29545–29557. https://doi.org/10.1074/jbc.M114.586784.

(14) Waldo, G. L.; Ricks, T. K.; Hicks, S. N.; Cheever, M. L.; Kawano, T.; Tsuboi, K.; Wang, X.; Montell, C.; Kozasa, T.; Sondek, J.; et al. Kinetic Scaffolding Mediated by a Phospholipase C–β and Gq Signaling Complex. *Science* **2010**, *330* (6006), 974–980. https://doi.org/10.1126/science.1193438.

(15) Lyon, A. M.; Tesmer, V. M.; Dhamsania, V. D.; Thal, D. M.; Gutierrez, J.; Chowdhury, S.; Suddala, K. C.; Northup, J. K.; Tesmer, J. J. G. An Autoinhibitory Helix in the C-Terminal Region of Phospholipase C-β Mediates Gαq Activation. *Nat. Struct. Mol. Biol.* **2011**, *18* (9), 999–1005. https://doi.org/10.1038/nsmb.2095.

(16) Lyon, A. M.; Dutta, S.; Boguth, C. A.; Skiniotis, G.; Tesmer, J. J. G. Full-Length Gαq–Phospholipase C-B3 Structure Reveals Interfaces of the C-Terminal Coiled-Coil Domain. *Nat. Struct. Mol. Biol.* **2013**, *20* (3), 355–362. https://doi.org/10.1038/nsmb.2497.

(17) Singer, A. U.; Waldo, G. L.; Harden, T. K.; Sondek, J. A Unique Fold of Phospholipase C-Beta Mediates Dimerization and Interaction with G Alpha q. *Nat. Struct. Biol.* **2002**, *9* (1), 32–36. https://doi.org/10.1038/nsb731.

(18) Illenberger, D.; Walliser, C.; Nurnberg, B.; Diaz Lorente, M.; Gierschik, P. Specificity and Structural Requirements of Phospholipase C-Beta Stimulation by Rho GTPases versus G Protein Beta Gamma Dimers. *J. Biol. Chem.* **2003**, *278* (5), 3006–3014. https://doi.org/10.1074/jbc.M208282200.

(19) Jenco, J. M.; Becker, K. P.; Morris, A. J. Membrane-Binding Properties of Phospholipase C-Beta1 and PhospholipaseC-Beta2: Role of the C-Terminus and Effects of Polyphosphoinositides, G-Proteins and Ca2+. *Biochem. J.* **1997**, *327* (Pt 2), 431–437.

(20) Romoser, V.; Ball, R.; Smrcka, A. V. Phospholipase C B2 Association with Phospholipid Interfaces Assessed by Fluorescence Resonance Energy Transfer G Protein Bγ Subunit-Mediated Translocation is Not Required For Enzyme Activation. *J. Biol. Chem.* **1996**, *271* (41), 25071–25078. https://doi.org/10.1074/jbc.271.41.25071.

(21) Illenberger, D.; Walliser, C.; Strobel, J.; Gutman, O.; Niv, H.; Gaidzik, V.; Kloog, Y.; Gierschik, P.; Henis, Y. I. Rac2 Regulation of Phospholipase C-Beta 2 Activity and Mode of Membrane Interactions in Intact Cells. *J. Biol. Chem.* **2003**, *278* (10), 8645–8652. https://doi.org/10.1074/jbc.M211971200.

(22) Schnabel, P.; Camps, M.; Carozzi, A.; Parker, P. J.; Gierschik, P. Mutational Analysis of Phospholipase C-B2. *Eur. J. Biochem.* **1993**, *217* (3), 1109–1115. https://doi.org/10.1111/j.1432-1033.1993.tb18343.x.

(23) Kim, C. G.; Park, D.; Rhee, S. G. The Role of Carboxyl-Terminal Basic Amino Acids in Gqα-Dependent Activation, Particulate Association, and Nuclear Localization of Phospholipase C-B1. *J. Biol. Chem.* **1996**, *271* (35), 21187–21192. https://doi.org/10.1074/jbc.271.35.21187.

(24) Park, D.; Jhon, D. Y.; Lee, C. W.; Ryu, S. H.; Rhee, S. G. Removal of the Carboxyl-Terminal Region of Phospholipase C-Beta 1 by Calpain Abolishes Activation by G Alpha q. *J. Biol. Chem.* **1993**, *268* (5), 3710–3714.

(25) Ilkaeva, O.; Kinch, L. N.; Paulssen, R. H.; Ross, E. M. Mutations in the Carboxyl-Terminal Domain of Phospholipase C-B1 Delineate the Dimer Interface and a Potential GαqInteraction Site. *J. Biol. Chem.* **2002**, *277* (6), 4294–4300. https://doi.org/10.1074/jbc.M109612200.

(26) Sahu, S.; Philip, F.; Scarlata, S. Hydrolysis Rates of Different Small Interfering RNAs (SiRNAs) by the RNA Silencing Promoter Complex, C3PO, Determines Their Regulation by Phospholipase Cβ. *J. Biol. Chem.* **2014**, *289* (8), 5134–5144. https://doi.org/10.1074/jbc.M113.531467.

(27) Sahu, S.; Williams, L.; Perez, A.; Philip, F.; Caso, G.; Zurawsky, W.; Scarlata, S. Regulation of the Activity of the Promoter of RNA- induced Silencing, C3PO. *Protein Sci. Publ. Protein Soc.* **2017**, *26* (9), 1807–1818. https://doi.org/10.1002/pro.3219.

(28) Yerramilli, V. S.; Scarlata, S. The Breast Cancer Susceptibility Gene Product (γ-Synuclein) Alters Cell Behavior through It Interaction with Phospholipase Cβ. *Cell. Signal.* **2016**, *28* (1), 91–99. https://doi.org/10.1016/j.cellsig.2015.10.018.

(29) Narayanan, V.; Guo, Y.; Scarlata, S. Fluorescence Studies Suggest a Role for α-Synuclein in the Phosphatidylinositol Lipid Signaling Pathway. *Biochemistry* **2005**, *44* (2), 462–470. https://doi.org/10.1021/bi0487140.

(30) Guo, Y.; Rosati, B.; Scarlata, S. α–Synuclein Increases the Cellular Level of Phospholipase Cβ1. *Cell. Signal.* **2012**, *24* (5), 1109–1114. https://doi.org/10.1016/j.cellsig.2012.01.007.

(31) Kan, W.; Adjobo-Hermans, M.; Burroughs, M.; Faibis, G.; Malik, S.; Tall, G. G.; Smrcka, A. V. M3 Muscarinic Receptor Interaction with Phospholipase C B3 Determines Its Signaling Efficiency. *J. Biol. Chem.* **2014**, *289* (16), 11206–11218. https://doi.org/10.1074/jbc.M113.538546.

(32) Grubb, D. R.; Luo, J.; Yu, Y. L.; Woodcock, E. A. Scaffolding Protein Homer 1c Mediates Hypertrophic Responses Downstream of Gq in Cardiomyocytes. *FASEB J. Off. Publ. Fed. Am. Soc. Exp. Biol.* **2012**, *26* (2), 596–603. https://doi.org/10.1096/fj.11-190330.

(33) Hwang, J.-I.; Kim, H. S.; Lee, J. R.; Kim, E.; Ryu, S. H.; Suh, P.-G. The Interaction of Phospholipase C-Beta3 with Shank2 Regulates MGluR-Mediated Calcium Signal. *J. Biol. Chem.* **2005**, *280* (13), 12467–12473. https://doi.org/10.1074/jbc.M410740200.

(34) Suh, P. G.; Hwang, J. I.; Ryu, S. H.; Donowitz, M.; Kim, J. H. The Roles of PDZ-Containing Proteins in PLC-Beta-Mediated Signaling. *Biochem. Biophys. Res. Commun.* **2001**, *288* (1), 1–7. https://doi.org/10.1006/bbrc.2001.5710.

(35) Adjobo-Hermans, M. J. W.; Goedhart, J.; Gadella, T. W. J. Regulation of PLCβ1a Membrane Anchoring by Its Substrate Phosphatidylinositol (4,5)-Bisphosphate. *J. Cell Sci.* **2008**, *121* (22), 3770–3777. https://doi.org/10.1242/jcs.029785.

(36) Adjobo-Hermans, M. J. W.; Crosby, K. C.; Putyrski, M.; Bhageloe, A.; van Weeren, L.; Schultz, C.; Goedhart, J.; Gadella Jr., T. W. J. PLCβ Isoforms Differ in Their Subcellular Location and Their CT-Domain Dependent Interaction with Gαq. *Cell. Signal.* **2013**, *25* (1), 255–263. https://doi.org/10.1016/j.cellsig.2012.09.022.

(37) Sun, L.; Mao, G.; Kunapuli, S. P.; Dhanasekaran, D. N.; Rao, A. K. Alternative Splice Variants of Phospholipase C-Beta2 Are Expressed in Platelets: Effect on Galphaq-Dependent Activation and Localization. *Platelets* **2007**, *18* (3), 217–223. https://doi.org/10.1080/09537100601016133.

(38) Cocco, L.; Faenza, I.; Follo, M. Y.; Billi, A. M.; Ramazzotti, G.; Papa, V.; Martelli, A. M.; Manzoli, L. Nuclear Inositides: PI-PLC Signaling in Cell Growth, Differentiation and Pathology. *Adv. Enzyme Regul.* **2009**, *49* (1), 2–10. https://doi.org/10.1016/j.advenzreg.2008.12.001.

(39) Faenza, I.; Matteucci, A.; Manzoli, L.; Billi, A. M.; Aluigi, M.; Peruzzi, D.; Vitale, M.; Castorina, S.; Suh, P. G.; Cocco, L. A Role for Nuclear Phospholipase Cbeta 1 in Cell Cycle Control. *J. Biol. Chem.* **2000**, *275* (39), 30520–30524. https://doi.org/10.1074/jbc.M004630200.

(40) Suh, P.-G.; *; Park, J.-I.; Manzoli, L.; Cocco, L.; Peak, J. C.; Katan, M.; Fukami, K.; Kataoka, T.; Ryu, S. Y. & S. H. Multiple Roles of Phosphoinositide-Specific Phospholipase C Isozymes. *BMB Rep.* **2008**, *41* (6), 415–434.

(41) Mende, U.; Kagen, A.; Meister, M.; Neer, E. J. Signal Transduction in Atria and Ventricles of Mice with Transient Cardiac Expression of Activated G Protein Alpha(q). *Circ. Res.* **1999**, *85* (11), 1085–1091.

(42) Böhm, D.; Schwegler, H.; Kotthaus, L.; Nayernia, K.; Rickmann, M.; Köhler, M.; Rosenbusch, J.; Engel, W.; Flügge, G.; Burfeind, P. Disruption of PLC-Beta 1-Mediated Signal Transduction in Mutant Mice Causes Age-Dependent Hippocampal Mossy Fiber Sprouting and Neurodegeneration. *Mol. Cell. Neurosci.* **2002**, *21* (4), 584–601.

(43) Aisiku, O. R.; Runnels, L. W.; Scarlata, S. Identification of a Novel Binding Partner of Phospholipase Cβ1: Translin-Associated Factor X. *PLoS ONE* **2010**, *5* (11). https://doi.org/10.1371/journal.pone.0015001.

(44) James, S. R.; Paterson, A.; Harden, T. K.; Demel, R. A.; Downes, C. P. Dependence of the Activity of Phospholipase Cβ on Surface Pressure and Surface Composition in Phospholipid Monolayers and Its Implications for Their Regulation. *Biochemistry* **1997**, *36* (4), 848–855. https://doi.org/10.1021/bi962108q.

(45) Demel, R. A.; Geurts van Kessel, W. S. M.; Zwaal, R. F. A.; Roelofsen, B.; van Deenen, L. L. M. Relation between Various Phospholipase Actions on Human Red Cell Membranes and the Interfacial Phospholipid Pressure in Monolayers. *Biochim. Biophys. Acta BBA - Biomembr.* **1975**, *406* (1), 97–107. https://doi.org/10.1016/0005-2736(75)90045-0.

(46) Boguslavsky, V.; Rebecchi, M.; Morris, A. J.; Jhon, D. Y.; Rhee, S. G.; McLaughlin, S. Effect of Monolayer Surface Pressure on the Activities of Phosphoinositide-Specific Phospholipase C-.Beta.1, -.Gamma.1, and -.Delta.1. *Biochemistry* **1994**, *33* (10), 3032–3037. https://doi.org/10.1021/bi00176a036.

(47) James, S. R.; Demel, R. A.; Downes, C. P. Interfacial Hydrolysis of Phosphatidylinositol 4-Phosphate and Phosphatidylinositol 4,5-Bisphosphate by Turkey Erythrocyte Phospholipase C. *Biochem. J.* **1994**, *298* (2), 499–506. https://doi.org/10.1042/bj2980499.

(48) Arduin, A.; Gaffney, P. R. J.; Ces, O. Regulation of PLCβ2 by the Electrostatic and Mechanical Properties of Lipid Bilayers. *Sci. Rep.* **2015**, *5*. https://doi.org/10.1038/srep12628.

(49) Kates, M. Techniques of Lipidology. 2. Rev. Ed. **1986**.

(50) Georgiev, G. A.; Kutsarova, E.; Jordanova, A.; Krastev, R.; Lalchev, Z. Interactions of Meibomian Gland Secretion with Polar Lipids in Langmuir Monolayers. *Colloids Surf. B Biointerfaces* **2010**, *78* (2), 317–327. https://doi.org/10.1016/j.colsurfb.2010.03.024.

(51) Levental, I.; Cēbers, A.; Janmey, P. A. Combined Electrostatics and Hydrogen Bonding Determine Intermolecular Interactions Between Polyphosphoinositides. *J. Am. Chem. Soc.* **2008**, *130* (28), 9025–9030. https://doi.org/10.1021/ja800948c.

(52) Mezzasalma, T. M.; Kranz, J. K.; Chan, W.; Struble, G. T.; Schalk-Hihi, C.; Deckman, I. C.; Springer, B. A.; Todd, M. J. Enhancing Recombinant Protein Quality and Yield by Protein Stability Profiling. *J. Biomol. Screen.* **2007**, *12* (3), 418–428. https://doi.org/10.1177/1087057106297984.

(53) Liu, X.; Villalta, P. W.; Sturla, S. J. Simultaneous Determination of Inositol and Inositol Phosphates in Complex Biological Matrices: Quantitative Ion-Exchange Chromatography/Tandem Mass Spectrometry. *Rapid Commun. Mass Spectrom.* **2009**, *23* (5), 705–712. https://doi.org/10.1002/rcm.3923.

(54) Ghosh, M.; Smrcka, A. V. Assay for G Protein-Dependent Activation of Phospholipase C Beta Using Purified Protein Components. *Methods Mol. Biol. Clifton NJ* **2004**, *237*, 67–75.

(55) Redfern, D. A.; Gericke, A. Domain Formation in Phosphatidylinositol Monophosphate/Phosphatidylcholine Mixed Vesicles. *Biophys. J.* **2004**, *86* (5), 2980–2992.

(56) Redfern, D. A.; Gericke, A. PH-Dependent Domain Formation in Phosphatidylinositol Polyphosphate/Phosphatidylcholine Mixed Vesicles. *J. Lipid Res.* **2005**, *46* (3), 504–515. https://doi.org/10.1194/jlr.M400367-JLR200.

(57) Illenberger, D.; Schwald, F.; Pimmer, D.; Binder, W.; Maier, G.; Dietrich, A.; Gierschik, P. Stimulation of Phospholipase C-Beta2 by the Rho GTPases Cdc42Hs and Rac1. *EMBO J.* **1998**, *17* (21), 6241–6249. https://doi.org/10.1093/emboj/17.21.6241.

(58) Runnels, L. W.; Jenco, J.; Morris, A.; Scarlata, S. Membrane Binding of Phospholipases C-Beta 1 and C-Beta 2 Is Independent of Phosphatidylinositol 4,5-Bisphosphate and the Alpha and Beta Gamma Subunits of G Proteins. *Biochemistry* **1996**, *35* (51), 16824–16832. https://doi.org/10.1021/bi961606w.

(59) Ellis, M. V.; James, S. R.; Perisic, O.; Downes, C. P.; Williams, R. L.; Katan, M. Catalytic Domain of Phosphoinositide-Specific Phospholipase C (PLC). Mutational Analysis of Residues within the Active Site and Hydrophobic Ridge of Plcdelta1. *J. Biol. Chem.* **1998**, *273* (19), 11650–11659.

(60) Qualmann, B.; Koch, D.; Kessels, M. M. Let's Go Bananas: Revisiting the Endocytic BAR Code. *EMBO J.* **2011**, *30* (17), 3501–3515. https://doi.org/10.1038/emboj.2011.266.

(61) Peter, B. J.; Kent, H. M.; Mills, I. G.; Vallis, Y.; Butler, P. J. G.; Evans, P. R.; McMahon, H. T. BAR Domains as Sensors of Membrane Curvature: The Amphiphysin BAR Structure. *Science* **2004**, *303* (5657), 495–499. https://doi.org/10.1126/science.1092586.

(62) Pykäläinen, A.; Boczkowska, M.; Zhao, H.; Saarikangas, J.; Rebowski, G.; Jansen, M.; Hakanen, J.; Koskela, E. V.; Peränen, J.; Vihinen, H.; et al. Pinkbar Is an Epithelial-Specific BAR Domain Protein That Generates Planar Membrane Structures. *Nat. Struct. Mol. Biol.* **2011**, *18* (8), 902–907. https://doi.org/10.1038/nsmb.2079.

(63) Zhao, H.; Michelot, A.; Koskela, E. V.; Tkach, V.; Stamou, D.; Drubin, D. G.; Lappalainen, P. Membrane-Sculpting BAR Domains Generate Stable Lipid Microdomains. *Cell Rep.* **2013**, *4* (6), 1213–1223. https://doi.org/10.1016/j.celrep.2013.08.024.

(64) McCullar, J. S.; Malencik, D. A.; Vogel, W. K.; Crofoot, K. M.; Anderson, S. R.; Filtz, T. M. Calmodulin Potentiates Gβγ Activation of Phospholipase C-Β3. *Biochem. Pharmacol.* **2007**, *73* (2), 270–278. https://doi.org/10.1016/j.bcp.2006.10.004.

(65) Hammond, G. R. V.; Fischer, M. J.; Anderson, K. E.; Holdich, J.; Koteci, A.; Balla, T.; Irvine, R. F. PI4P and PI(4,5)P2 Are Essential but Independent Lipid Determinants of Membrane Identity. *Science* **2012**, *337* (6095), 727–730. https://doi.org/10.1126/science.1222483.

(66) Willars, G. B.; Nahorski, S. R.; Challiss, R. A. Differential Regulation of Muscarinic Acetylcholine Receptor-Sensitive Polyphosphoinositide Pools and Consequences for Signaling in Human Neuroblastoma Cells. *J. Biol. Chem.* **1998**, *273* (9), 5037–5046. https://doi.org/10.1074/jbc.273.9.5037.

(67) Yadav, S.; Garner, K.; Georgiev, P.; Li, M.; Gomez-Espinosa, E.; Panda, A.; Mathre, S.; Okkenhaug, H.; Cockcroft, S.; Raghu, P. RDGBα, a PtdIns-PtdOH Transfer Protein, Regulates G-Protein-Coupled PtdIns(4,5)P2 Signalling during Drosophila Phototransduction. *J. Cell Sci.* **2015**, *128* (17), 3330–3344. https://doi.org/10.1242/jcs.173476.

(68) Kim, S.; Kedan, A.; Marom, M.; Gavert, N.; Keinan, O.; Selitrennik, M.; Laufman, O.; Lev, S. The Phosphatidylinositol-Transfer Protein Nir2 Binds Phosphatidic Acid and Positively Regulates Phosphoinositide Signalling. *EMBO Rep.* **2013**, *14* (10), 891–899. https://doi.org/10.1038/embor.2013.113.

(69) Zhang, H.; Craciun, L. C.; Mirshahi, T.; Rohács, T.; Lopes, C. M. B.; Jin, T.; Logothetis, D. E. PIP(2) Activates KCNQ Channels, and Its Hydrolysis Underlies Receptor-Mediated Inhibition of M Currents. *Neuron* **2003**, *37* (6), 963–975.

(70) Whorton, M. R.; MacKinnon, R. X-Ray Structure of the Mammalian GIRK2-Bγ G-Protein Complex. *Nature* **2013**, *498* (7453), 190–197. https://doi.org/10.1038/nature12241.

(71) Suh, B.-C.; Hille, B. Regulation of Ion Channels by Phosphatidylinositol 4,5-Bisphosphate. *Curr. Opin. Neurobiol.* **2005**, *15* (3), 370–378. https://doi.org/10.1016/j.conb.2005.05.005.

(72) Zhang, Y.; Vogel, W. K.; McCullar, J. S.; Greenwood, J. A.; Filtz, T. M. Phospholipase C-Beta3 and -Beta1 Form Homodimers, but Not Heterodimers, through Catalytic and Carboxyl-Terminal Domains. *Mol. Pharmacol.* **2006**, *70* (3), 860–868. https://doi.org/10.1124/mol.105.021923.

CHAPTER 3. G ALPHA Q AND THE PHOSPHOLIPASE C BETA 3 X–Y LINKER REGULATE ADSORPTION AND ACTIVITY ON COMPRESSED LIPID MONOLAYERS

This manuscript is currently in revision for *Biochemistry*.

3.1 Abstract

Phospholipase Cβ (PLCβ) enzymes are peripheral membrane proteins required for normal cardiovascular function. PLCβ hydrolyzes phosphatidylinositol-4,5-bisphosphate (PIP_2), producing second messengers that increase intracellular Ca^{2+} and activate protein kinase C (PKC). Under basal conditions, PLCβ is autoinhibited by its C-terminal domains and by the X–Y linker, which contains a stretch of conserved acidic residues required for interfacial activation. Following stimulation of G protein-coupled receptors, the heterotrimeric G protein subunit $G\alpha_q$ allosterically activates PLCβ and helps orient the activated complex at the membrane for efficient lipid hydrolysis. However, the molecular basis for how the PLCβ X–Y linker, its C-terminal domains, $G\alpha_q$, and the membrane coordinately regulate activity is not well understood. Using compressed lipid monolayers and atomic force microscopy, we found that a highly conserved acidic region of the X–Y linker is sufficient to regulate adsorption. Furthermore, regulation of adsorption and activity by the X–Y linker also occurs independently of the C-terminal domains. We next investigated whether $G\alpha_q$-dependent activation of PLCβ altered interactions with the model membrane. $G\alpha_q$ increased PLCβ adsorption to the monolayer independently of the PLCβ regulatory elements and targeted adsorption to specific regions of the monolayer in the absence of the C-terminal domains. Thus, the mechanism of $G\alpha_q$-dependent activation likely includes a spatial component.

3.2 Introduction

Phospholipase C (PLC) enzymes are peripheral membrane proteins that hydrolyze the plasma membrane lipid phosphatidylinositol-4,5-bisphosphate (PIP_2) to generate the second messengers inositol-1,4,5-triphosphate (IP_3) and diacylglycerol (DAG)[1,2]. IP_3 binds to receptors in the endoplasmic or sarcoplasmic reticulum, releasing calcium from intracellular stores[1,2]. DAG

remains in the membrane, and together with increased Ca^{2+}, activates protein kinase C (PKC). These events activate numerous downstream pathways, including those involved in cell survival and proliferation[1,3,4]. PLCβ enzymes have low basal activity and are stimulated up to ~60-fold through direct interactions with the heterotrimeric G protein subunits $G\alpha_q$ and $G\beta\gamma$, which are released upon activation of G_q- and G_i-coupled receptors, respectively[1,5]. Increased PLCβ expression and/or activation is associated with vascular smooth muscle contraction, cardiac arrhythmias, hypertrophy, and heart failure[6–12].

PLC enzymes, including PLCβ, share a highly conserved set of core domains including an N-terminal pleckstrin homology (PH) domain, four tandem EF hand repeats, a catalytic TIM barrel domain which is split by the autoinhibitory X–Y linker, and a C2 domain (Figure 3.1A)[1,13]. The defining feature of the PLCβ subfamily is a ~400-amino acid C-terminal extension immediately following the C2 domain, which is subdivided into proximal and distal C-terminal domains (CTDs)[1,13]. The proximal CTD is required for activation by $G\alpha_q$ and autoinhibition[14,15], while the distal CTD contributes to membrane association and maximum basal and $G\alpha_q$-stimulated activity[16,17].

The basal activity of PLCβ is regulated by three known elements: the X–Y linker, the Hα2′ helix in the proximal CTD, and the distal CTD[13,14,18,19]. The X–Y linker is largely unconserved in sequence and length, with the exception of its C-terminus which features a highly conserved 10-15 acidic residue stretch and a short α helix (Figure 3.1B,C)[1,13,18]. This helix interacts with residues adjacent to the active site and acts as a lid, preventing the substrate from binding to the active site (Figure 3.1B,C)[1,18]. In this mechanism, electrostatic repulsion between the negatively charged membrane and the acidic region of the X–Y linker eject the lid helix and expose the active site. In addition, the Hα2' helix in the proximal CTD must also be displaced for maximum lipase activity[1,13,14,18]. Under basal conditions, Hα2' is bound to a cleft between the TIM barrel and C2 domains and protrudes into the predicted membrane binding plane where it sterically hinders membrane association[14,19]. However, whether this helix is displaced through an interfacial mechanism has not been established. Finally, the distal CTD increases membrane association as well as basal and G protein-stimulated activity[19–23]. The distal CTD also interacts with the TIM barrel in solution, which may help regulate the distribution of membrane-bound and cytosolic populations of PLCβ[13]. More recently, the PLCβ3 distal CTD was shown to target the enzyme to

specific regions of PIP_2-containing lipid monolayers, consistent with its reported PIP_2 binding site[11,19].

PLCβ is activated through direct binding of the heterotrimeric G protein subunits $G\alpha_q$ and Gβγ. $G\alpha_q$ allosterically activates PLCβ by binding to Hα1/ Hα2 in the proximal CTD, displacing the autoinhibitory Hα2′ helix from the core[16, 18]. $G\alpha_q$ also interacts with the membrane via its palmitoylated N-terminus and with the PLCβ distal CTD, and these combined integrations are proposed to facilitate interfacial activation[16, 18]. Thus, maximum PIP_2 hydrolysis by PLCβ requires multivalent interactions between $G\alpha_q$, PLCβ, and the membrane[15]. In contrast, the mechanism of Gβγ-mediated activation is largely unknown but is proposed to prolong the dwell time of the Gβγ–PLCβ complex at the membrane [5,22–31]. Both $G\alpha_q$- and Gβγ-dependent activation are dependent upon the lipidation of the heterotrimeric G protein subunit[32–34]. The differences in the type of lipid modification on the G protein may also contribute to regulation. Palmitoylated $G\alpha_q$ may help localize PLCβ to raft-like regions of the membrane, which are also enriched in PIP_2. In contrast, the prenylated Gγ subunit would exclude Gβγ and its activated complexes from raft-like regions [20,24–26].

PLCβ enzymes must interact with the membrane for efficient catalysis, and under basal conditions, membrane association is hindered by the X–Y linker and proximal CTD. While heterotrimeric G proteins stimulate activity, in part by displacing autoinhibitory elements and/or facilitating interfacial activation, this is insufficient for full lipase activity. Thus, the membrane itself must contribute to PLCβ activation. In this study, we used biochemical assays and atomic force microscopy (AFM) on compressed lipid monolayers to begin characterizing how the PLCβ regulatory elements and $G\alpha_q$ regulates adsorption and activation. Specifically, the role of the X–Y linker and the contribution of interfacial activation to both basal and $G\alpha_q$-stimulated activity were investigated using a series of PLCβ3 domain deletion variants. We found that PLCβ3 variants lacking the X–Y linker, in whole or in part, had increased monolayer adsorption through a mechanism independent of the proximal and distal CTDs. The addition of activated $G\alpha_q$ to the model membrane system was sufficient to further increase protein adsorption to specific regions of the monolayer, suggesting that $G\alpha_q$-dependent activation of PLCβ includes a spatial component.

3.3 Materials and Methods

3.3.1 Protein Expression, Purification, and Mutagenesis

cDNA encoding N-terminally His-tagged *H. sapiens* PLCβ3 (UniProt entry Q01970 and residues 10-1234) and C-terminal truncation variants PLCβ3-Δ847 (residues 10-847) and PLCβ3-Δ892 (residues 10-892) were subcloned into pFastBac Dual vectors (Invitrogen) and expressed and purified as previously described[19]. The ΔXY1 (residues 471-569) and ΔXY2 (residues 471-584) deletions were generated using site-directed mutagenesis (Stratagene, San Diego, CA, USA), and sequenced over the entire open reading frame[18]. All PLCβ3 variants were purified as previously described[19]. We attempted to express and purify the PLCβ3-Δ847 ΔXY1 variant, but despite expression trials using multiple baculoviruses and High5 and Sf9 cells[13], the protein was not expressed at a high enough yield for purification.

The cDNA encoding murine $G\alpha_q$ (UniProt entry P21279 and residues 7-359) was subcloned into pFastbac HTA (Invitrogen), co-transfected with Ric-8A-GST[40] in baculovirus-infected High5 cells, and expressed and purified as previously described, with some modifications[13,19,40]. Following elution from the Ni-NTA column, the protein was concentrated to 1 mL, filtered through a 0.2 μm filter (Millipore), and applied to tandem Superdex S200 columns (GE Healthcare) pre-equilibrated with $G\alpha_q$ S200 activation buffer (20 mM HEPES pH 8, 100 mM NaCl, 2 mM DTT, 5 mM $MgCl_2$, 10 μm GDP pH 8, 30 μm $AlCl_3$, and 10 mM NaF)[14,16,18].

3.3.2 $G\alpha_q$–PLCβ3 Variant Complex Formation

Activated $G\alpha_q$ ($G\alpha_q$·GDP-ALF_4^-) was incubated with purified PLCβ3 variants in a 1:1.5 molar ratio in Buffer A (20 mM HEPES pH 8, 200 mM NaCl, 2 mM DTT, 0.9 mM $CaCl_2$, 5 mM $MgCl_2$, 10 mM NaF, 30 μM $AlCl_3$, and 50 μM GDP pH 8) for 30 min on ice. The reaction was concentrated to 500 μL and loaded on a Superdex S200 column equilibrated with buffer A. Fractions containing the $G\alpha_q$–PLCβ3 variant complexes were identified by SDS-PAGE, pooled, concentrated in an Amicon concentrator (Millipore), and flash frozen in liquid nitrogen[16].

3.3.3 Formation of Compressed Lipid Monolayers

Chicken egg white phosphatidylethanolamine (PE) and porcine brain phosphatidylinositol-4,5-bisphosphate (PIP_2) from Avanti Polar Lipids (Alabaster, AL, USA) were mixed in a 7:3 molar ratio, aliquoted, and stored under N_2 prior their use in compressed lipid monolayers as previously

described[19], with one modification to the protocol. The subphase of the monolayers contained 25 mL of 20 mM H_2NaPO_4 pH 8.0, and all monolayers were compressed at a rate of 56.1 mm/min.

3.3.4 Atomic Force Microscopy

All samples were imaged using a Veeco MultiMode atomic force microscope equipped with a Nanoscope V controller in tapping mode as previously described, with some modifications[19]. Gwyddion scanning probe microscopy data visualization software was used to perform plane flattening, median line corrections, scar artifact removal, contrast adjustment, column statistical analysis, and grain analysis[19,41]. Protein adsorption was detected qualitatively by the appearance of lighter colors, corresponding to increases in height, in the false-colored AFM micrographs. Quantitative changes in the monolayer after protein incubation were determined by measuring the maximum height as a function of position[41]. All AFM data was collected as line scans along the x-axis and then combined to generate a two-dimensional micrograph, where z is the second dimension. The height profile of the monolayer was determined by the maximum height sampled in regular intervals along the x-axis. The step size of the intervals was based on the full scan size, and the number of data points per line. In these experiments, all samples were imaged with a scan size of 1 x 1 μm and a total of 512 data points per line. The distance between each data point per line is equal to the step size of the interval. Additional quantitative information was obtained by grain analysis of each micrograph, which takes the sample background into account[41]. The heights for all grains on the monolayer surface were quantified and plotted as a histogram. Protein adsorption to the monolayer changes the grain height distribution relative to monolayers in the absence of protein[41]. The maximum height values for each micrograph and the normal distribution of height values of each grain were plotted in GraphPad Prism v8.0[41].

3.3.5 DSF Assays

Melting temperature (T_m) values for all PLCβ3 variants were determined by monitoring the binding of SYPRO Orange (Molecular Probes, Eugene, OR, USA) to hydrophobic regions of the proteins at increasing temperatures as previously described[19]. At least three experiments were carried out in triplicate using proteins from three independent purifications.

3.3.6 Activity Assays

300 μM hen egg white phosphatidylethanolamine (PE) and 750 μM soy phosphatidylinositol (PI) (Avanti Polar Lipids) were resuspended in $CHCl_3$, mixed, and dried in 312 μl aliquots in borosilicate glass tubes under a low stream of N_2. Lipids were sealed and stored at -20 °C until use. Liposomes were resuspended in 312 μl of sonication buffer (50 mM HEPES pH 7, 80 mM KCl, 2 mM EGTA, and 1 mM DTT), vortexed, incubated at room temperature for 5 minutes, then sonicated for two 30 s pulses using a bath sonicator (Avanti Polar Lipids). For basal activity measurements, each reaction contained 10 μL of PLC dilution buffer (50 mM HEPES pH 7, 3 mM EGTA, 80 mM KCl, 3 mM DTT, and 3 mg/ml BSA), 5 μL of G-protein control buffer (50 mM HEPES pH 7, 100 mM NaCl, 5 mM MgCl, 1 mM DTT, and 3 mM EGTA), and 5 μL of $CaCl_2$ solution (50 mM HEPES pH 7, 3 mM EGTA, 80 mM KCl, 1 mM DTT, and 13.6 μM $CaCl_2$). Control reactions contained all components except $CaCl_2$. Concentrations of the PLCβ3 variants were chosen such that activity was in the linear range over the time course (2-10 min) of the assay. Reactions were terminated by the addition of ice-cold quench solution (50 mM HEPES pH 7, 80 mM KCl, 210 mM EGTA, and 1 mM DTT) and incubated on ice. The final protein concentrations were: 15 ng/μL PLCβ3, 15 or 20 ng/μL PLCβ3 ΔXY1, 5 ng/μL PLCβ3 ΔXY2, 15 ng/μL PLCβ3-Δ847, 30 ng/μL PLCβ3-Δ847 ΔXY2, 30 ng/μL PLCβ3-Δ892, and 30 ng/μL PLCβ3-Δ892 ΔXY2. $G\alpha_q$-dependent increases in lipase activity were measured by adding activated $G\alpha_q$–PLCβ3 variant complexes to the reactions such that activity remained in the linear range from 2-10 min. The final protein concentrations used were 20 ng/μL $G\alpha_q$–PLCβ3, $G\alpha_q$–PLCβ3 ΔXY1, and $G\alpha_q$–PLCβ3 ΔXY2, and 30 ng/μL $G\alpha_q$–PLCβ3-Δ892, $G\alpha_q$–PLCβ3-Δ892 ΔXY1, and $G\alpha_q$–PLCβ3-Δ892 ΔXY2. Inositol phosphate (IP_1) production was quantified using a modified version of the CisBio IP-One G_q assay kit. Following termination, 14 μL of each reaction, 3 μL d_2-labeled IP_1, and 3 μL cryptate-labeled anti-IP_1 antibody (CisBio) were added to a 384-well low-volume white microplate at room temperature (Corning, Corning, NY, USA). Positive controls contained assay buffer, d_2-labeled IP_1, cryptate-labeled anti-IP_1, and negative controls contained assay buffer, lysis and detection buffer, and cryptate-labeled anti-IP_1. The plate was centrifuged at 1000 x g for 1 min, incubated at room temperature for 1 h, and read on a Synergy4 plate reader (BioTek, Winooski, VT, USA). The concentration of IP_1 was calculated from a standard curve and normalized following the

manufacturer's protocol (CisBio). At least four experiments were performed in duplicate with protein from three different purifications.

3.4 Results

3.4.1 Deletions within the X–Y linker Perturb Stability and Activity

Interfacial activation is thought to require the acidic stretch within the X–Y linker. To determine whether this region is sufficient for autoinhibition, or if the entire X–Y linker is required, we expressed and purified a series of PLCβ3 variants lacking the unconserved N-terminus and acidic stretch of the X–Y linker (residues 471-569, referred to as ΔXY1), or the entire X–Y linker (residues 471-584, referred to as ΔXY2). These deletions were introduced in the background of PLCβ3 and two previously characterized C-terminal truncations, PLCβ3-Δ892 and PLCβ3-Δ847, which lack the distal CTD or the proximal and distal CTDs, respectively (Figures 3.1A,B)[14,18,19]. Differential scanning fluorimetry (DSF) was used to determine whether these deletions altered the melting temperature (T_m) of the PLCβ3 variants. PLCβ3 had a T_m of 55.5 ± 0.2 °C, while the T_ms of PLCβ3 ΔXY1 and PLCβ3 ΔXY2 were increased by ~3°C (Figure 3.2 and Table 3.1). PLCβ3-Δ892 had a T_m of 59.4 ± 0.1 °C, but the T_m of PLCβ3-Δ892 ΔXY1 was decreased by ~2.5 °C, and was ~5 °C lower for PLCβ3-Δ892 ΔXY2 (Figure 3.2 and Table 3.1). Finally, PLCβ3-Δ847 had the lowest thermal stability of the PLCβ3 variants, consistent with loss of the proximal CTD, with a T_m of 53.3 ± 0.1 °C. Deletion of the X–Y linker in PLCβ3-Δ847 ΔXY2 decreased the T_m by an additional ~2 °C (Figure 3.2 and Table 3.1).

The basal activity of the PLCβ3 variants was then measured using a modified version of the CisBio IP-One assay, wherein PI was incorporated into liposomes, and the amount of inositol phosphate (IP_1) produced was quantified[42–44]. PLCβ3 had a specific activity of 0.11 ± 0.01 nmol IP_1/min/nmol PLCβ3 variant (Figure 3.3A and Table 3.2), while PLCβ3 ΔXY1 and PLCβ3 ΔXY2 had ~11-fold higher basal activity (1.20 ± 0.11 nmol IP_1/min/nmol PLCβ3 variant and 1.20 ± 0.16 nmol IP_1/min/nmol PLCβ3 variant, respectively), consistent with deletions in the X–Y linker relieving autoinhibition (Figure 3.3A and Table 3.2). PLCβ3-Δ847 has ~2-fold lower basal activity than PLCβ3, due to loss of membrane association by the distal CTD. PLCβ3-Δ847 ΔXY2 increased activity ~10-fold over that of PLCβ3-Δ847 (Figure 3.3B and Table 3.2). Finally, PLCβ3-

Δ892 had the lowest specific activity at 0.01 ± 0.001 nmol IP_1/min/nmol PLCβ3 variants, due to autoinhibition by both the X–Y linker and the proximal CTD. Deletion of the acidic stretch or the entire linker in this variant increased basal activity over ~60-fold compared to PLCβ3-Δ892 (Figure 3.3C and Table 3.2). The modest changes in $T_{m,}$ together with the measurable basal activity, demonstrate the deletions within the X–Y linker do not compromise the structure of the PLCβ3 variants. In addition, deletion of the acidic in the X–Y linker increases basal activity to the same extent as deletion of the entire X–Y linker.

3.4.2 The Acidic Stretch of the X–Y Linker Regulates Adsorption to Lipid Monolayers

Deletions within the PLCβ3 X–Y linker increase basal activity, potentially by exposing the active site and eliminating unfavorable interactions between the acidic stretch of the X–Y linker and liposomes. To determine whether the increased activity of the ΔXY variants is due, at least in part, to increased membrane binding, the PLCβ3 variants were added to the subphases of compressed PE:PIP_2 lipid monolayers, allowed to incubate, and then the monolayer containing adsorbed protein was visualized by atomic force microscopy[19]. In these experiments, adsorption to the monolayer is detected as changes in the appearance of the monolayer surface, where taller features are shown in lighter colors in the false-colored AFM micrographs. The relative height of these surface features were quantified by measuring the maximum height above the supporting surface as a function of position, and the number of surface features with a specific height range were quantified using grain analysis of the micrograph (Figure 3.4).

Compressed lipid monolayers incubated with 10 nM PLCβ3 showed an increase in the maximum height of surface features, as illustrated by the lighter puncta on the surface and the increased height of surface features from ~4 nm on the monolayer alone to ~20 nm after protein addition. Adsorption of protein is also observed in the grain height distribution, where the majority of surface features are ~10-20 nm in height (Figures 3.4A, B and Figure 3.5). Addition of 50 nM PLCβ3 to the subphase increased the number of elevated surface features in the grain analysis but did not further increase the height of the surface features compared to the 10 nM PLCβ3 monolayers (Figures 3.4A-C and Figure 3.5). In contrast, monolayers incubated with 10 nM PLCβ3 ΔXY1 had a more uniform appearance, with smaller surface features only ~4-6 nm in height (Figures 3.4B-D and Figure 3.5). Monolayers incubated with 50 nM PLCβ3 ΔXY1 lacked clear surface features, as supported by the uniform absence of light puncta in the micrographs and

had a further decrease in the height frequency distribution to ~2 nm, relative to monolayers incubated with lower concentrations of PLCβ ΔXY1 (Figures 3.4D, E and Figure 3.5). Similar trends were observed for monolayers incubated with PLCβ3 ΔXY2 (Figure 3.4F-G and Figure 3.5).

The more uniform adsorption of PLCβ3 ΔXY1 and PLCβ3 ΔXY2 to monolayers could be due to depletion of the PIP_2 clusters caused by their higher basal activity[19,37,45–47]. Therefore, monolayers were incubated with 10 nM PLCβ3 ΔXY1 or 10 nM PLCβ3 ΔXY2 for shorter times (Figure 3.6). After 5 minutes, monolayers incubated with 10 nM PLCβ3 ΔXY1 had large elevated surface features ~8-20 nm in height (Figure 3.6A), similar in size and appearance to features observed on monolayers incubated with PLCβ3 (Figure 3.4B,C and Figure 3.5). Similar trends were observed for monolayers incubated with 10 nM PLCβ3 ΔXY2, with surface features ~12-22 nm in height (Figure 3.6B). At longer incubation times, the height of the surface features decreased by ~10 nm on monolayers incubated with either PLCβ3 ΔXY variant (Figure 3.6C,D), but the features can still be clearly resolved in the micrographs. After 20 minutes, the monolayers incubated with PLCβ3 ΔXY1 or PLCβ3 ΔXY2 have a more uniform appearance, with the majority of surface features ~6-7 nm in height (Figure 3.6E, F). Given the time-dependent decrease in the height of surface features, a possible explanation for these results is that the PLCβ3 ΔXY variants deplete PIP_2 clusters from the monolayer.

3.4.3 The X–Y Linker Increases Adsorption Independently of the Proximal CTD

The proximal CTD negatively regulates adsorption by sterically preventing interactions between the active site and the membrane [14,18,19]. However, whether the X–Y linker and the proximal CTD coordinately regulate adsorption is unknown. To investigate the roles of these two regulatory elements, monolayers were incubated with increasing concentrations of the PLCβ3-Δ847 and PLCβ3-Δ892 ΔXY variants.

At all concentrations tested, PLCβ3-Δ847 and PLCβ3-Δ847 ΔXY2 adsorbed nonspecifically to the monolayer, consistent with the ~2-4 nm changes in height across the surface and the lack of well-defined, elevated features on the surface (Figure 3.7 and Figure 3.8). PLCβ3-Δ892 also adsorbed uniformly to the monolayer, but to a lesser extent than PLCβ3-Δ847, due to the presence of the proximal CTD (Figure 3.1, Figure 3.7, Figure 3.8, Figure 3.9, and Figure 3.10).

Even at 50 nM PLCβ3-Δ892, the surface features only vary by ~1 nm in height (Figure 3.9B,C and Figure 3.10). In contrast, monolayers incubated with 10 nM PLCβ3-Δ892 ΔXY1 show increased protein adsorption, with an overall lighter appearance and increased number of features ~3-5 nm in height (Figures 3.9D, E and Figure 3.10). At 50 nM PLCβ3-Δ892 ΔXY1, the micrographs are lighter in color and nearly uniform in height compared to PLCβ3-Δ892 or lower concentrations of PLCβ3-Δ892 ΔXY1 (Figure 3.9B-E and Figure 3.10). Similar trends were observed for monolayers incubated with PLCβ3-Δ892 ΔXY2 (Figure 3.9F, G and Figure 3.10). Therefore, deletion of the acidic stretch increases adsorption to the same extent as deletion of the entire X–Y linker, independently of the proximal CTD (Figure 3.4, Figure 3.6, Figure 3.7, and Figure 3.9).

3.4.4 $G\alpha_q$ Increases Adsorption to Compressed Lipid Monolayers

$G\alpha_q$ allosterically activates PLCβ by displacing Hα2′ from the core and can facilitate interfacial activation by increasing interactions with the membrane[13,14]. To evaluate the contribution of interfacial activation to $G\alpha_q$-dependent activation of PLCβ, stoichiometric complexes of $G\alpha_q$–PLCβ3 and $G\alpha_q$–PLCβ3 Δ892 were isolated by size exclusion chromatography, and their basal activity and adsorption to compressed lipid monolayers was evaluated.

The specific activities of the $G\alpha_q$–PLCβ3 variant complexes were measured using the PI liposome-based activity assay. The $G\alpha_q$–PLCβ3 complex had a specific activity of 0.89 ± 0.15 nmol IP_1/min/nmol complex, an ~8-fold increase over the basal activity of PLCβ3 (Figure 3.3A, Table 3.2, Figure 3.11A, and Table 3.3). $G\alpha_q$–PLCβ3 ΔXY1 and $G\alpha_q$–PLCβ3 ΔXY2 had specific activities ~2-4-fold greater than the basal activity of the PLCβ3 ΔXY variants alone (5.2 ± 1.0 nmol IP_1/min/nmol complex and 1.8 ± 0.40 nmol IP_1/min/nmol complex, respectively), and ~2-6 fold higher than the wild-type $G\alpha_q$–PLCβ3 complex (Figures 3.3A, Tables 3.2, Figure 3.11A, and Table 3.3). The activity of the $G\alpha_q$–PLCβ3-Δ892 complex was ~22-fold higher than PLCβ3-Δ892 (0.24 ± 0.06 nmol IP_1/min/nmol complex, Figures 3.3C, Tables 3.2, Figure 3.11B, and Table 3.3). The activities of the $G\alpha_q$–PLCβ3-Δ892 ΔXY1 and $G\alpha_q$–PLCβ3-Δ892 ΔXY2 were ~2-3-fold higher over the PLCβ3-Δ892 ΔXY variants alone (1.1 ± 0.20 nmol IP_1/min/nmol complex and 2.1 ± 0.40 nmol IP_1/min/nmol complex, respectively, Figures 3.3C, Tables 3.2, Figure 3.11B, and Table 3.3), and ~5-9 fold greater than the $G\alpha_q$–PLCβ3-Δ892 complex (Figure 3.11B and Table

3.3). As PLCβ3-Δ847 lacks the proximal CTD, it is unresponsive to $G\alpha_q$-dependent activation at all concentrations and was not included in these experiments[14].

The $G\alpha_q$–PLCβ3 variant complexes were then assessed for their ability to adsorb to the compressed PE:PIP_2 monolayers. Addition of 10 nM $G\alpha_q$–PLCβ3 to the subphase resulted in the formation of elevated surface features similar in appearance to monolayers incubated with PLCβ3 alone (Figure 3.4, Figures 3.5, Figure 3.12, and Figure 3.13). The majority of these features were ~10-16 nm in height. Increasing the concentration of $G\alpha_q$–PLCβ3 in the subphase also increased the height of the surface features to ~16-26 nm. Thus, the inclusion of $G\alpha_q$ increases PLCβ3 adsorption (Figure 3.12B, C and Figure 3.13). The roles of the acidic stretch within the X–Y linker or the entire X–Y linker were then assessed in the presence of $G\alpha_q$. Given that the monolayers incubated with the PLCβ3 ΔXY variants were relatively uniform in appearance the $G\alpha_q$–PLCβ3 ΔXY variant complexes may show similar trends. Alternatively, the complexes could adsorb to regions of the monolayer enriched in PIP_2, as palmitoylated $G\alpha_q$ has been reported to preferentially localize to these regions[32–34]. Monolayers incubated with 10 nM $G\alpha_q$–PLCβ3 ΔXY1 had a uniform appearance, with only ~2 nm changes in height over the monolayer surface (Figures 3.12D and Figure 3.13). At higher concentrations, adsorption of the $G\alpha_q$–PLCβ3 ΔXY1 complex showed a modest increase in the height of the small surface features to ~2-4 nm across the surface, as shown in the micrographs (Figure 3.12E and Figure 3.13). We next investigated whether deletion of the entire X–Y linker in the $G\alpha_q$–PLCβ3 ΔXY2 complex altered adsorption. At low concentrations, the monolayers are largely uniform in appearance with few clustered regions ~2-4 nm in height (Figure 3.12F and Figure 3.13). Addition of 50 nM $G\alpha_q$–PLCβ3 ΔXY2 to the subphase increased the number of elevated surface features with heights of ~4-6 (Figure 3.12F, G and Figure 3.13). These small changes in the monolayer surface contrast with the well-defined ~10-14 nm features observed on monolayers incubated with the wild-type $G\alpha_q$–PLCβ3 complex (Figure 3.12 and Figure 3.13).

3.4.5 $G\alpha_q$ Increases Specific Adsorption to the Monolayer in the Absence of the Distal CTD

We next assessed whether $G\alpha_q$ increased and/or altered the distribution of PLCβ3-Δ892 and its ΔXY variants at the monolayer. As PLCβ3-Δ892 lacks the distal CTD, the addition of $G\alpha_q$ could increase adsorption, resulting in taller and/or more extended features compared to

monolayers incubated with PLCβ3-Δ892. $G\alpha_q$ could also promote adsorption to PIP_2-enriched regions of the monolayer via its palmitoylated N-terminus. Addition of 10 nM $G\alpha_q$–PLCβ3-Δ892 to the subphase resulted in the formation of large, elevated surface features ~10-14 nm in height, similar in appearance to monolayers incubated with the $G\alpha_q$–PLCβ3 complex (Figures 3.12B,C, Figure 3.13, Figure 3.14B and Figure 3.15). At higher concentrations of $G\alpha_q$–PLCβ3-Δ892, the monolayers retained large, elevated clusters, but the height of these features decreased to ~8-12 nm (Figure 3.14C and Figure 3.15). This contrasts with the monolayers incubated with PLCβ3-Δ892 alone, which have a uniform appearance (Figure 3.9B,C and Figure 3.10), suggesting that $G\alpha_q$ may contribute to the spatial distribution of protein complex at the monolayer.

The ability of $G\alpha_q$ to alter the adsorption and/or distribution of PLCβ3-Δ892 ΔXY variants to the monolayer was then assessed. Addition of 10 nM $G\alpha_q$–PLCβ3-Δ892 ΔXY1 also resulted in the formation of small, clustered features ~4-6 nm in height (Figure 3.14D and Figure 3.15). Higher concentrations of the $G\alpha_q$–PLCβ3-Δ892 ΔXY1 complex further increased adsorption and the height of the features to ~4-10 nm (Figure 3.14E and Figure 3.15). These features are taller than those observed in monolayers incubated with $G\alpha_q$–PLCβ3-Δ892, again demonstrating that adsorption increases when the acidic stretch of the X–Y linker is removed (Figure 3.14A-E and Figure 3.15). Addition of 10 nM $G\alpha_q$–PLCβ3-Δ892 ΔXY2 to the monolayer increased the number of clustered regions ~2-8 nm in height (Figure 3.14F and Figure 3.15). However, at higher concentrations of $G\alpha_q$–PLCβ3-Δ892 ΔXY2, the monolayers lacked well-defined surface features and had a more uniform appearance (Figure 3.14E and Figure 3.15). This could be due to PIP_2 depletion from the monolayer, given the significantly higher basal activity of $G\alpha_q$–PLCβ3-Δ892 ΔXY2 complex (Figure 3.11 and Table 3.3).

3.5 Discussion

PLCβ enzymes are maintained in a catalytically quiescent state by its X–Y linker and CTDs. The X–Y linker regulates activity through an interfacial mechanism that requires a highly conserved stretch of acidic residues. The Hα2′ helix in the proximal CTD also inhibits interactions between the active site and the membrane. Finally, the distal CTD can interact with the rest of the PLCβ core, partitioning the enzyme between membrane and cytosolic populations. However, whether the acidic stretch within the X–Y linker is responsible for the autoinhibitory function of

this element, and whether or how the X–Y linker and CTDs coordinately regulate membrane association and activity remain unclear.

To establish whether the acidic stretch of the linker is necessary and sufficient for adsorption independently of the CTDs, a series of PLCβ3 variants lacking the disordered N-terminus and acidic stretch (ΔXY1 variants) or the entire linker (ΔXY2 variants) in the background of PLCβ3 variants lacking the distal and/or proximal CTDs (Figure 3.1) were assessed for stability and activity. While deletions within the X–Y linker caused modest changes in T_m values, deletion of the acidic stretch was sufficient to increase basal activity to the same extent as deletion of the entire linker in all PLCβ3 backgrounds (Figure 3.1, Figure 3.2, Figure 3.3, Table 3.1, and Table 3.2). The increased activity could be due to increased lipid interactions, which can be detected as changes in the topographical features of compressed PE:PIP_2 monolayers using AFM. PLCβ3 adsorbed to specific regions of the monolayer, forming large, clearly defined elevated features on the surface (Figure 3.4B,C and Figure 3.5). Deletion of the acidic stretch in the X–Y linker or the entire X–Y linker resulted in monolayers more uniform in height and lacking elevated clusters, consistent with either nonspecific adsorption and/or depletion of PIP_2 clusters (Figure 3.4 and Figure 3.5)[19]. To distinguish between these possibilities, the PLCβ3 ΔXY variants were incubated for shorter times in the monolayer subphases (Figure 3.6). At shorter time points, elevated clustered features were clearly visible, suggesting that the flatter monolayers observed at long incubation times are likely due to PIP_2 depletion (Figure 3.6). PLCβ3-Δ847, which lacks the proximal and distal CTDs, and PLCβ3-Δ892, which lacks only the distal CTD, adsorbed uniformly to the monolayer (Figure 3.7- Figure 3.10). Deletion of the X–Y linker in these variants, in whole or in part, increased adsorption but did not alter spatial distribution (Figure 3.7- Figure 3.10). In all cases, deletion of the acidic stretch increases monolayer adsorption to a similar extent as deletion of the entire X–Y linker, demonstrating that the acidic stretch is responsible for autoinhibition by the X–Y linker (Figure 3.4, Figure 3.5, and Figures 3.7- 3.10).

We next investigated whether the heterotrimeric G protein subunit $G\alpha_q$ altered adsorption and/or spatial localization to the model membrane. The inclusion of $G\alpha_q$ increases adsorption of both PLCβ3 and PLCβ3-Δ892 to the monolayer, as compared to the PLCβ3 variants alone (Figure 3.4, Figure 3.5, Figure 3.9, Figure 3.10, and Figures 3.12- 3.15). While previous studies have found that $G\alpha_q$ does not increase the affinity of PLCβ for the membrane, $G\alpha_q$ may stabilize PLCβ at the

monolayer, increasing the amount of protein on the monolayer [20,23–25]. Our results suggest that $G\alpha_q$ also promotes adsorption of PLCβ3 to specific regions of the monolayer. We previously showed that the PLCβ3 distal CTD was required for specific adsorption, while PLCβ3 variants lacking the distal CTD adsorbed nonspecifically [19]. Monolayers incubated with the $G\alpha_q$–PLCβ3-Δ892 complex had clearly defined, elevated features on the surface (Figure 3.14B, C and Figure 3.15), similar to those observed on PLCβ3 and $G\alpha_q$–PLCβ3 monolayers (Figure 3.3, Figure 3.4, Figure 3.12, and Figure 3.13). Thus, $G\alpha_q$ appears to rescue specific adsorption to the monolayer in the absence of the distal CTD.

As $G\alpha_q$ increases PLCβ3 adsorption to specific regions of the monolayer, an additional component in its activation of PLCβ may include the targeting of the complex to regions enriched in PIP_2, (Figure 3.16). Recent studies have found that PIP_2 is highly concentrated at the rim of caveolae, and these regions also have increased $G\alpha_q$-dependent PLCβ activation[48,49]. In the cell, this localization could, in turn, regulate other signaling proteins and processes dependent upon PIP_2, including ion channel and transporter activity, cell motility, and vesicular trafficking[50–57]. PLCβ is also regulated by the Gβγ heterodimer, but the prenylation of the Gγ subunit would result in exclusion from PIP_2-enriched regions[,20,24–26], which may impact the amplitude or duration of PLC-dependent PIP_2 hydrolysis. Future studies exploring the spatial component of PLCβ activity, alone and following GPCR stimulation, will be essential for understanding the role of the membrane in these dynamic processes.

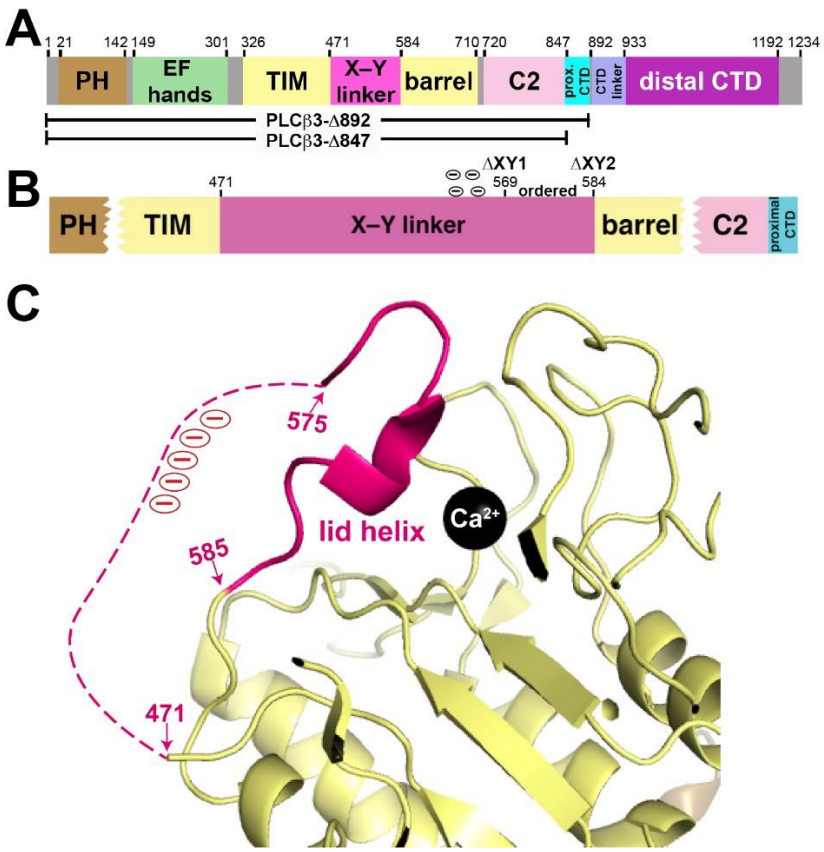

Figure 3.1. PLCβ3 Domain Architecture and Autoinhibition by the X–Y linker.
(A) Domain diagram of PLCβ3. Numbers above the diagram correspond to amino acids at domain boundaries. C-terminal truncations used in this study are shown below. (B) Schematic of the PLCβ3 X–Y linker. Internal deletions used in this study remove the unconserved N-terminus and the acidic stretch (ΔXY1, residues 471-569), or the entire X–Y linker (ΔXY2, residues 471-584). (C) The C-terminus of the X–Y linker occludes the active site (PDB ID 4GNK)[16]. Domains are colored as in (A). The disordered region of the X–Y linker is shown as a dashed hot pink link, and the acidic region is labeled with circled minus signs (red). The catalytic Ca^{2+} ion is shown as a black sphere.

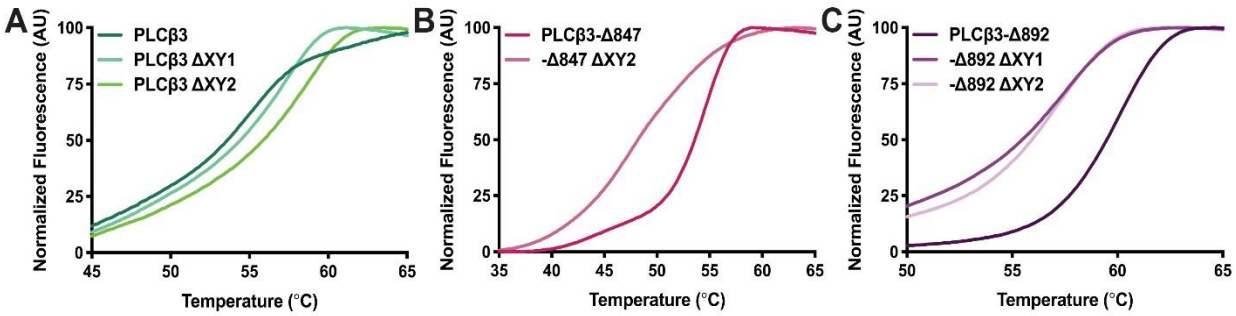

Figure 3.2. Deletions in the X–Y linker Alter Thermal Stability.
Representative thermal denaturation curves of (A) PLCβ3 ΔXY variants, (B) PLCβ3-Δ847 ΔXY variants, and (C) PLCβ3-Δ892 ΔXY variants. In these experiments, each protein was incubated with a fluorescent dye, and the change in fluorescence due to protein unfolding is monitored as a function of temperature. The data were fit using a Boltzmann distribution, and the melting temperature (T_m) calculated from the inflection point.

Table 3.1. Thermal Stability of PLCβ3 variants.

PLCβ3 Variant	T_m (°C)[a]
PLCβ3	55.5 ± 0.2
PLCβ3 ΔXY1	58.7 ± 0.1
PLCβ3 ΔXY2	58.5 ± 0.1[b]
PLCβ3-Δ847	53.3 ± 0.1
PLCβ3-Δ847 ΔXY2	48.2 ± 0.2[c]
PLCβ3-Δ892	59.4 ± 0.1
PLCβ3-Δ892 ΔXY1	56.8 ± 0.1[d]
PLCβ3-Δ892 ΔXY2	57.4 ± 0.2[d]

[a]Data represents the average of at least three experiments ± SEM. [b]Significant relative to PLCβ3 (*$p \leq 0.05$). [c]Significant relative to PLCβ3-Δ847 (****$p \leq 0.0001$). [d]Significant relative to PLCβ3-Δ892 (****$p \leq 0.0001$).

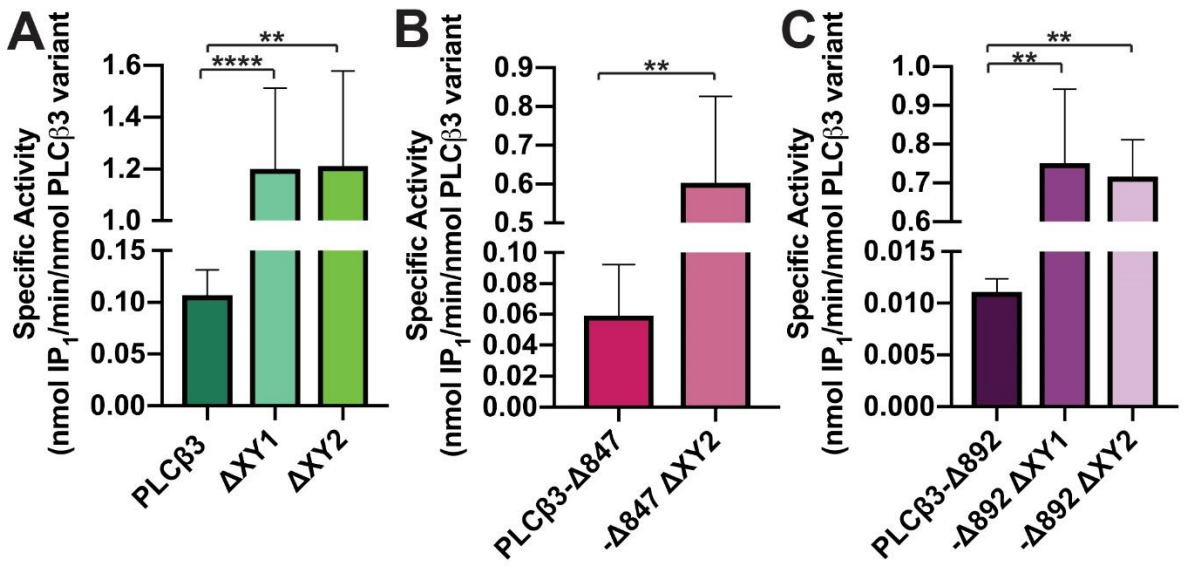

Figure 3.3. Deletions Within the X–Y Linker Increase Basal Specific Activity. Deletion of the X–Y linker, in whole or in part, in the background of (A) PLCβ3 or (B) PLCβ3-Δ847 increases basal activity ~10-11-fold. PLCβ3-Δ847 has lower basal activity than PLCβ3 due to the absence of the distal CTD. (C) PLCβ3-Δ892 has the lowest basal activity of the PLCβ3 variants tested, with deletions in the X–Y linker increasing activity ~65-fold. Data shown represent the average of at least four individual experiments in duplicate ± SEM (****$p \leq 0.0001$, **$p \leq 0.01$).

Table 3.2. Basal Activity of PLCβ3 variants.

PLCβ3 Variant	Basal Specific Activity (nmol IP_1/min/nmol PLCβ3)[a]	Fold Increase Relative to Wild-Type
PLCβ3 (wt)	0.11 ± 0.01	1
PLCβ3 ΔXY1	1.20 ± 0.11[b]	11
PLCβ3 ΔXY2	1.20 ± 0.16[c]	11
PLCβ3-Δ847 (wt)	0.06 ± 0.01	1
PLCβ3-Δ847 ΔXY2	0.60 ± 0.09[d]	10
PLCβ3-Δ892 (wt)	0.01 ± 0.001	1
PLCβ3-Δ892 ΔXY1	0.75 ± 0.19[e]	68
PLCβ3-Δ892 ΔXY2	0.72 ± 0.10[e]	65

[a]The data shown represent at least four experiments performed in duplicate ± SEM. [b]Significant relative to PLCβ3 (****$p \leq 0.0001$). [c]Significant relative to PLCβ3 (**$p \leq 0.01$). [d]Significant relative to PLCβ3-Δ847 **(*****$p \leq 0.01$). [e]Significant relative to PLCβ3-Δ892 **(*****$p \leq 0.01$).

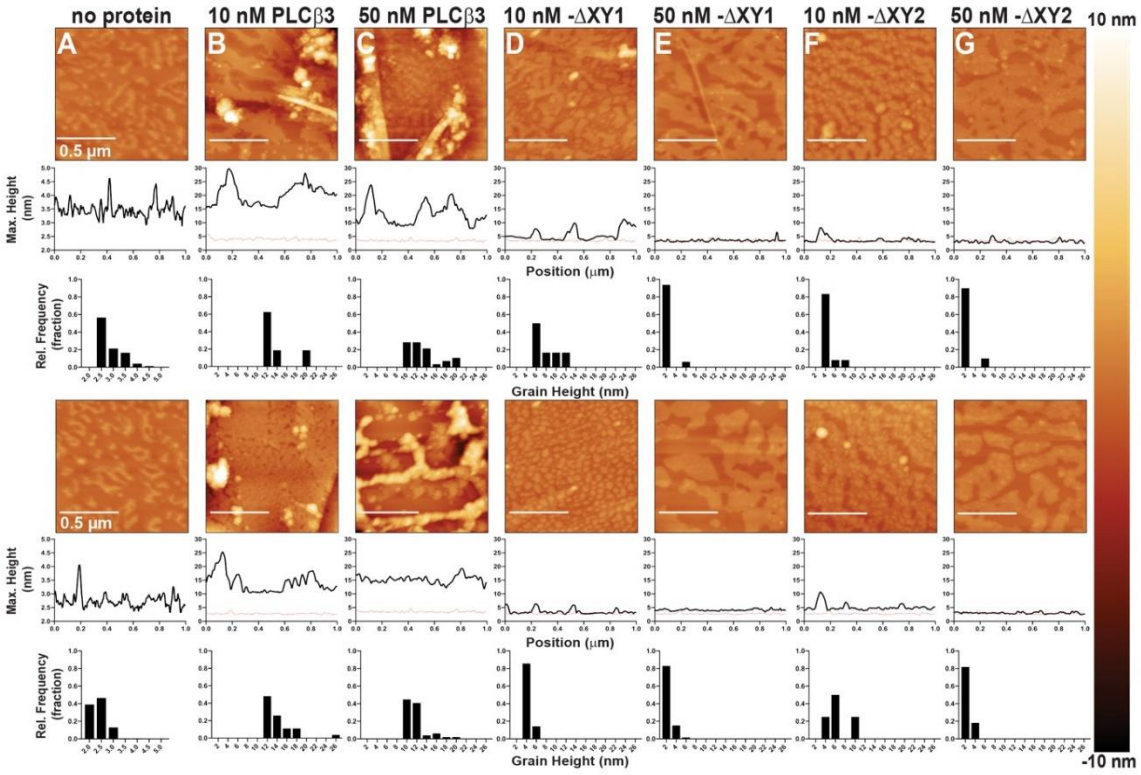

Figure 3.4. Representative AFM Tapping Mode Images of Compressed PE:PIP_2 Monolayers Incubated with PLCβ3 ΔXY Variants.

Two representative images of each condition are shown, with sample variations most likely due to lipid distribution in the monolayer and/or Langmuir-Schaefer transfer to the HOPG substrate. Topographical changes upon protein addition are detected as changes in the appearance of the monolayer surface, with taller features shown in lighter colors, and increases in the height and/or size of surface features. The maximum heights above the HOPG surface as a function of position and the grain analysis for the relative height frequency of surface features are quantified below each micrograph. For comparison, a representative height profile from a compressed monolayer in the absence of protein is shown on each height profile as a dashed red line. Monolayers in the (A) absence of protein or incubated with (B) 10 nM PLCβ3, (C) 50 nM PLCβ3, (D) 10 nM PLCβ3 ΔXY1, (E) 50 nM PLCβ3 ΔXY1, (F) 10 nM PLCβ3 ΔXY2, or (G) 50 nM PLCβ3 ΔXY2.

Figure 3.5. Representative AFM Tapping Mode Images of Compressed PE:PIP_2 Monolayers Incubated with Increasing Concentrations of PLCβ3 ΔXY Variants.
One representative image of each condition is shown. Sample variations are most likely due to differences in lipid distribution and Langmuir-Schaefer transfer to the HOPG substrate. Topographical changes are detected as changes in the appearance of the monolayer surface, where taller features are shown in lighter colors in the false-colored micrographs. Below each micrograph are height profiles of the monolayer surface quantifying the maximum heights measured above the supporting surface as a function of position. For comparison, a representative height profile from a compressed monolayer in the absence of protein is shown on each height profile as a dashed red line. Grain analysis by height thresholding was also performed for each monolayer and shown in height distribution histograms below each height profile. Protein adsorption changes the grain height distribution of features across the monolayer surface. Monolayers in the (A-C) absence of protein or incubated with (D) 5 nM PLCβ3, (E) 5 nM PLCβ3 ΔXY1, (F) 5 nM PLCβ3 ΔXY2, (G) 10 nM PLCβ3, (H) 10 nM PLCβ3 ΔXY1, (I) 10 nM PLCβ3 ΔXY2, (J) 30 nM PLCβ3, (K) 30 nM PLCβ3 ΔXY1, (L) 30 nM PLCβ3 ΔXY2, (M) 50 nM PLCβ3, (N) 50 nM PLCβ3 ΔXY1, (O) 50 nM PLCβ3 ΔXY2 for 20 min. at room temperature prior to Langmuir-Schaefer transfer.

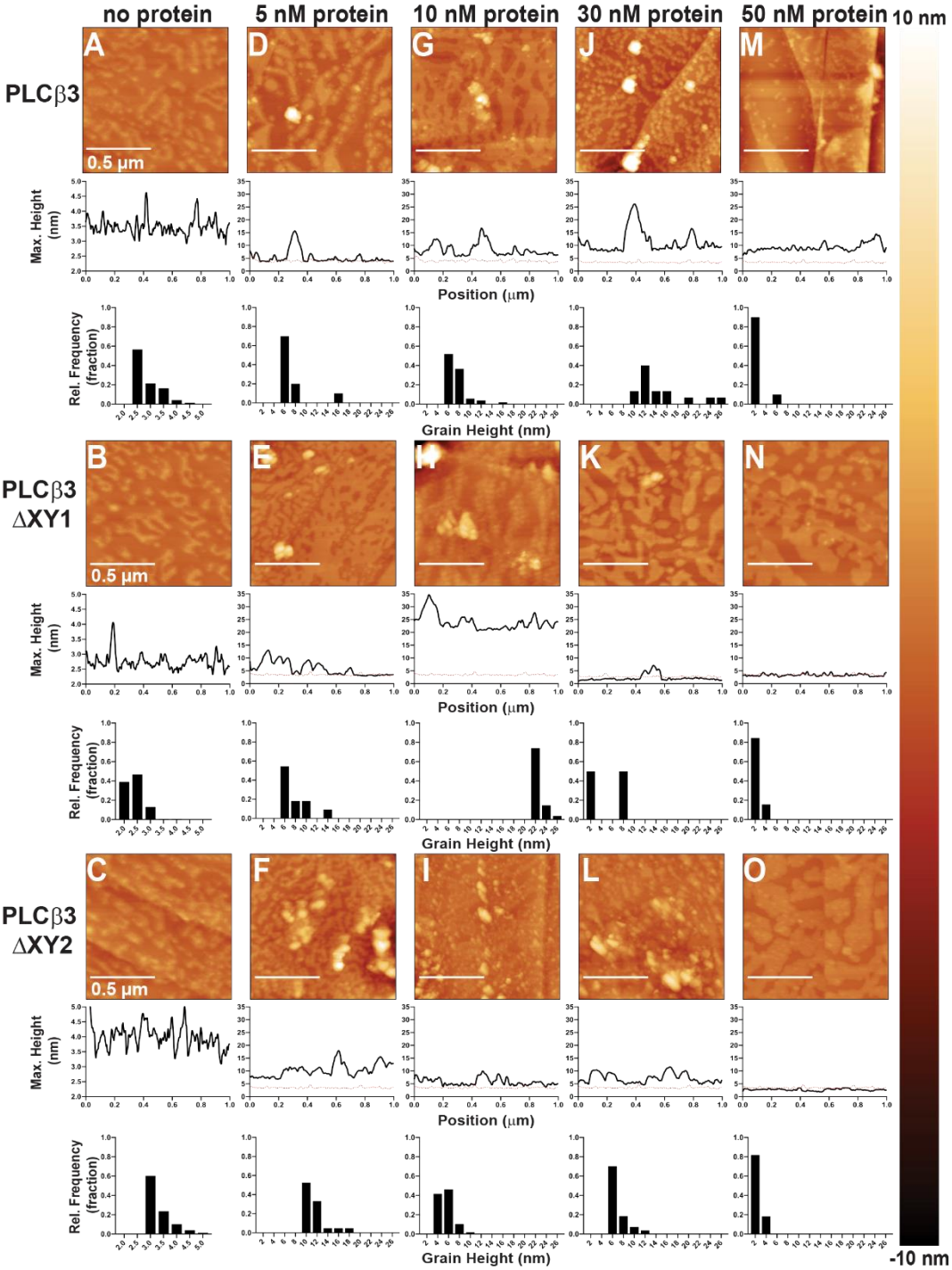
no protein
5 nM protein
10 nM protein
30 nM protein
50 nM protein
10 nm
-10 nm
PLCβ3
PLCβ3 ΔXY1
PLCβ3 ΔXY2
A
B
C
D
E
F
G
H
I
J
K
L
M
N
O
0.5 μm
Max. Height (nm)
Position (μm)
Rel. Frequency (fraction)
Grain Height (nm)

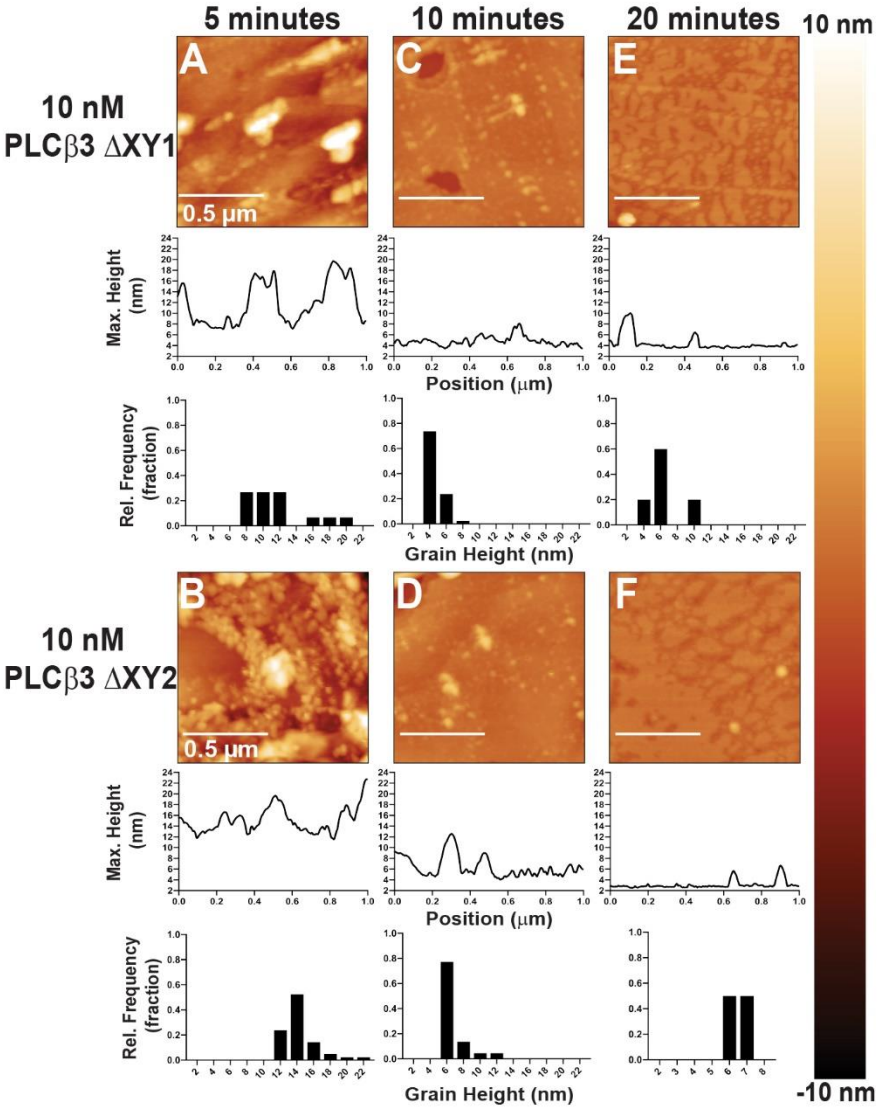

Figure 3.6. Representative AFM Tapping Mode Images of Compressed PE:PIP_2 Monolayers Incubated with PLCβ3 ΔXY Variants for Varying Incubation Times.
Changes in the maximum height and height frequency distributions due to protein adsorption are quantified below each micrograph. For comparison, a representative height profile from a compressed monolayer in the absence of protein is shown on each height profile as a dashed red line. Monolayers incubated with 10 nM (A) PLCβ3 ΔXY1 or (B) PLCβ3 ΔXY2 for 5 min., (C, D) 10 min., or (E, F) 20 min.

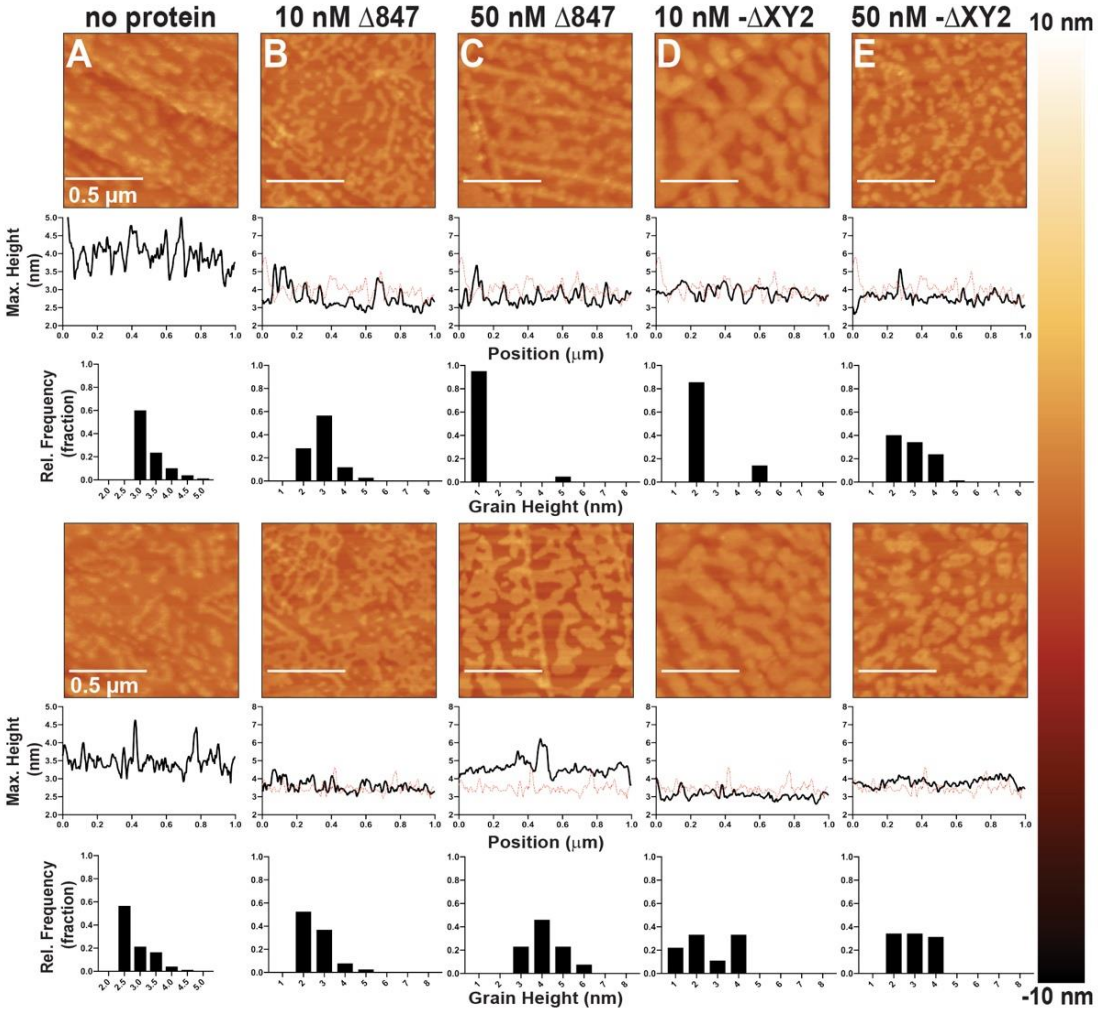

Figure 3.7. Representative AFM Tapping Mode Images of PE:PIP_2 Monolayers Incubated with PLCβ3-Δ847 or PLCβ3-Δ847 ΔXY2.

Two representative images of each condition are shown, with sample variations most likely due to lipid distribution in the monolayer and/or Langmuir-Schaefer transfer to the HOPG substrate. Topographical changes upon protein addition are detected as changes in the appearance of the monolayer surface, where taller features are shown in lighter colors, and increases in the height and/or size of surface features. The maximum heights above the HOPG surface as a function of position and the grain analysis for the relative height frequency of surface features are quantified below each micrograph. For comparison, a representative height profile from a compressed monolayer in the absence of protein is shown on each height profile as a dashed red line. Monolayers in the (A) absence of protein or incubated with (B) 10 nM PLCβ3-Δ847, (C) 50 nM PLCβ3-Δ847, (D) 10 nM PLCβ3-Δ847 ΔXY2, or (E) 50 nM PLCβ3-Δ847 ΔXY2.

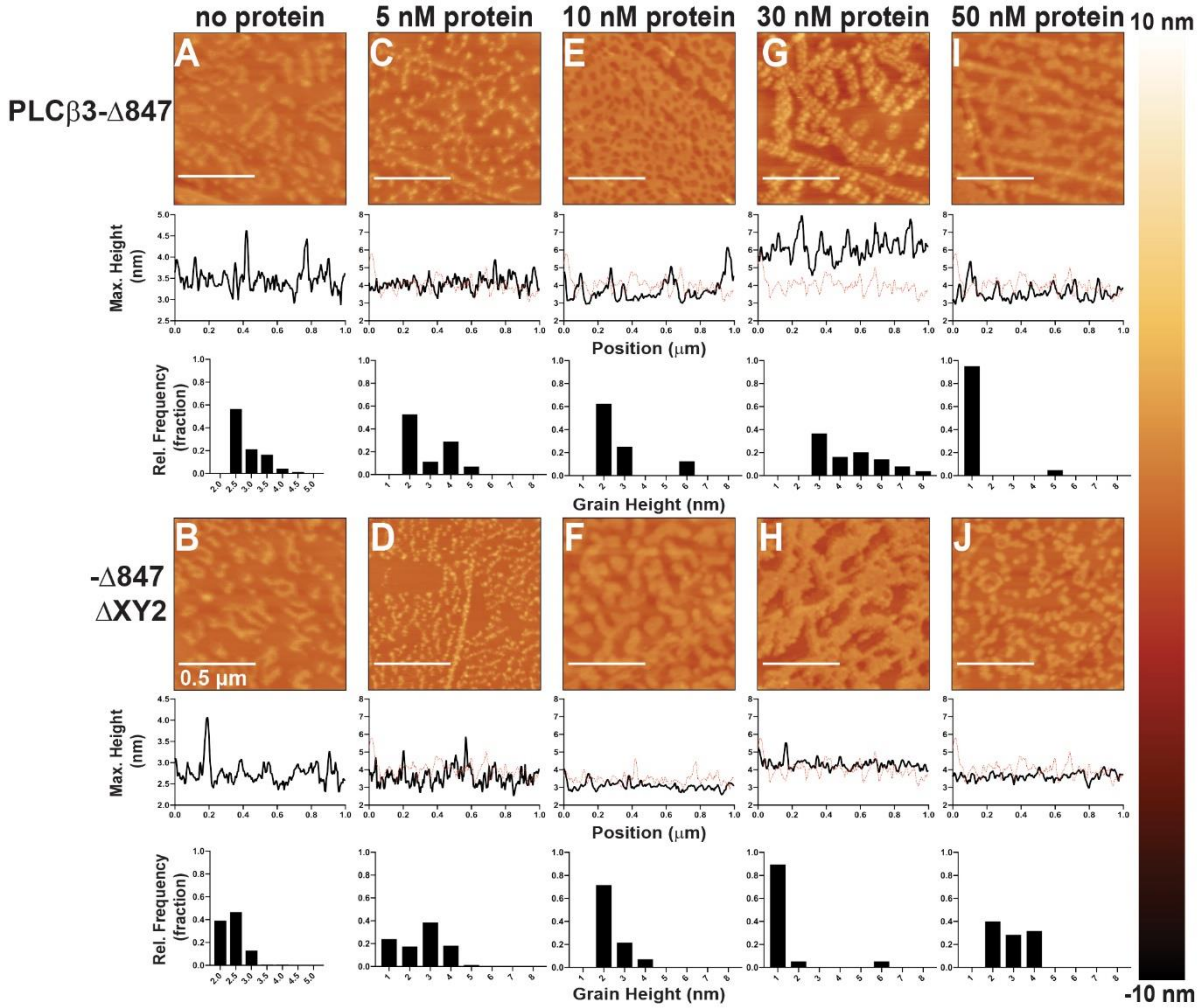

Figure 3.8. Representative AFM Tapping Mode Images of Compressed PE:PIP_2 Monolayers Incubated with Increasing Concentrations of PLCβ3-Δ847 ΔXY Variants.
One representative image of each condition is shown. Sample variations are most likely due to differences in lipid distribution and Langmuir-Schaefer transfer to the HOPG substrate. Topographical changes are detected as changes in the appearance of the monolayer surface, where taller features are shown in lighter colors in the false-colored micrographs. For comparison, a representative height profile from a compressed monolayer in the absence of protein is shown on each height profile as a dashed red line. Below each micrograph are height profiles of the monolayer surface quantifying the maximum heights measured above the supporting surface as a function of position. Grain analysis by height thresholding was also performed for each monolayer and shown in height distribution histograms below each height profile. Protein adsorption changes the grain height distribution of features across the monolayer surface. Monolayers in the (A-B) absence of protein or incubated with (C) 5 nM PLCβ3-Δ847, (D) 5 nM PLCβ3-Δ847 ΔXY2, (E) 10 nM PLCβ3-Δ847, (F) 10 nM PLCβ3-Δ847 ΔXY2, (G) 30 nM PLCβ3-Δ847, (H) 30 nM PLCβ3-Δ847 ΔXY2, (I) 50 nM PLCβ3-Δ847, (J) 50 nM PLCβ3-Δ847 ΔXY2 for 20 min. at room temperature prior to Langmuir-Schaefer transfer.

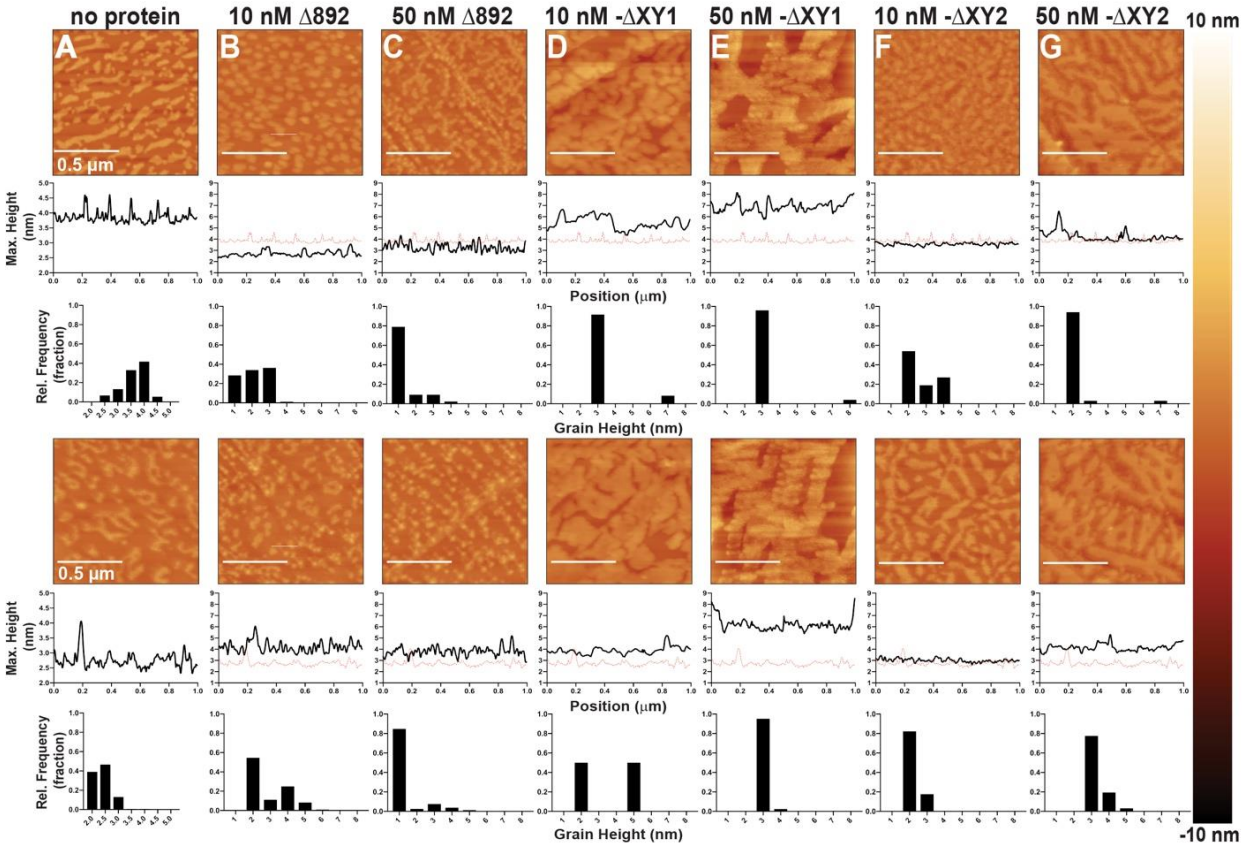

Figure 3.9. Representative AFM Tapping Mode Images of PE:PIP_2 Monolayers Incubated with PLCβ3-Δ892 ΔXY Variants.

Two representative images of each condition are shown, with sample variations most likely due to lipid distribution in the monolayer and/or Langmuir-Schaefer transfer to the HOPG substrate. Topographical changes are detected as changes in the appearance of the monolayer surface, with taller features shown in lighter colors, and increases in the height and/or size of surface features. The maximum heights above the HOPG surface as a function of position and the grain analysis for the relative height frequency of surface features are quantified below each micrograph. For comparison, a representative height profile from a compressed monolayer in the absence of protein is shown on each height profile as a dashed red line. Monolayers in the (A) absence of protein or incubated with (B) 10 nM PLCβ3-Δ892, (C) 50 nM PLCβ3-Δ892, (D) 10 nM PLCβ3-Δ892 ΔXY1, (E) 50 nM PLCβ3-Δ892 ΔXY1, (F) 10 nM PLCβ3-Δ892 ΔXY2, and (F) 50 nM PLCβ3-Δ892 ΔXY2.

Figure 3.10. Representative AFM Tapping Mode Images of Compressed PE:PIP_2 Monolayers Incubated with Increasing Concentrations of PLCβ3-Δ892 ΔXY Variants.
One representative image of each condition is shown. Sample variations are most likely due to differences in lipid distribution and Langmuir-Schaefer transfer to the HOPG substrate. Topographical changes are detected as changes in the appearance of the monolayer surface, where taller features are shown in lighter colors in the false-colored micrographs. Below each micrograph are height profiles of the monolayer surface quantifying the maximum heights measured above the supporting surface as a function of position. For comparison, a representative height profile from a compressed monolayer in the absence of protein is shown on each height profile as a dashed red line. Grain analysis by height thresholding was also performed for each monolayer and shown in height distribution histograms below each height profile. Protein adsorption changes the grain height distribution of features across the monolayer surface. Monolayers in the (A-B) absence of protein or incubated with (D) 5 nM PLCβ3-Δ892, (E) 5 nM PLCβ3-Δ892 ΔXY1, (F) 5 nM PLCβ3-Δ892 ΔXY2, (G) 10 nM PLCβ3-Δ892, (H) 10 nM PLCβ3-Δ892 ΔXY1, (I) 10 nM PLCβ3-Δ892 ΔXY2, (J) 30 nM PLCβ3-Δ892, (K) 30 nM PLCβ3-Δ892 ΔXY1, (L) 30 nM PLCβ3-Δ892 ΔXY2, (M) 50 nM PLCβ3-Δ892, (N) 50 nM PLCβ3-Δ892 ΔXY1, (O) 50 nM PLCβ3-Δ892 ΔXY2 for 20 min. at room temperature prior to Langmuir-Schaefer transfer.

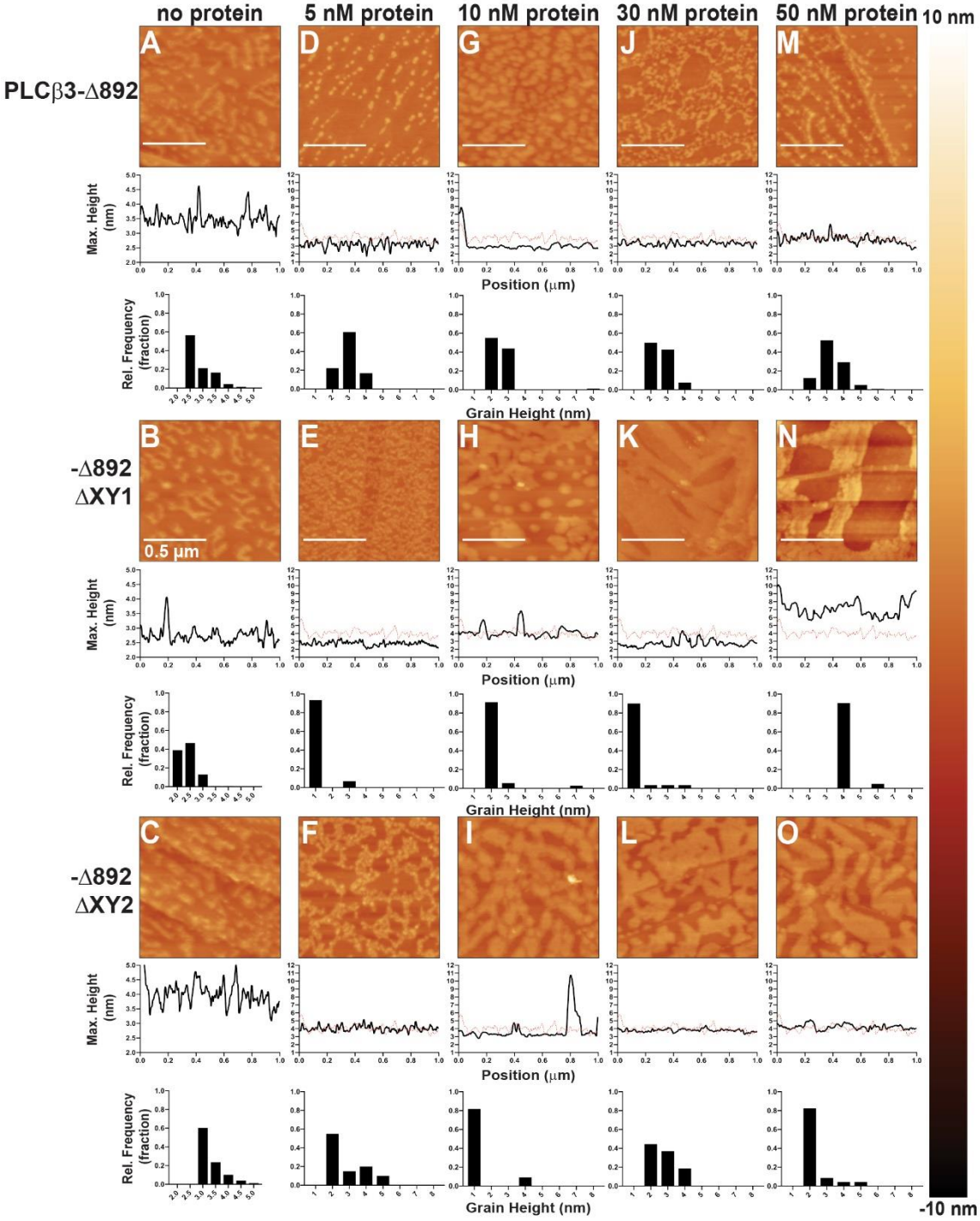
no protein
5 nM protein
10 nM protein
30 nM protein
50 nM protein
10 nm
-10 nm
PLCβ3-Δ892
-Δ892 ΔXY1
-Δ892 ΔXY2
A
B
C
D
E
F
G
H
I
J
K
L
M
N
O
0.5 μm
Max. Height (nm)
Position (μm)
Rel. Frequency (fraction)
Grain Height (nm)

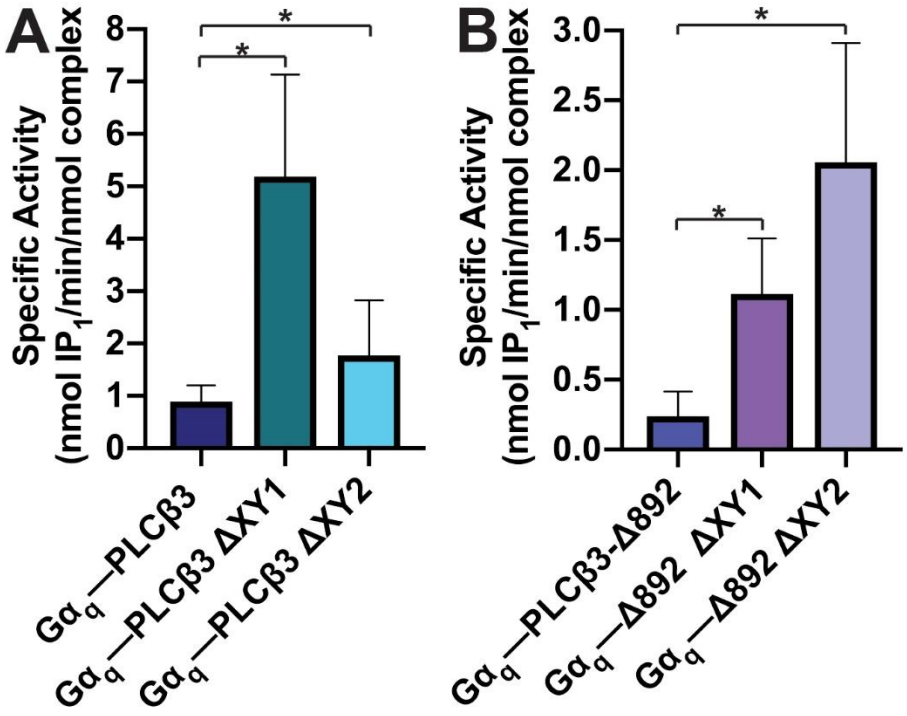

Figure 3.11. Deletions in the PLCβ3 X–Y Linker Increase $G\alpha_q$-Dependent Activation.
The specific activities of $G\alpha_q$–PLCβ3 variant complexes were measured using a liposome-based activity assay. (A) $G\alpha_q$–PLCβ3 complexes have higher activity than the (B) $G\alpha_q$–PLCβ3-Δ892 complexes and its ΔXY variants. This is consistent with the absence of the distal CTD in the PLCβ3-Δ892 variants. Data represent the average of at least four experiments in duplicate ± SEM (*$p \leq 0.05$).

Table 3.3. $G\alpha_q$-Dependent Activation of PLCβ3 Variants.

Variant Complex	Increase in Specific Activity (nmol IP_1/min/nmol complex)[a]	Fold Max. Activity Over Basal[d]
$G\alpha_q$–PLCβ3	0.89 ± 0.15	8
$G\alpha_q$–PLCβ3 ΔXY1	5.2 ± 1.0[b]	4
$G\alpha_q$–PLCβ3 ΔXY2	1.8 ± 0.40[b]	2
$G\alpha_q$–PLCβ3-Δ892	0.24 ± 0.06	22
$G\alpha_q$–PLCβ3-Δ892 ΔXY1	1.1 ± 0.20[c]	2
$G\alpha_q$–PLCβ3-Δ892 ΔXY2	2.1 ± 0.40[c]	3

[a] Data represents the average of four experiments in duplicate ± SEM. [b] Significant relative to $G\alpha_q$–PLCβ3 (*$p \leq 0.05$). [c] Significant relative to $G\alpha_q$–PLCβ3-Δ892 (*$p \leq 0.05$). [d] Fold activation was calculated by dividing the basal activity of the $G\alpha_q$–PLCβ3 ΔXY complex by the basal activity of the PLCβ3 variant (Table 3.2).

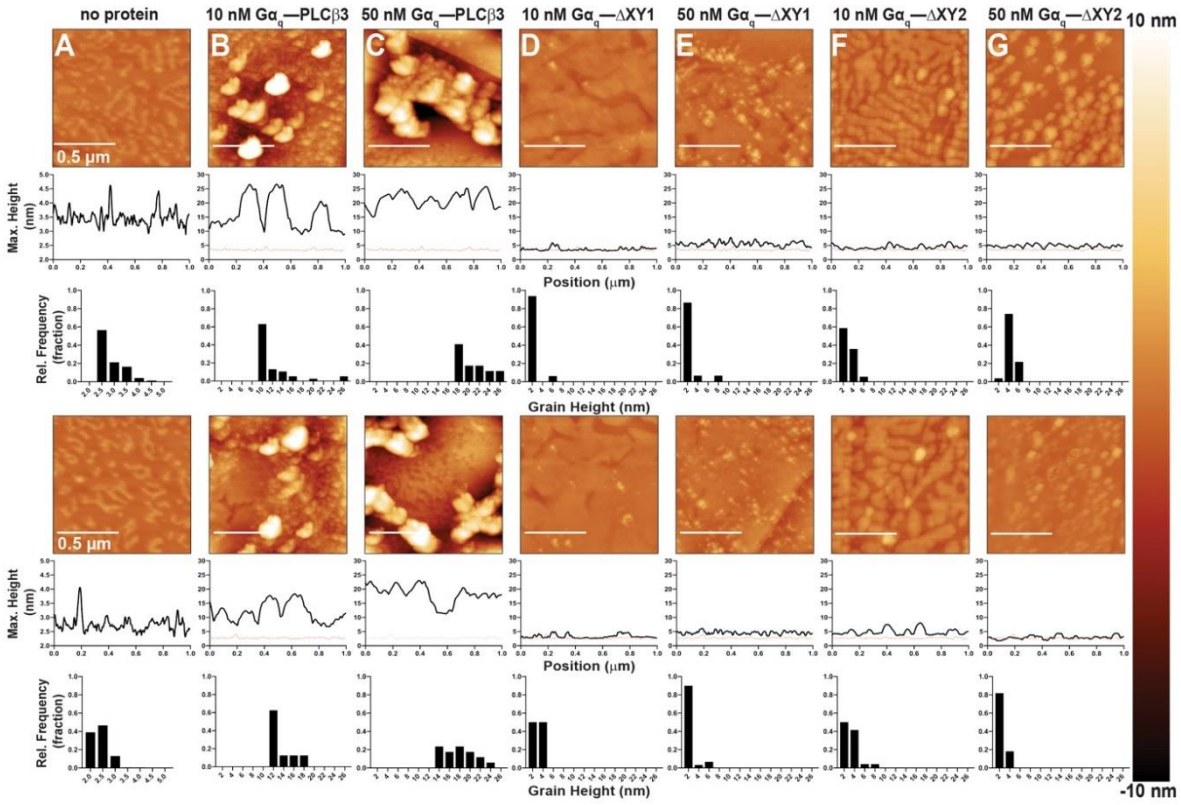

Figure 3.12. Representative AFM Tapping Mode Images of PE:PIP_2 Monolayers Incubated with $G\alpha_q$–PLCβ3 ΔXY Variant Complexes.

Two representative images of each condition are shown, with sample variations most likely due to lipid distribution in the monolayer and/or Langmuir-Schaefer transfer to the HOPG substrate. Topographical changes upon protein addition are detected as changes in the appearance of the monolayer surface, where taller features are shown in lighter colors, and increases in the height and/or size of surface features. The maximum heights above the HOPG surface as a function of position and the grain analysis for the relative height frequency of surface features are quantified below each micrograph. For comparison, a representative height profile from a compressed monolayer in the absence of protein is shown on each height profile as a dashed red line. Monolayers in the (A) absence of protein or incubated with (B) 10 nM $G\alpha_q$–PLCβ3, (C) 50 nM $G\alpha_q$–PLCβ3, (D) 10 nM $G\alpha_q$–PLCβ3 ΔXY1, (E) 50 nM $G\alpha_q$–PLCβ3 ΔXY1, (F) 10 nM $G\alpha_q$–PLCβ3 ΔXY2, or (F) 50 nM $G\alpha_q$–PLCβ3 ΔXY2.

Figure 3.13. Representative AFM Tapping Mode Images of Compressed PE:PIP_2 Monolayers Incubated with Increasing Concentrations of $G\alpha_q$–PLCβ3 ΔXY Variant Complexes. One representative image of each condition is shown. Sample variations are most likely due to differences in lipid distribution and Langmuir-Schaefer transfer to the HOPG substrate. Topographical changes are detected as changes in the appearance of the monolayer surface, where taller features are shown in lighter colors in the false-colored micrographs. Below each micrograph are height profiles of the monolayer surface quantifying the maximum heights measured above the supporting surface as a function of position. For comparison, a representative height profile from a compressed monolayer in the absence of protein is shown on each height profile as a dashed red line. Grain analysis by height thresholding was also performed for each monolayer and shown in height distribution histograms below each height profile. Protein adsorption changes the grain height distribution of features across the monolayer surface. Monolayers in the (A-B) absence of protein or incubated with (D) 5 nM $G\alpha_q$–PLCβ3, (E) 5 nM $G\alpha_q$–PLCβ3 ΔXY1, (F) 5 nM $G\alpha_q$–PLCβ3 ΔXY2, (G) 10 nM $G\alpha_q$–PLCβ3, (H) 10 nM $G\alpha_q$–PLCβ3 ΔXY1, (I) 10 nM $G\alpha_q$–PLCβ3 ΔXY2, (J) 30 nM $G\alpha_q$–PLCβ3, (K) 30 nM $G\alpha_q$–PLCβ3 ΔXY1, (L) 30 nM $G\alpha_q$–PLCβ3 ΔXY2, (M) 50 nM $G\alpha_q$–PLCβ3, (N) 50 nM $G\alpha_q$–PLCβ3 ΔXY1, (O) 50 nM $G\alpha_q$–PLCβ3 ΔXY2 for 20 min. at room temperature prior to Langmuir-Schaefer transfer.

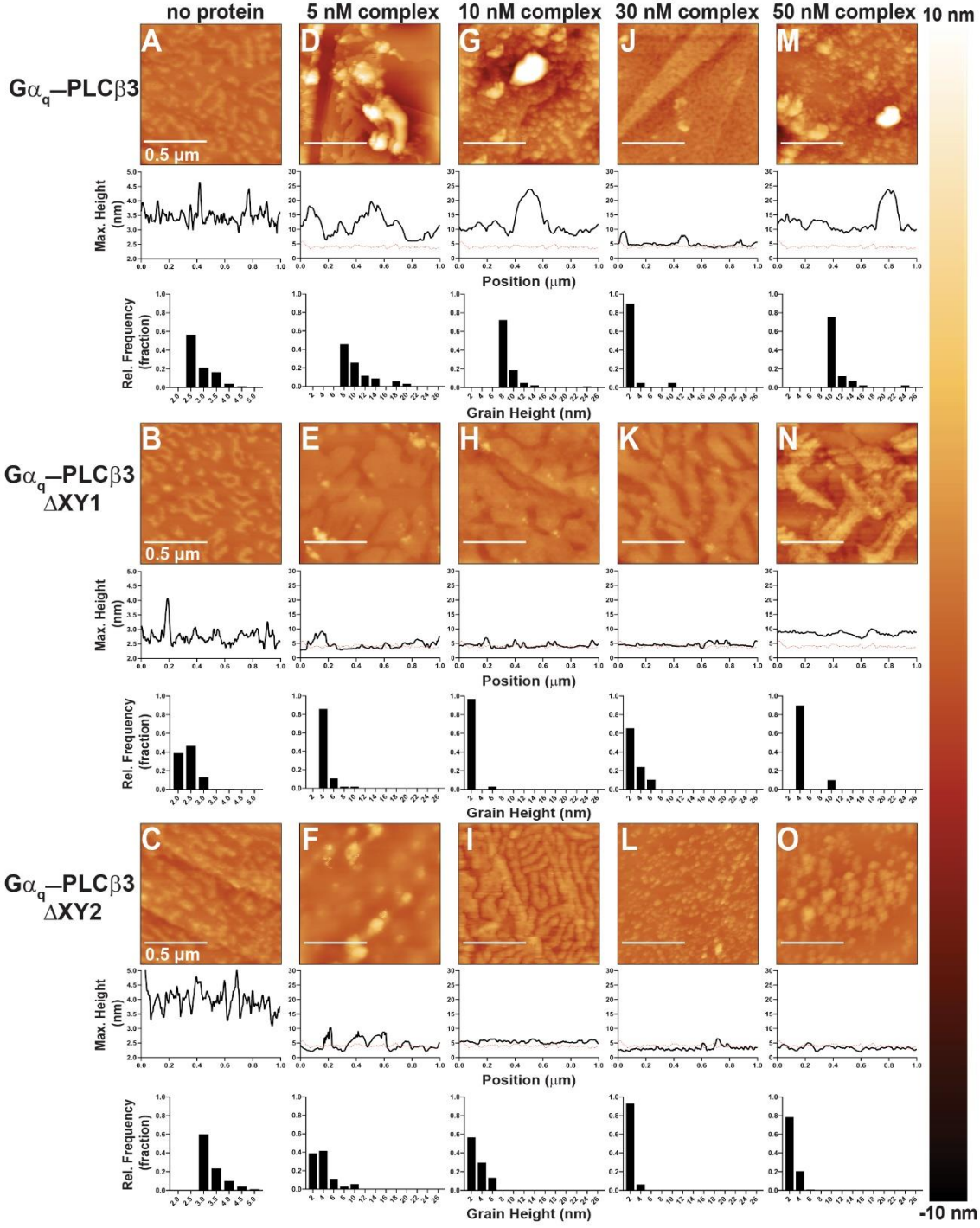
no protein
5 nM complex
10 nM complex
30 nM complex
50 nM complex
10 nm
-10 nm
Gαq–PLCβ3
Gαq–PLCβ3 ΔXY1
Gαq–PLCβ3 ΔXY2
A
B
C
D
E
F
G
H
I
J
K
L
M
N
O
0.5 μm
Max. Height (nm)
Position (μm)
Rel. Frequency (fraction)
Grain Height (nm)

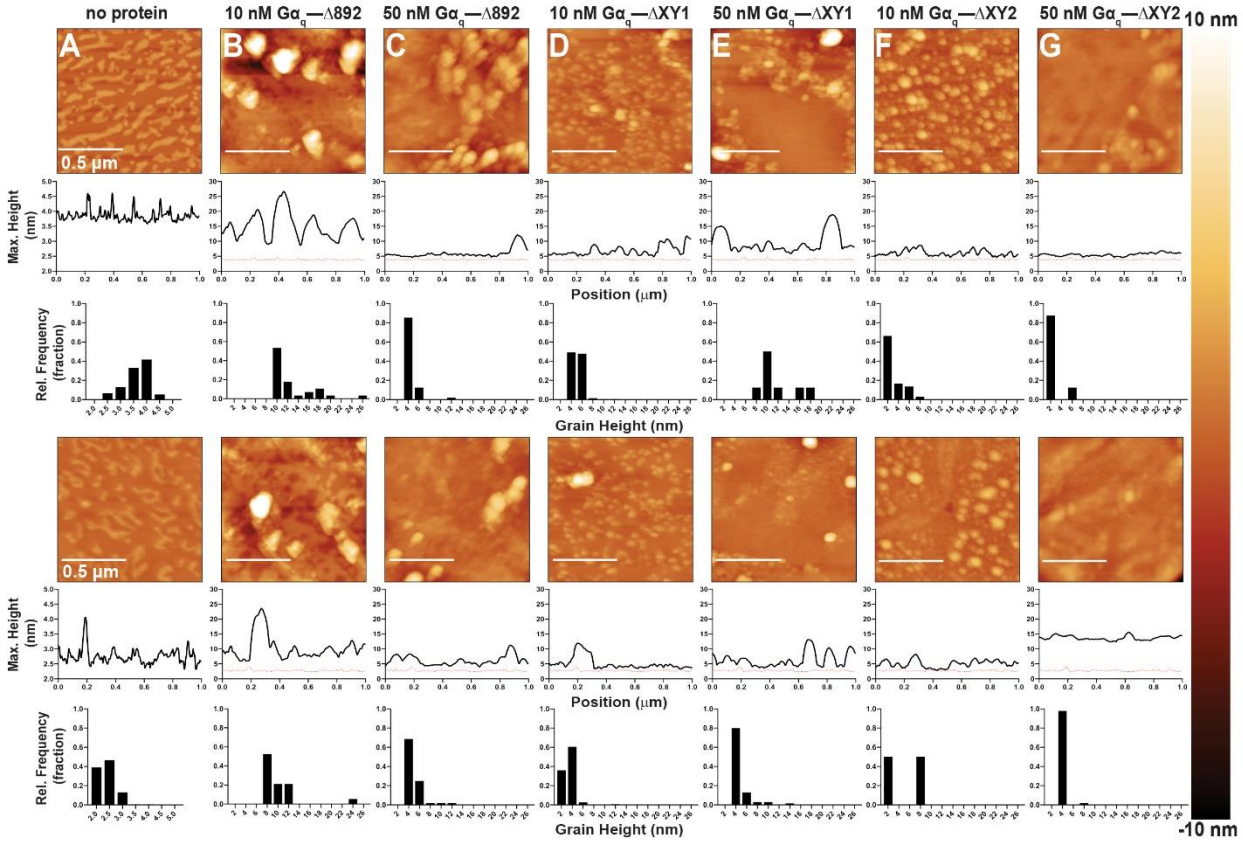

Figure 3.14. Representative AFM Tapping Mode Images of PE:PIP_2 Monolayers Incubated with $G\alpha_q$–PLCβ3 Δ892 ΔXY Variant Complexes.

Two representative images of each condition are shown, with sample variations most likely due to lipid distribution in the monolayer and/or Langmuir-Schaefer transfer to the HOPG substrate. Topographical changes upon protein addition are detected as changes in the appearance of the monolayer surface, where taller features are shown in lighter colors, and increases in the height and/or size of surface features. The maximum heights above the HOPG surface as a function of position and the grain analysis for the relative height frequency of surface features are quantified below each micrograph. For comparison, a representative height profile from a compressed monolayer in the absence of protein is shown on each height profile as a dashed red line. Monolayers in the (A) absence of protein or incubated with (B) 10 nM $G\alpha_q$–PLCβ3 Δ892, (C) 50 nM $G\alpha_q$–PLCβ3 Δ892, (D) 10 nM $G\alpha_q$–PLCβ3 Δ892 ΔXY1, (E) 50 nM $G\alpha_q$–PLCβ3 Δ892 ΔXY1, (F) 10 nM $G\alpha_q$–PLCβ3 Δ892 ΔXY2, or (F) 50 nM $G\alpha_q$–PLCβ3 Δ892 ΔXY2.

Figure 3.15. Representative AFM Tapping Mode Images of Compressed PE:PIP_2 Monolayers Incubated with $G\alpha_q$–PLCβ3-Δ892 ΔXY Variant Complexes.
One representative image of each condition is shown. Sample variations are most likely due to differences in lipid distribution and Langmuir-Schaefer transfer to the HOPG substrate. Topographical changes are detected as changes in the appearance of the monolayer surface, where taller features are shown in lighter colors in the false-colored micrographs. Below each micrograph are height profiles of the monolayer surface quantifying the maximum heights measured above the supporting surface as a function of position. For comparison, a representative height profile from a compressed monolayer in the absence of protein is shown on each height profile as a dashed red line. Grain analysis by height thresholding was also performed for each monolayer and shown in height distribution histograms below each height profile. Protein adsorption changes the grain height distribution of features across the monolayer surface. Monolayers in the (A-B) absence of protein or incubated with (D) 5 nM $G\alpha_q$–PLCβ3-Δ892, (E) 5 nM $G\alpha_q$–PLCβ3-Δ892 ΔXY1, (F) 5 nM $G\alpha_q$–PLCβ3-Δ892 ΔXY2, (G) 10 nM $G\alpha_q$–PLCβ3-Δ892, (H) 10 nM $G\alpha_q$–PLCβ3-Δ892 ΔXY1, (I) 10 nM $G\alpha_q$–PLCβ3-Δ892 ΔXY2, (J) 30 nM $G\alpha_q$–PLCβ3-Δ892, (K) 30 nM $G\alpha_q$–PLCβ3-Δ892 ΔXY1, (L) 30 nM $G\alpha_q$–PLCβ3-Δ892 ΔXY2, (M) 50 nM $G\alpha_q$–PLCβ3-Δ892, (N) 50 nM $G\alpha_q$–PLCβ3-Δ892 ΔXY1, (O) $G\alpha_q$–50 nM PLCβ3-Δ892 ΔXY2 for 20 min. at room temperature prior to Langmuir-Schaefer transfer.

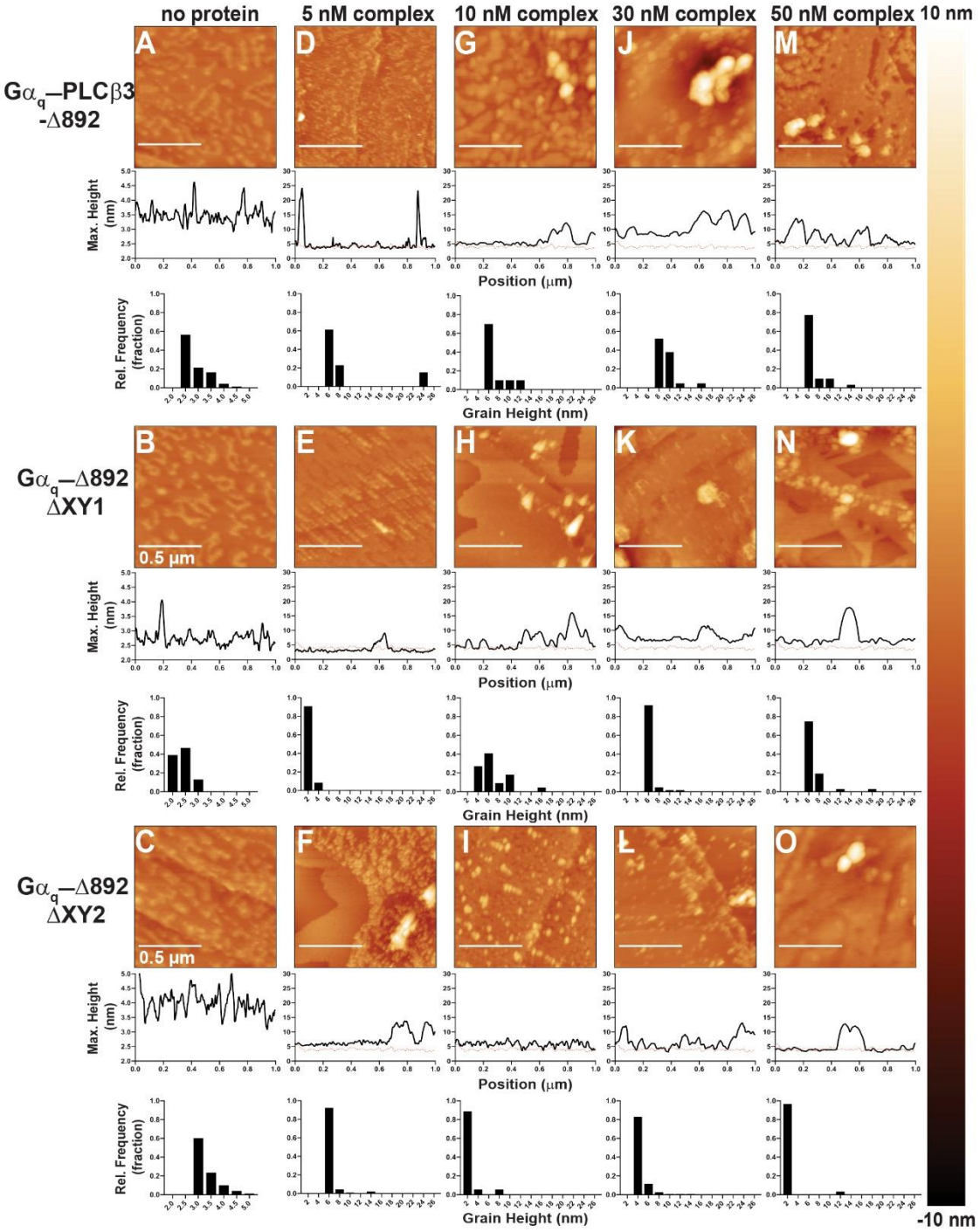
no protein
5 nM complex
10 nM complex
30 nM complex
50 nM complex
10 nm
Gαq–PLCβ3 -Δ892
Gαq–Δ892 ΔXY1
Gαq–Δ892 ΔXY2
A
B
C
D
E
F
G
H
I
J
K
Ł
M
N
O
0.5 μm
0.5 μm
Max. Height (nm)
Position (μm)
Rel. Frequency (fraction)
Grain Height (nm)
-10 nm

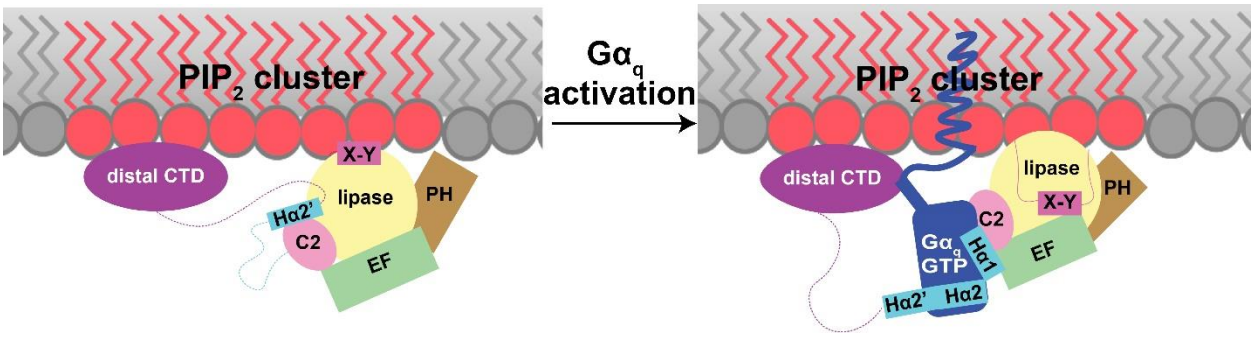

Figure 3.16. Regulation of PLCβ Adsorption by the X–Y Linker and $G\alpha_q$.
Under basal conditions, PLCβ3 can adsorb to regions of the monolayer enriched in PIP_2 via interactions between the distal CTD and the negatively charged PIP_2. Unfavorable electrostatic interactions between the acidic stretch of the X–Y linker and the membrane expose the active site and facilitate substrate binding. The Hα2′ helix remains bound to the core and regulates activity by limiting adsorption to the membrane. Upon activation of G_q-coupled receptors, $G\alpha_q$ binds to the proximal CTD, displacing Hα2′ helix and allosterically activate PLCβ3. Interactions between $G\alpha_q$, the core, and the distal CTD promote interfacial activation to expose the active site and regulate the spatial distribution of the complex.

3.6 References

(1) Kadamur, G.; Ross, E. M. Mammalian Phospholipase C. *Annu. Rev. Physiol.* **2013**, *75* (1), 127–154. https://doi.org/10.1146/annurev-physiol-030212-183750.

(2) Gresset, A.; Sondek, J.; Harden, T. K. The Phospholipase C Isozymes and Their Regulation. *Subcell. Biochem.* **2012**, *58*, 61–94. https://doi.org/10.1007/978-94-007-3012-0_3.

(3) Shortridge, R. D.; McKay, R. R. Invertebrate Phosphatidylinositol-Specific Phospholipases C and Their Role in Cell Signaling. *Invertebr. Neurosci. IN* **1995**, *1* (3), 199–206.

(4) McKay, R. R.; Chen, D. M.; Miller, K.; Kim, S.; Stark, W. S.; Shortridge, R. D. Phospholipase C Rescues Visual Defect in NorpA Mutant of Drosophila Melanogaster. *J. Biol. Chem.* **1995**, *270* (22), 13271–13276.

(5) Park, D.; Jhon, D. Y.; Lee, C. W.; Lee, K. H.; Rhee, S. G. Activation of Phospholipase C Isozymes by G Protein Beta Gamma Subunits. *J. Biol. Chem.* **1993**, *268* (7), 4573–4576.

(6) Filtz, T. M.; Grubb, D. R.; McLeod-Dryden, T. J.; Luo, J.; Woodcock, E. A. Gq-Initiated Cardiomyocyte Hypertrophy Is Mediated by Phospholipase Cβ1b. *FASEB J.* **2009**, *23* (10), 3564–3570. https://doi.org/10.1096/fj.09-133983.

(7) Grubb, D. R.; Crook, B.; Ma, Y.; Luo, J.; Qian, H. W.; Gao, X.-M.; Kiriazis, H.; Du, X.-J.; Gregorevic, P.; Woodcock, E. A. The Atypical 'b' Splice Variant of Phospholipase Cβ1 Promotes Cardiac Contractile Dysfunction. *J. Mol. Cell. Cardiol.* **2015**, *84*, 95–103. https://doi.org/10.1016/j.yjmcc.2015.04.016.

(8) Atef, M. E.; Anand-Srivastava, M. B. Role of PKCδ in Enhanced Expression of Gqα/PLCβ1 Proteins and VSMC Hypertrophy in Spontaneously Hypertensive Rats. *PLOS ONE* **2016**, *11* (7), e0157955. https://doi.org/10.1371/journal.pone.0157955.

(9) Woodcock, E. A.; Grubb, D. R.; Filtz, T. M.; Marasco, S.; Luo, J.; McLeod-Dryden, T. J.; Kaye, D. M.; Sadoshima, J.; Du, X.-J.; Wong, C.; et al. Selective Activation of the "b" Splice Variant of Phospholipase Cβ1 in Chronically Dilated Human and Mouse Atria. *J. Mol. Cell. Cardiol.* **2009**, *47* (5), 676–683. https://doi.org/10.1016/j.yjmcc.2009.08.020.

(10) Dent, M. R.; Dhalla, N. S.; Tappia, P. S. Phospholipase C Gene Expression, Protein Content, and Activities in Cardiac Hypertrophy and Heart Failure Due to Volume Overload. *Am. J. Physiol.* **2004**, *287* (2), H719–H727. https://doi.org/10.1152/ajpheart.01107.2003.

(11) Adjobo-Hermans, M. J. W.; Goedhart, J.; Gadella, T. W. J. Regulation of PLCβ1a Membrane Anchoring by Its Substrate Phosphatidylinositol (4,5)-Bisphosphate. *J. Cell Sci.* **2008**, *121* (22), 3770–3777. https://doi.org/10.1242/jcs.029785.

(12) Mathews, J. L.; Smrcka, A. V.; Bidlack, J. M. A Novel Gβγ-Subunit Inhibitor Selectively Modulates μ-Opioid-Dependent Antinociception and Attenuates Acute Morphine-Induced Antinociceptive Tolerance and Dependence. *J. Neurosci.* **2008**, *28* (47), 12183–12189. https://doi.org/10.1523/JNEUROSCI.2326-08.2008.

(13) Lyon, A. M.; Tesmer, J. J. G. Structural Insights into Phospholipase C-β Function. *Mol. Pharmacol.* **2013**, *84* (4), 488–500. https://doi.org/10.1124/mol.113.087403.

(14) Lyon, A. M.; Tesmer, V. M.; Dhamsania, V. D.; Thal, D. M.; Gutierrez, J.; Chowdhury, S.; Suddala, K. C.; Northup, J. K.; Tesmer, J. J. G. An Autoinhibitory Helix in the C-Terminal Region of Phospholipase C-β Mediates Gαq Activation. *Nat. Struct. Mol. Biol.* **2011**, *18* (9), 999–1005. https://doi.org/10.1038/nsmb.2095.

(15) Waldo, G. L.; Ricks, T. K.; Hicks, S. N.; Cheever, M. L.; Kawano, T.; Tsuboi, K.; Wang, X.; Montell, C.; Kozasa, T.; Sondek, J.; et al. Kinetic Scaffolding Mediated by a Phospholipase C–β and Gq Signaling Complex. *Science* **2010**, *330* (6006), 974–980. https://doi.org/10.1126/science.1193438.

(16) Lyon, A. M.; Dutta, S.; Boguth, C. A.; Skiniotis, G.; Tesmer, J. J. G. Full-Length Gαq–Phospholipase C-B3 Structure Reveals Interfaces of the C-Terminal Coiled-Coil Domain. *Nat. Struct. Mol. Biol.* **2013**, *20* (3), 355–362. https://doi.org/10.1038/nsmb.2497.

(17) Singer, A. G.; Ghomashchi, F.; Calvez, C. L.; Bollinger, J.; Bezzine, S.; Rouault, M.; Sadilek, M.; Nguyen, E.; Lazdunski, M.; Lambeau, G.; et al. Interfacial Kinetic and Binding Properties of the Complete Set of Human and Mouse Groups I, II, V, X, and XII Secreted Phospholipases A2. *J. Biol. Chem.* **2002**, *277* (50), 48535–48549. https://doi.org/10.1074/jbc.M205855200.

(18) Lyon, A. M.; Begley, J. A.; Manett, T. D.; Tesmer, J. J. G. Molecular Mechanisms of PLCβ3 Autoinhibition. *Struct. Lond. Engl. 1993* **2014**, *22* (12), 1844–1854. https://doi.org/10.1016/j.str.2014.10.008.

(19) Hudson, B. N.; Hyun, S.-H.; Thompson, D. H.; Lyon, A. M. Phospholipase Cβ3 Membrane Adsorption and Activation Are Regulated by Its C-Terminal Domains and Phosphatidylinositol 4,5-Bisphosphate. *Biochemistry* **2017**, *56* (41), 5604–5614. https://doi.org/10.1021/acs.biochem.7b00547.

(20) Jenco, J. M.; Becker, K. P.; Morris, A. J. Membrane-Binding Properties of Phospholipase C-Beta1 and PhospholipaseC-Beta2: Role of the C-Terminus and Effects of Polyphosphoinositides, G-Proteins and Ca2+. *Biochem. J.* **1997**, *327* (Pt 2), 431–437.

(21) Illenberger, D.; Schwald, F.; Pimmer, D.; Binder, W.; Maier, G.; Dietrich, A.; Gierschik, P. Stimulation of Phospholipase C-Beta2 by the Rho GTPases Cdc42Hs and Rac1. *EMBO J.* **1998**, *17* (21), 6241–6249. https://doi.org/10.1093/emboj/17.21.6241.

(22) Illenberger, D.; Walliser, C.; Nurnberg, B.; Diaz Lorente, M.; Gierschik, P. Specificity and Structural Requirements of Phospholipase C-Beta Stimulation by Rho GTPases versus G Protein Beta Gamma Dimers. *J. Biol. Chem.* **2003**, *278* (5), 3006–3014. https://doi.org/10.1074/jbc.M208282200.

(23) Romoser, V.; Ball, R.; Smrcka, A. V. Phospholipase C B2 Association with Phospholipid Interfaces Assessed by Fluorescence Resonance Energy Transfer G Protein Beta Gamma Subunit-Mediated Translocation Is Not Required for Enzyme Activation. *J. Biol. Chem.* **1996**, *271* (41), 25071–25078. https://doi.org/10.1074/jbc.271.41.25071.

(24) Runnels, L. W.; Jenco, J.; Morris, A.; Scarlata, S. Membrane Binding of Phospholipases C-Beta 1 and C-Beta 2 Is Independent of Phosphatidylinositol 4,5-Bisphosphate and the Alpha and Beta Gamma Subunits of G Proteins. *Biochemistry* **1996**, *35* (51), 16824–16832. https://doi.org/10.1021/bi961606w.

(25) Scarlata, S. Regulation of the Lateral Association of Phospholipase Cbeta2 and G Protein Subunits by Lipid Rafts. *Biochemistry* **2002**, *41* (22), 7092–7099.

(26) Gutman, O.; Walliser, C.; Piechulek, T.; Gierschik, P.; Henis, Y. I. Differential Regulation of Phospholipase C-Beta2 Activity and Membrane Interaction by Galphaq, Gbeta1gamma2, and Rac2. *J. Biol. Chem.* **2010**, *285* (6), 3905–3915. https://doi.org/10.1074/jbc.M109.085100.

(27) Schnabel, P.; Camps, M.; Carozzi, A.; Parker, P. J.; Gierschik, P. Mutational Analysis of Phospholipase C-B2. *Eur. J. Biochem.* **1993**, *217* (3), 1109–1115. https://doi.org/10.1111/j.1432-1033.1993.tb18343.x.

(28) Camps, M.; Carozzi, A.; Schnabel, P.; Scheer, A.; Parker, P. J.; Gierschik, P. Isozyme-Selective Stimulation of Phospholipase C-B2 by G Protein Bγ-Subunits. *Nature* **1992**, *360* (6405), 684–686. https://doi.org/10.1038/360684a0.

(29) Katz, A.; Wu, D.; Simon, M. I. Subunits Beta Gamma of Heterotrimeric G Protein Activate Beta 2 Isoform of Phospholipase C. *Nature* **1992**, *360* (6405), 686–689. https://doi.org/10.1038/360686a0.

(30) Smrcka, A. V.; Sternweis, P. C. Regulation of Purified Subtypes of Phosphatidylinositol-Specific Phospholipase C Beta by G Protein Alpha and Beta Gamma Subunits. *J. Biol. Chem.* **1993**, *268* (13), 9667–9674.

(31) Lee, S. B.; Shin, S. H.; Hepler, J. R.; Gilman, A. G.; Rhee, S. G. Activation of Phospholipase C-Beta 2 Mutants by G Protein Alpha q and Beta Gamma Subunits. *J. Biol. Chem.* **1993**, *268* (34), 25952–25957.

(32) Hepler, J. R.; Biddlecome, G. H.; Kleuss, C.; Camp, L. A.; Hofmann, S. L.; Ross, E. M.; Gilman, A. G. Functional Importance of the Amino Terminus of G. *J. Biol. Chem.* **1996**, *271* (1), 496–504. https://doi.org/10.1074/jbc.271.1.496.

(33) Wedegaertner, P. B.; Chu, D. H.; Wilson, P. T.; Levis, M. J.; Bourne, H. R. Palmitoylation Is Required for Signaling Functions and Membrane Attachment of Gq Alpha and Gs Alpha. *J. Biol. Chem.* **1993**, *268* (33), 25001–25008.

(34) Dietrich, A.; Brazil, D.; Jensen, O. N.; Meister, M.; Schrader, M.; Moomaw, J. F.; Mann, M.; Illenberger, D.; Gierschik, P. Isoprenylation of the G Protein γ Subunit Is Both Necessary and Sufficient for Bγ Dimer-Mediated Stimulation of Phospholipase C. *Biochemistry* **1996**, *35* (48), 15174–15182. https://doi.org/10.1021/bi960305j.

(35) Demel, R. A.; Geurts van Kessel, W. S. M.; Zwaal, R. F. A.; Roelofsen, B.; van Deenen, L. L. M. Relation between Various Phospholipase Actions on Human Red Cell Membranes and the Interfacial Phospholipid Pressure in Monolayers. *Biochim. Biophys. Acta BBA - Biomembr.* **1975**, *406* (1), 97–107. https://doi.org/10.1016/0005-2736(75)90045-0.

(36) James, S. R.; Demel, R. A.; Downes, C. P. Interfacial Hydrolysis of Phosphatidylinositol 4-Phosphate and Phosphatidylinositol 4,5-Bisphosphate by Turkey Erythrocyte Phospholipase C. *Biochem. J.* **1994**, *298* (2), 499–506. https://doi.org/10.1042/bj2980499.

(37) James, S. R.; Paterson, A.; Harden, T. K.; Demel, R. A.; Downes, C. P. Dependence of the Activity of Phospholipase Cβ on Surface Pressure and Surface Composition in Phospholipid Monolayers and Its Implications for Their Regulation. *Biochemistry* **1997**, *36* (4), 848–855. https://doi.org/10.1021/bi962108q.

(38) Boguslavsky, V.; Rebecchi, M.; Morris, A. J.; Jhon, D. Y.; Rhee, S. G.; McLaughlin, S. Effect of Monolayer Surface Pressure on the Activities of Phosphoinositide-Specific Phospholipase C-.Beta.1, -.Gamma.1, and -.Delta.1. *Biochemistry* **1994**, *33* (10), 3032–3037. https://doi.org/10.1021/bi00176a036.

(39) Arduin, A.; Gaffney, P. R. J.; Ces, O. Regulation of PLCβ2 by the Electrostatic and Mechanical Properties of Lipid Bilayers. *Sci. Rep.* **2015**, *5*. https://doi.org/10.1038/srep12628.

(40) Chan, P.; Gabay, M.; Wright, F. A.; Kan, W.; Oner, S. S.; Lanier, S. M.; Smrcka, A. V.; Blumer, J. B.; Tall, G. G. Purification of Heterotrimeric G Protein α Subunits by GST-Ric-8 Association Primary Characterization of Purified Gαolf. *J. Biol. Chem.* **2011**, *286* (4), 2625–2635. https://doi.org/10.1074/jbc.M110.178897.

(41) Nečas, D.; Klapetek, P. Gwyddion: An Open-Source Software for SPM Data Analysis. *Cent. Eur. J. Phys.* **2012**, *10* (1), 181–188. https://doi.org/10.2478/s11534-011-0096-2.

(42) Zhang, J. Y.; Kowal, D. M.; Nawoschik, S. P.; Dunlop, J.; Pausch, M. H.; Peri, R. Development of an Improved IP $_1$ Assay for the Characterization of 5-HT $_{2C}$ Receptor Ligands. Assay *Drug Dev. Technol.* **2010**, *8* (1), 106–113. https://doi.org/10.1089/adt.2009.0205.

(43) Bergsdorf, C.; Kropp-Goerkis, C.; Kaehler, I.; Ketscher, L.; Boemer, U.; Parczyk, K.; Bader, B. A One-Day, Dispense-Only IP-One HTRF Assay for High-Throughput Screening of Galphaq Protein-Coupled Receptors: Towards Cells as Reagents. *Assay Drug Dev. Technol.* **2008**, *6* (1), 39–53. https://doi.org/10.1089/adt.2007.108.

(44) Trinquet, E.; Fink, M.; Bazin, H.; Grillet, F.; Maurin, F.; Bourrier, E.; Ansanay, H.; Leroy, C.; Michaud, A.; Durroux, T.; et al. D-Myo-Inositol 1-Phosphate as a Surrogate of D-Myo-Inositol 1,4,5-Tris Phosphate to Monitor G Protein-Coupled Receptor Activation. *Anal. Biochem.* **2006**, *358* (1), 126–135. https://doi.org/10.1016/j.ab.2006.08.002.

(45) Levental, I.; Cēbers, A.; Janmey, P. A. Combined Electrostatics and Hydrogen Bonding Determine Intermolecular Interactions Between Polyphosphoinositides. *J. Am. Chem. Soc.* **2008**, *130* (28), 9025–9030. https://doi.org/10.1021/ja800948c.

(46) Redfern, D. A.; Gericke, A. PH-Dependent Domain Formation in Phosphatidylinositol Polyphosphate/Phosphatidylcholine Mixed Vesicles. *J. Lipid Res.* **2005**, *46* (3), 504–515. https://doi.org/10.1194/jlr.M400367-JLR200.

(47) Redfern, D. A.; Gericke, A. Domain Formation in Phosphatidylinositol Monophosphate/Phosphatidylcholine Mixed Vesicles. *Biophys. J.* **2004**, *86* (5), 2980–2992.

(48) Fujita, A.; Cheng, J.; Tauchi-Sato, K.; Takenawa, T.; Fujimoto, T. A Distinct Pool of Phosphatidylinositol 4,5-Bisphosphate in Caveolae Revealed by a Nanoscale Labeling Technique. *Proc. Natl. Acad. Sci.* **2009**, *106* (23), 9256–9261. https://doi.org/10.1073/pnas.0900216106.

(49) Qifti, A.; Garwain, O.; Scarlata, S. Mechanical Stretch Redefines Membrane Gαq–Calcium Signaling Complexes. *J. Membr. Biol.* **2019**. https://doi.org/10.1007/s00232-019-00063-8.

(50) Zhang, H.; Craciun, L. C.; Mirshahi, T.; Rohács, T.; Lopes, C. M. B.; Jin, T.; Logothetis, D. E. PIP(2) Activates KCNQ Channels, and Its Hydrolysis Underlies Receptor-Mediated Inhibition of M Currents. *Neuron* **2003**, *37* (6), 963–975.

(51) Whorton, M. R.; MacKinnon, R. X-Ray Structure of the Mammalian GIRK2-Bγ G-Protein Complex. *Nature* **2013**, *498* (7453), 190–197. https://doi.org/10.1038/nature12241.

(52) Suh, B.-C.; Hille, B. Regulation of Ion Channels by Phosphatidylinositol 4,5-Bisphosphate. *Curr. Opin. Neurobiol.* **2005**, *15* (3), 370–378. https://doi.org/10.1016/j.conb.2005.05.005.

(53) Golebiewska, U.; Scarlata, S. The Effect of Membrane Domains on the G Protein – Phospholipase Cβ Signaling Pathway. *Crit. Rev. Biochem. Mol. Biol.* **2010**, *45* (2), 97–105. https://doi.org/10.3109/10409231003598812.

(54) Gamper, N.; Shapiro, M. S. Target-Specific PIP2 Signalling: How Might It Work? *J. Physiol.* **2007**, *582* (Pt 3), 967–975. https://doi.org/10.1113/jphysiol.2007.132787.

(55) Yeung, T.; Terebiznik, M.; Yu, L.; Silvius, J.; Abidi, W. M.; Philips, M.; Levine, T.; Kapus, A.; Grinstein, S. Receptor Activation Alters Inner Surface Potential during Phagocytosis. *Science* **2006**, *313* (5785), 351–350.

(56) Heo, W. D.; Inoue, T.; Park, W. S.; Kim, M. L.; Park, B. O.; Wandless, T. J.; Meyer, T. PI(3,4,5)P3 and PI(4,5)P2 Lipids Target Proteins with Polybasic Clusters to the Plasma Membrane. *Science* **2006**, *314* (5804), 1458–1461. https://doi.org/10.1126/science.1134389.

(57) Hammond, G. R. V.; Fischer, M. J.; Anderson, K. E.; Holdich, J.; Koteci, A.; Balla, T.; Irvine, R. F. PI4P and PI(4,5)P2 Are Essential but Independent Lipid Determinants of Membrane Identity. *Science* **2012**, *337* (6095), 727–730. https://doi.org/10.1126/science.1222483.

CHAPTER 4. CONCLUSION AND FUTURE DIRECTIONS

Many functional activities of membrane-associated proteins in cells are modulated by the lipids in the membrane. Therefore, the composition of the membrane itself affects inter- and intra-molecular interactions between the lipid bilayer and proteins that are localized to and/or act on the membrane. Protein-lipid interactions can regulate the subcellular localization, distribution, and activities of numerous proteins. In addition, many membrane-associated proteins can modulate the shape, lipid composition, and dynamics of the cell membrane. Therefore, determining the precise mechanism by which a protein interacts with lipids is essential to understanding its biological function. However, the biological complexity of cell membranes has not been recapitulated *in vitro* to date. Thus, model membrane systems are commonly used to study protein-membrane interactions.

The studies presented in this dissertation used atomic force microscopy and compressed lipid monolayers as a model system to investigate how the known PLCβ3 regulatory elements and/or $G\alpha_q$ modulate PLCβ adsorption and activity. My first studies, discussed in Chapter 2, focused on determining the role of the PLCβ3 C-terminal extension in regulating monolayer adsorption and activity under basal conditions. I confirmed that deletion of both the proximal and distal CTDs (PLCβ3-Δ847) or deletion of only the distal CTD (PLCβ3-Δ892) decreases basal activity, likely due to decreased interactions with liposomes. This is consistent with the nonspecific adsorption of these proteins to compressed PE:PIP_2 monolayers. PLCβ3-Δ892 has the lowest basal activity and based on the AFM studies, this is likely due to steric hindrance by the proximal CTD. I also showed for the first time that PLCβ3 preferentially adsorbs to specific regions of the monolayer and that this spatial distribution is dependent upon the distal CTD. These regions are likely regions enriched in PIP_2, as PIP_2 spontaneously forms clusters on compressed lipid monolayers. I used mass spectrometry to confirm that the PLCβ3 variants all retained catalytic activity at the monolayer by quantifying the amount of IP_3 in the subphase. This confirmed that all variants were active under these assay conditions and that increased protein adsorption to the monolayer results in increased IP_3 production. I also found that mutations disrupting PIP_2 hydrolysis in the background of PLCβ3, PLCβ3-Δ847, or PLCβ3-Δ892 altered adsorption to the monolayer, demonstrating a role for the active site in membrane binding.

In Chapter 3, I expanded this approach to investigate the role of the acidic stretch within the X-Y linker and the entire X-Y linker in regulating PLCβ3 activity and adsorption to compressed lipid monolayers. Deletion of the acidic stretch (ΔXY1) or the entire X-Y linker (ΔXY2) increased basal activity in a liposome-based activity assay, demonstrating its autoinhibitory function. Surprisingly, the addition of PLCβ3 ΔXY1 and PLCβ3 ΔXY2 to the subphases of compressed lipid monolayers resulted in uniform protein adsorption with few elevated surface features compared to PLCβ3. This is most likely due to PIP_2 depletion caused by the ~10-fold higher basal activity of these variants. In contrast, the PLCβ3-Δ847 ΔXY and PLCβ3-892 ΔXY variants had increased non-specific adsorption compared to wild-type PLCβ3-Δ847 and PLCβ3-Δ892, respectively. Finally, under all conditions tested, the acidic stretch of the X-Y linker is sufficient to regulate PLCβ3 activity and adsorption to compressed lipid monolayers independently of the proximal and distal CTDs.

How the PLCβ3 regulatory elements regulate adsorption and activity in the context of $G\alpha_q$-dependent activation is largely unknown. To address this question, I purified stoichiometric $G\alpha_q$−PLCβ3 complexes and assessed their ability to adsorb to compress lipid monolayers. Addition of $G\alpha_q$−PLCβ3 to the subphases of compressed lipid monolayers resulted in specific adsorption to monolayers, comparable to those incubated with PLCβ3. In contrast, the addition of $G\alpha_q$−PLCβ3 ΔXY1 or $G\alpha_q$−PLCβ3 ΔXY2 lead to the flattening of monolayers, likely due to PIP_2 depletion. Monolayers incubated with $G\alpha_q$−PLCβ3-Δ892 showed adsorption to specific regions of the monolayer, similar to those incubated with $G\alpha_q$−PLCβ3 or PLCβ3. This suggests that $G\alpha_q$ is sufficient to target PLCβ3 to specific regions of the monolayer, likely those enriched in PIP_2, independently of the distal CTD. In contrast, monolayers incubated with $G\alpha_q$−PLCβ3-Δ892 ΔXY1 and $G\alpha_q$−PLCβ3-Δ892 ΔXY2 resulted in an increase in non-specific adsorption compared to monolayers incubated with PLCβ3-Δ892 ΔXY1 and PLCβ3-Δ892 ΔXY2, consistent with local PIP_2 depletion due to the increased lipase activity of these PLCβ3 variants. Together, this data is consistent with the X−Y linker, the regulatory CTDs, and $G\alpha_q$ coordinately regulating the adsorption and spatial distribution of PLCβ3 at the membrane.

Our studies suggest that the distal CTD and $G\alpha_q$ target PLCβ3 to regions of the monolayer enriched in PIP_2. Previous studies have shown that $G\alpha_q$ segregates into caveolae, which are enriched in PIP_2, and PLCβ has been shown to partition between raft and non-raft domains. Therefore, the distal CTD and/or $G\alpha_q$ may help target PLCβ to caveolae. This would add an

additional layer of complexity in PLCβ activation by $G\alpha_q$. For example, localization of PLCβ3 could result in increased local PIP_2 hydrolysis, which would have an impact on PIP_2-dependent cell processes. Thus, future studies exploring the spatial distribution of PLCβ, $G\alpha_q$, and lipid raft regions are needed. One possible approach would be to generate compressed lipid monolayers with raft-like properties by combining cholesterol and sphingomyelin, phospholipids [phosphatidylethanolamine (PE), phosphatidylserine (PS), and/or phosphatidylcholine (PC)], and PIP_2. It may also be interesting to add caveolin-1 to monolayers to mimic caveolae. AFM could then be used to detect the formation of lipid rafts, as rafts would be expected to have increased height compared to non-raft regions.

Furthermore, all of the studies presented in this dissertation explored PLCβ3 protein adsorption and activation under basal conditions or $G\alpha_q$-mediated activation. PLCβ3 is also activated by the Gβγ heterodimer. Thus, additional studies identifying how membrane properties influence Gβγ-dependent activation of PLCβ3 are needed. These studies can be conducted using a similar approach to our $G\alpha_q$-PLCβ3 experiments, and the synergistic activation of PLCβ by both $G\alpha_q$ and Gβγ could be investigated. Finally, these experiments could be performed in the presence and absence of lipid rafts.

Structural and functional studies suggest that PLCβ is regulated in part through interfacial activation. However, it is unclear how membrane composition contributes to this process, and whether the composition impacts regulation by the autoinhibitory Hα2' helix or the distal CTD. For example, the displacement of the X-Y linker is thought to require electrostatic repulsion between the acidic stretch and the negatively charged membrane. This repulsion may also facilitate the displacement of Hα2'. Therefore, it would be interesting to explore how membrane properties, such as charge and surface pressure, affect PLCβ adsorption and activity using compressed lipid monolayers and AFM. For these experiments, monolayers containing 30% PIP_2 and varying percentages of phosphatidylethanolamine, phosphatidylcholine, and/or phosphatidylserine could be used to generate monolayers ranging from strongly acidic to strongly basic in surface charge.

VITA

Brianna Hudson was born in Cincinnati, Ohio to David and Chaunda Hudson. She has two sisters, Brittney and Brielle. Brianna graduated from Clark Montessori High School with honors in May 2011 and moved to Atlanta, Georgia to attend Agnes Scott College. She graduated with honors from Agnes Scott College in May 2015 with a B.S. in Biochemistry and Molecular Biology. Brianna then moved to Lafayette, Indiana to attend Purdue University in June 2015, where she joined Dr. Angeline Lyon's lab. Following her graduation from Purdue University in August 2019, Brianna plans to move to San Diego where she will work as a Scientist at GenWay Biotech.